Biocompatible zwitterionic polymer chemistries and hydrogels for gene therapy, drug delivery, and regenerative medicine

Andrew Sinclair

A dissertation
submitted in partial fulfillment of the
requirements for the degree of

Doctor of Philosophy

University of Washington

2016

Reading Committee:

Shaoyi Jiang, Chair

Cole DeForest

Elizabeth Nance

Program Authorized to Offer Degree:
Department of Chemical Engineering

University of Washington

Abstract

Biocompatible zwitterionic polymer chemistries and hydrogels for gene therapy, drug delivery, and regenerative medicine

Andrew Sinclair

Chair of the Supervisory Committee:
Shaoyi Jiang
Chemical Engineering

Zwitterionic polymers have recently gained significant attention as a unique class of biomaterials, with their superhydrophilicity and unrivaled biocompatibility setting them apart from non-ionic and single-charged polymers. In particular, polycarboxybetaine (PCB) is easy to functionalize, highly resistant to nonspecific cell and protein interactions, and able to evade immunological responses in the body. The work described in this dissertation uses several strategies to add new functionality to PCB-based materials; specifically, it strives for simple and elegant approaches to engineer the chemical and material properties of PCB-based polymers and hydrogels toward clinical applications.

First, PCB-ester side chain chemistries were tailored to engineer a nontoxic gene delivery platform, based on optimized pH buffering during gene trafficking and cationic-to-zwitterionic charge switching through hydrolytic and photolabile groups. Next, step-growth polymerization strategies were investigated to design a new class of heterodifunctional "linear" PCB architectures featuring zwitterionic groups positioned directly along the polymer backbone; these polymers are promising candidates to reduce immunogenicity and extend the circulation time of biologics. Then, new physical and chemical crosslinking strategies were explored to expand the capabilities of PCB hydrogels. In one approach, bioorthogonal thiol chemistries were combined with star-shaped PCB architectures to facilitate cytocompatible stem cell encapsulation and robust *ex vivo* expansion. Finally, a versatile strategy was developed to give PCB hydrogels dynamic viscoelasticity. These "zwitterionic injectable pellet" (*ZIP*) hydrogels exhibit tunable shear-thinning and self-healing attributes, are simple to make and use at any scale, and can be sterilized, lyophilized, and reconstituted into custom injectable drug formulations and cell-protective materials.

TABLE OF CONTENTS

LIST OF FIGURES

LIST OF TABLES

LIST OF ABBREVIATIONS

Abbreviation	Meaning	Ref.
PEG	poly(ethylene glycol)	Fig. 1.2
PCB	poly(carboxybetaine) *(any backbone)*	Fig. 1.4
PCBMA	poly(carboxybetaine methacrylate)	Fig. 1.4
PCBAA	poly(carboxybetaine acrylamide)	Fig. 1.4
PCBMA-**1** or -**2**	Distance between N^+ and COO^-	Fig. 1.5
PCBMA-**3**°	Tertiary amine in place of quaternary ammonium	Fig. 1.5
CBAA-X	carboxybetaine diacrylamide crosslinker	Fig. 1.5
RGD	arginylglycylaspartic acid	Fig. 1.5
CBMA-NBE	carboxybetaine methacrylate o-nitrobenzyl ester	Fig. 2.1
(b)PEI	(branched) polyethyleneimine	Fig. 2.10
PLGA	poly(lactic-co-glycolic acid)	various
PBAE	poly(β-amino ester)	Fig. 3.2
PAA	poly(amidoamine)	Fig. 3.2
PACB	poly(amidocarboxybetaine)	Fig. 3.3
PECB	poly(estercarboxybetaine)	Fig. 3.4
PSCB	poly(sulfidecarboxybetaine)	Fig. 3.5
sPCB	star-shaped poly(carboxybetaine acrylamide)	Fig. 4.1
sPCB-SH	thiol-terminated sPCB	Fig. 4.1
sPCB-DP	disulfide pyridine-terminated sPCB	Fig. 4.1
ZIP	"Zwitterionic injectable pellet"	Fig. 5.2

ACKNOWLEDGMENTS

This work was financially supported by the National Science Foundation (DMR-1005699 and DMR-1307375) and Defense Threat Reduction Agency (HDTRA1-13-1-0044). The author appreciates fellowship support from the Department of Education (P200A120023).

The author would like to thank members of the Jiang Lab, especially Prof. Zhiqiang Cao for early inspiration, Dr. Louisa Carr and Prof. Lei Zhang for gene delivery assistance, Drs. Jean-Rene Ella-Menye and Priyesh Jain for monomer synthesis and design expertise, Mr. Tao Bai and Ms. Mary Beth O'Kelly for fruitful hydrogel collaborations, Mr. Erik J. Liu for protein and travel expertise, and Drs. Harihara Sundaram, Hsiang-Chieh Hung, Andrew Keefe, Andrew White, George Sellhorn and Sijun Liu for helpful discussions throughout.

Peptide depot studies were done in collaboration with Warren Ladiges and Peter Rabinovich (NIH 5P01AG001751-31) in the Dept. of Comparative Medicine. Drs. John Morton and Xuan Ge assisted with *in vivo* work. Electron microscopy was conducted at the University of Washington Molecular Analysis Facility (MAF). The author would like to thank Arne Biermans for custom machining and device fabrication assistance and appreciates the teaching experience gained in the Depts. of Chemistry and Chemical Engineering at the University of Washington.

In all the work presented here, the author is especially grateful for the support of his supervisory committee members—Prof. Cole DeForest for hydrogel and artistic inspiration, Prof. Elizabeth Nance for superhuman inspiration, and Prof. Bruce Hinds for valuable suggestions. In particular, the author thanks his PhD advisor Prof. Shaoyi Jiang for priceless mentorship and creating an exciting environment for scientific discovery.

Finally, the author is most grateful for his parents, who encouraged his curiosity from the very beginning; his sister, who taught him that art is important; his friends, who remind him to occasionally stay up all night dancing instead of working; and his incredible wife Kim, who gives him unconditional support and love.

DEDICATION

to my amazing wife Kim, who is finally starting to care about polymers.

Chapter 1

INTRODUCTION

Continued medical breakthroughs promise to prolong life and cure diseases once considered fatal—these advancements are among the most uplifting products of technological progress and human ingenuity. Medicine has traditionally been as much of an art as a true science, but this balance has tipped towards the latter in recent decades. Academic discoveries and clinical findings are now disseminated around the globe instantly; this has accelerated research and finally begun to illuminate many of the "black boxes" of physiology and pathology. Treatments of the near future will be highly personalized, precisely targeted, and likely created through collaborative work spanning biology, chemistry, technology, and engineering.

1.1 Biomaterials and "biocompatibility"

One key to developing these advanced treatments is a deep understanding of interactions between physiological systems and engineered materials. These materials—biomaterials—play an irreplaceable role in more and more modern medical and biotechnological advances, but the importance of optimized biomaterials is still underestimated.

Early biomaterials were typically discovered through trial and error, as various polymers, metals and ceramics were adopted and occasionally modified before experimental use by surgeons.[1] Many synthetic polymers still considered the "gold-standard" for a particular intervention rose to prominence simply because of luck and convenience, and remain there in part because of regulatory or cost hurdles faced by their modern competitors. A continuous stream of new products based on crude and often disproven decades-old assumptions are promoted as advanced medical technologies. Thus, these material strategies should be periodically reevaluated to ensure the best outcomes, particularly in light of our evolving understanding of material-tissue interactions. This is particularly true in regards to the loosely-defined concept of "*biocompatibility*".

Many classes of biomaterials are routinely referenced as *biocompatible* when they would be more accurately termed *bio-tolerable*—this shift in perspective has been suggested by

Buddy Ratner.[2] That is, while these materials may be nontoxic and traditionally suitable for implantation or injection, the body will eventually recognize them as foreign and work to eliminate, sequester, or separate them from physiological interaction. This process, illustrated in Fig. 1.1, typically begins with nonspecific protein interactions, also known as biofouling.

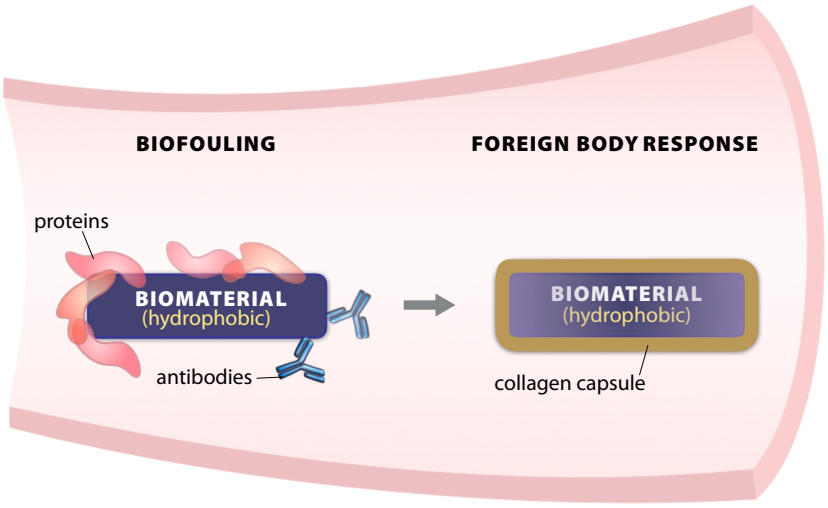

Figure 1.1 – Biofouling and the foreign-body response. **Left:** When hydrophobic materials are implanted in the body or injected into circulation, nonspecific interactions with proteins ("fouling") eventually lead to immune attack or sequestration (**right**).

Biofouling initiates a cascade resulting in many undesirable outcomes—clotting around catheters and implants,[3] premature clearance of polymeric nanocarriers[4] and even dangerous anaphylactic responses. Some outcomes of biofouling and immune system activation are helpful in specific situations; for example, the "foreign-body response" prevents systemic lead poisoning from gunshot wounds as a dense fibrous capsule is formed around bullet fragments. However, the goal of most modern biomaterials is to specifically interact with targeted biomolecules, cells, or tissues with a high sensitivity and specificity that enables their designed functionality. In practice, nonspecific protein interactions present a huge challenge to these targeted interactions.[5] The propensity of a material to foul typically increases along with its hydrophobicity. Therefore, several types of hydrophilic materials have been highly researched in recent years for their ability to avoid fouling, and these nonfouling materials have seen growing applications in engineering and medicine.

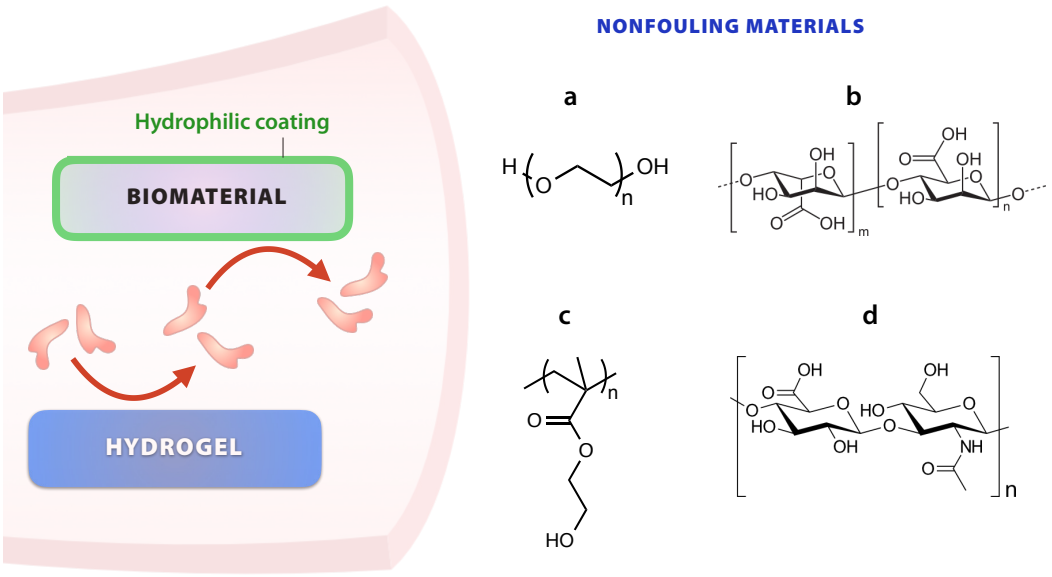

Figure 1.2 – Popular strategies to reduce fouling and improve biocompatibility. **Left:** Biomaterials can be coated with hydrophilic "nonfouling" polymers, or the hydrophilic polymers can be made into a hydrogel. Popular non-ionic nonfouling materials include: **a,** poly(ethylene glycol) (PEG); **b,** alginate; **c,** poly(2-hydroxyethyl methacrylate) (PHEMA); and **d**, hyaluronic acid.

1.2 Nonfouling materials

Selected non-ionic nonfouling materials are highlighted in Fig. 1.2. Among these, polyethylene glycol (PEG) (Fig. 1.2a) has seen the widest use. Other popular choices include polysaccharides such as alginate, dextran, and hyaluronic acid. All of these significantly mitigate most nonspecific interactions, but there are drawbacks to each as well. In long-term use, PEG is susceptible to oxidation in physiological environments,[6] and is also more accurately characterized as *amphiphilic* instead of purely *hydrophilic*; proteins and other biomolecules still have some nonspecific interactions with the carbon atoms in its backbone. Notably, reports of anti-PEG antibodies induced by PEGylated therapies and PEG-containing cosmetics have been increasing, raising serious concerns about its future potential.[7–9] Polysaccharides also have poor long-term physiological stability, varying biocompatibility, and are difficult to purify from natural sources to medical grade materials.[10]

Most nonfouling materials represent incremental steps towards true biocompatibility; a more modern definition of this term may be closer to physiological interaction or integration instead of a simple lack of toxicity. However, simply reducing nonspecific interactions or delaying an immune response is insufficient for long-term biocompatibility. A universal

strategy to eliminate nonspecific interactions and immunogenicity completely remains an open and important challenge.

1.3 Current trends in materials and medicine

In recent years, most research into biomaterials and nonfouling materials has moved beyond macroscopic surface modification. Two of the most rapidly growing interest areas are nanomedicine and regenerative medicine.

1.3.1 Nanomedicine

TNanomedicine has developed novel strategies to enhance medical imaging, diagnosis and treatment by leveraging the unique attributes of physiology at the sub-micron-scale. For example, nano-encapsulated chemotherapies can exploit the so-called enhanced permeation and retention (EPR) effect to passively target rapidly-growing tumor tissues through their "leaky" vasculature.[11] In addition, therapeutic proteins (or *biologics*) have become ubiquitous treatments and account for nearly half of prescription drug expenditures in the United States.[12] Biologics are costly to develop and face many practical challenges, with many exhibiting poor stability during production, formulation, storage, or physiological circulation. This has given rise to biomaterials-based strategies such as PEGylation, or the conjugation of PEG to proteins. PEGylation generally improves protein stability and circulation time, but is typically detrimental to bioactivity and product homogeneity.[13–15] Notably, reports of anti-PEG antibodies induced by PEGylated therapies and PEG-containing cosmetics have been increasing, raising particular concerns about its future in treatments requiring repeated administrations.[7,8] Nevertheless, this approach remains the gold standard in the field. Finding alternative materials and strategies to stabilize proteins and prolong their circulation and bioactivity should be a priority, to prevent unexpected setbacks for many pending and approved biologics and other nanomedicines. Along with conjugating alternative polymers to biologics, some researchers have recently employed hydrophilic peptides instead,[16–18] which can be genetically linked to the protein for one-step expression.

Gene-level manipulations are creatively combined with the engineered practicality of biomaterials in another way as well—as nonviral gene delivery vectors. By influencing a target protein's expression instead of simply supplementing or inhibiting its activity, DNA and siRNA-based gene therapies act at a more fundamental level of biology than most small-molecule drugs and biologics. This demands a particularly high bar for safety. The 1999

clinical trial death of Jesse Gelsinger focused intense scrutiny on the immunogenicity of adenovirus-based vectors and slowed gene therapy research for years,[19] but also spurred rapid development of a biomaterials-based alternative. Nonviral transfection gained attention as a capable strategy that mitigates the immunogenicity, manufacturing, and scalability concerns of viruses.[20,21] In particular, nucleic acid-complexing polymers were found to be highly customizable and facilitate the safe transport of nucleic acids to target cells. This tunability has inspired studies revealing fundamental aspects of nanoparticle uptake and cellular trafficking that apply broadly to drug and gene delivery strategies.[22–24] Viral vector safety has improved substantially in the past two decades, but biomaterials have increasingly proven their pivotal role in realizing the next generation of medicine.

1.3.2 Regenerative medicine

Cell-based regenerative treatments dominate headlines and may finally be the proverbial "cure" to many cancers and other diseases. However, many regenerative breakthroughs rely on expanding a limited number of a patient's own cells into a large and homogeneous population while maintaining their pluripotency or therapeutic value. This *ex vivo* expansion is proving to be a key bottleneck; cells frequently lose bioactivity and change their phenotype when expanded using typical culture platforms, which dramatically reduces their therapeutic value. Its becoming clear that expansion success is critically dependent on *ex vivo* culture environments, as biophysical interactions between a stem cell and its niche combine with biochemical signals to control its growth and fate.[25–27] Does its culture environment mimic the physiological niche closely enough to support desired differentiation behavior and maintain high viability? To what extent can we program or restrict cell activities through external stimuli? How can we maximize the therapeutic activity of cells or drugs at a tumor site? These are questions biomaterials are playing a key role in answering, and I explore these among others in this work.

1.4 Zwitterionic polymers

Zwitterionic polymers (or polyzwitterions) have recently gained significant attention as a unique class of biomaterials. These polymers contain an equal number of cationic and anionic groups repeated along their polymer chain. Though most in this class are synthetically produced, they take inspiration from many important molecules in the natural world; Fig. 1.3 shows some examples of zwitterions in nature. Glycine betaine, a nutritious zwit-

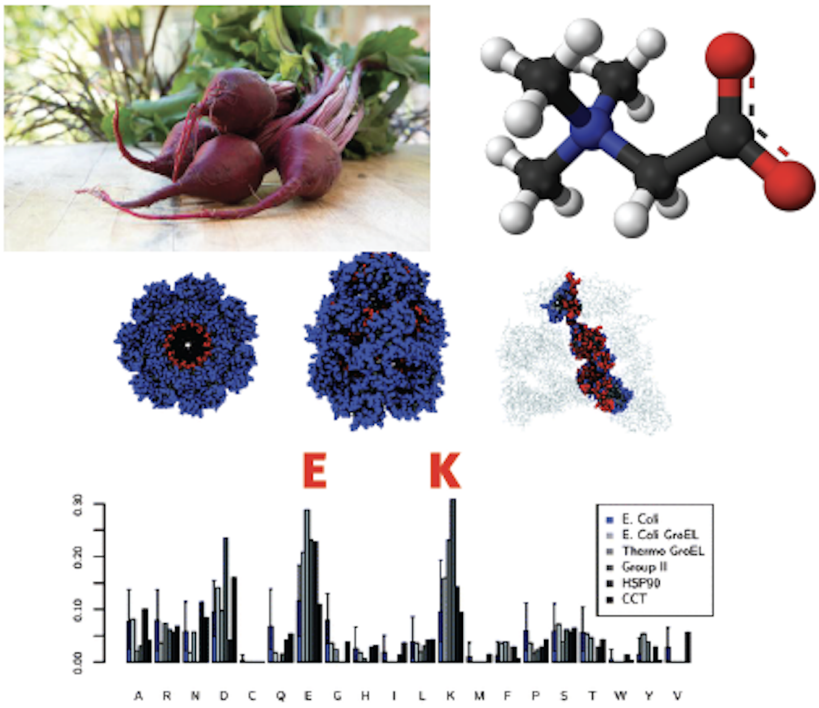

Figure 1.3 – Natural insight into zwitterionic materials. **Top:** Glycine betaine, found in beets, is a natural protein stabilizer. **Bottom**: Analysis of surface residues (White et al) has found charged amino acids in equal proportions (+ and -) to enable the natural stability of proteins in many organisms and environments.

terion found in beets, is widely known to stabilize protein structures and prevent denaturation and aggregation.[28,29] Phospholipids' zwitterionic phosphorylcholine head groups enable the formation and integrity of double-layer cell membranes, and recent investigations have found most proteins to exhibit quasi-zwitterionic surfaces dominated by cationic and anionic amino acids in equal proportions.[30,31]

The synthetic polyzwitterions derived from these natural phenomena are uniquely suitable for many biomedical applications. Their ultra-low fouling attribute is linked to their very high hydrophilicity and strong hydration in aqueous solutions,[28,32] which are typically superior to non-ionic materials such as PEG and polysaccharides. Several families of polyzwitterions have been developed, nearly all based on phosphorylcholine,[33] phosphobetaine, sulfobetaine, or carboxybetaine zwitterionic moieties. Fig. 1.4 shows the structures of some of the most popular types of zwitterionic polymers, with their charged groups highlighted.

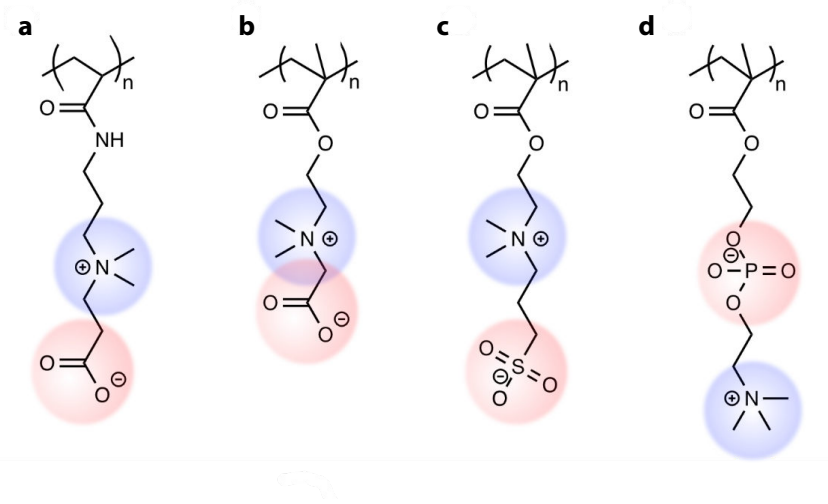

Figure 1.4 – Zwitterionic polymers used for biomedical applications. a) poly(carboxybetaine acrylamide) (pCBAA), b) poly(carboxybetaine methacrylate) (pCBMA), c) poly(sulfobetaine methacrylate) (pSBMA), and d) poly(methacryloyloxyethyl phosphorylcholine) (MPC).

More recently, polyzwitterions have also been successfully applied to several biomedical applications that reach beyond surface modification. In particular, zwitterionic polymers based on carboxybetaine have shown significant promise in nanomedicine and as highly biocompatible hydrogels. Polycarboxybetaines (PCBs) are unique among polyzwitterions in several ways; particularly important to the work in this dissertation, many molecular attributes of the CB monomer and PCB polymers can be systematically modified without compromising the superhydrophilicity for which they are known. Fig. 1.5 highlights some of the variations and derivatives of PCB studied in this work. As seen in the figure, the amine substitution (b), alkyl spacer length between the charged groups (c), and backbone group (d) can all be modified, and derivatives incorporating a hydrolytically degradable ester (e), cell-binding RGD (f), or dual acrylic groups for crosslinking (g) can be produced.

PCB polymers made from these and similar monomers have enabled many groundbreaking platforms over the previous decade. Nanoparticles incorporating a functionalized PCB shell—including liposomes,[?] PLGA,[34] gold,[35] silica,[36] iron oxide[37,38] and quantum dots[39]—can target specific tissues to release their drug cargo locally or enhance diagnostic imaging. At the same time, PCB-based nanoparticles exhibit prolonged circulation times, slow MPS clearance and and do not elicit immunogenicity.[35] Similarly, proteins conjugated to PCB[40,41] or encapsulated in PCB nanogels[8,42] see their circulation half-life enhanced, sta-

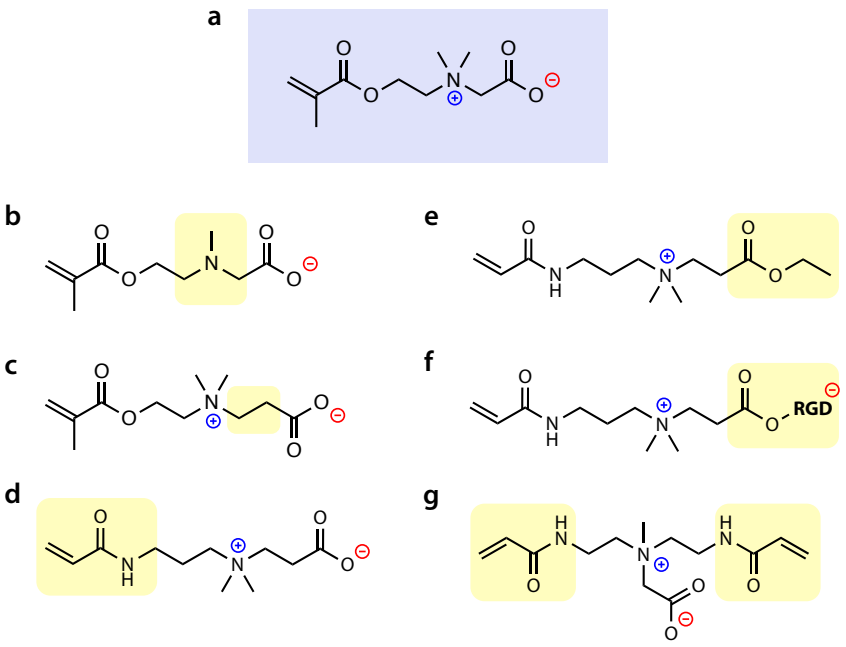

Figure 1.5 – Selected varieties and derivatives of carboxybetaine monomers used in this work. Notable differences from **a**, carboxybetaine methacrylate-1 (CBMA-1) highlighted. **b)** carboxybetaine methacrylate-1-tertiary amine (CBMA-1-3°; **c)** carboxybetaine methacrylate-2 (CBMA-2); **d)** carboxybetaine acrylamide-2 (CBAA-2); e) carboxybetaine acrylamide-2-ethyl ester (CBAA-2-EE); **f)** carboxybetaine acrylamide-2-RGD (CBAA-2-RGD); and **g)** carboxybetaine diacrylamide crosslinker (CBAAX-1).

bility heightened and opsonization reduced or eliminated—all without a significant reduction in bioactivity. This positions zwitterionic modification as a promising alternative to PEGylation.

This "stealthy" biocompatibility is not limited to the nanoscale. Purely zwitterionic PCB hydrogels made with zwitterionic crosslinkers were shown not to produce a foreign-body reaction or induce collagenous capsule formation for three months when implanted subcutaneously in mice, and even promote healing around the implant.[43] This result was later highlighted by the journal *Nature Biotechnology* as one of eight major breakthroughs published over the past 20 years. The growing evidence showing polyzwitterions uniquely able to avoid this adversarial response is exciting and motivates more application-specific development towards clinical use. PCB hydrogels also act as excellent cell culture platforms, and human stem cells grown on or inside PCB hydrogels are restrained from prematurely differentiating.[44,45] As demonstrated in *Chapter 4* of this work, these and other cell lines can

be expanded in PCB hydrogel platforms while retaining high viability and full functional bioactivity. This may prove incredibly useful for many regenerative medicine applications, and also help elucidate fundamental mechanisms driving stem cell fate choices. Clearly, zwitterionic polymers have the potential to overcome many longstanding limitations faced by biomaterials and in the biotechnology field in general.

1.5 Organization of thesis

1.5.1 Adding new functionality to polyzwitterions for nanomedicine

Many polymers commonly used as biomaterials feature a "backbone–side-chain" design, in which a material's unique functionality is primarily defined by the side chain structure, while its acrylic backbone is shared with many varied classes of polymers. This is frequently valuable, as it allows researchers to design and synthesize homopolymers and copolymers or various linear and branched architectures using established polymer chemistries. Since the side-chain functionality is relatively independent of the polymer architecture and polymerization process, polymers of similar overall structures but varying side chain functions to be designed, synthesized, and compared more easily for each targeted application. Zwitterionic polymers use this design as well—with the zwitterionic moiety in the side chain—and are commonly based on methacrylate and acrylamide backbones, as shown in Fig. 1.4.

Acrylic-backbone polyzwitterions are thus excellent platforms for exploring structure–function relationships through systematic side-chain modifications or comparisons between different zwitterions. In particular, carboxybetaine-based materials have invited creative monomer modifications that enable functionalities beyond the intrinsic hydrophilicity of PCB. The carboxylate group in CB is amenable to many conjugation chemistries, and CB-ester monomers can be easily synthesized.[46] PCB-esters are capable of switching charge, changing their hydrophilicity, or degrading into synergistic products.[47,48] Likewise, while

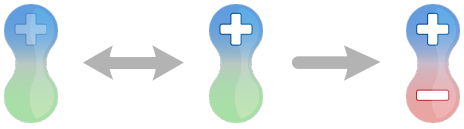

Figure 1.6 – Switchable PCB

the cationic amine in CB is most commonly a quaternary ammonium (so that the polymer retains a zwitterionic charge over a wide pH range) secondary and tertiary amines are reliably cationic (protonated) at some pH values and neutral at others, motivating the development of pH-responsive CB-based polymers for specific applications.

In *Chapter 2* of this work, I present our work exploring some of these switchable and pH-responsive variations and applying them to gene delivery applications. Results from this work have been published in *Biomacromolecules*.[49] Then in *Chapter 3*, I propose a new class of zwitterionic polymers that enable a similar degree of tunability to their polymer backbone. Variations in this class are formed through step-growth, Michael-type polyaddition or thiol-ene "click" reactions, and are designed to be more flexible and have greater hydrodynamic volumes than acrylic-backbone polyzwitterions at comparable molecular weights. This architecture is advantageous for protein conjugation and other drug delivery applications, and enables fully degradable backbone chemistries.

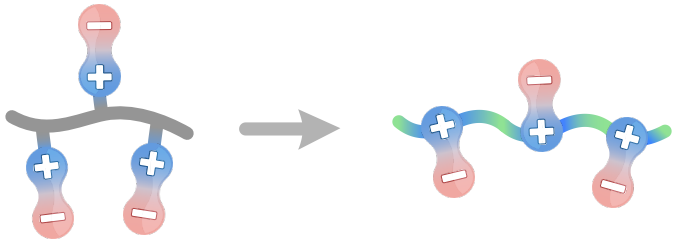

Figure 1.7 – Linear-backbone PCB

1.5.2 In situ-forming and injectable zwitterionic hydrogels

The exciting recent findings that polycarboxybetaine hydrogels are able to avoid the foreign-body response and eliminate nonspecific cell interactions suggest that commercial clinical uses are imminent. Our lab and others typically produce hydrogels by mixing acrylic monomers, crosslinkers, and free-radical initiators in a mold under the necessary conditions for radical generation such as UV light exposure. This method of making bulk hydrogels is well-established and allows many material properties (such as modulus) to be accurately programmed by changing the monomer:crosslinker ratio or intensity of localized light exposure.

As hydrogels have shown growing promise as ECM mimics to study and improve *ex vivo* cell growth and behavior, a need had arisen for alternative gelation chemistries. These are generally known as *in situ* forming strategies, and avoid radical-based chain reactions that can damage cells, leave behind toxic molecules, and are difficult to initiate in physiological environments. Thiol-ene coupling and refinements of azide-alkyne cycloaddition reactions such as SPAAC are now popularly employed to add this functionality to PEG- or polysaccharide-based hydrogels.[26,50–53]

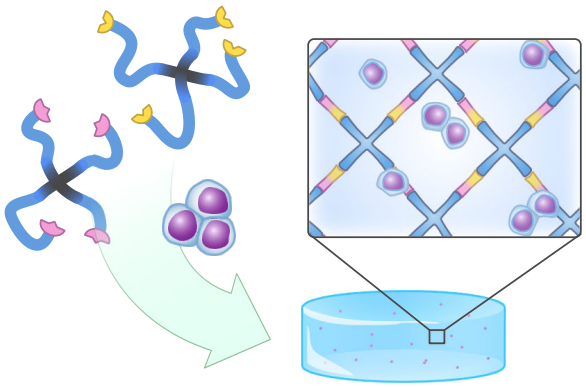

Figure 1.8 – *In situ*-forming sPCB hydrogels

In *Chapter 4*, I present our work to integrate *in situ* crosslinking and unique polymer architectures to enable one-step formation of degradable constructs for cell expansion. We explore a new star-shaped PCB architecture (spCB), and functionalize the stars' termini to produce two complementary variations: spCB-SH (thiol-terminated) and spCB-DP (disulfide pyridine-terminated). An extension of this work currently in review[54] substituted enzymatically degradable SPAAC crosslinking and achieved robust expansion of hematopoietic stem cells derived from cord blood and bone marrow. We hope these platforms will continue to be useful tools with which to study fundamental cell-matrix interactions, as well as lead to expanded clinical applications of stem cell based therapies.

For many of their growing clinical applications—including cosmetic procedures, localized chemotherapy and as regenerative cell scaffolds—injectable hydrogels are in high demand to avoid invasive implantation surgery and enable reshaping to fill unique 3-D spaces.[55–57] Most traditional hydrogels architectures are elastic until they break, and these

hydrogels cannot be injected through a needle, evenly spread on a surface or tissue (i.e. like jam on toast), or reconfigured into new self-supporting shapes without dramatic changes in their overall properties.

In *Chapter 5*, I present a simple and scalable strategy to create injectable, shear-thinning, and self-healing PCB hydrogels by reconstructing microgel units into new bulk materials. The unique combination of chemical crosslinking and dynamic supramolecular interactions in these zwitterionic injectable pellet (*ZIP*) constructs, known as "zwitterionic fusion",[58] give them a supportive modulus and tunable viscoelasticity. Their uniquely tunable and desirable rheological properties, including shear-thinning and self-healing behavior, are demonstrated and discussed. Lyophilized *ZIP* powders retain their strength and elasticity upon rehydration, simplifying sterilization and storage. When reconstituted with aqueous suspensions of cells, proteins, or drug-loaded microspheres, *ZIP* powders rapidly self-heal into a homogeneous composite hydrogel formulation without requiring any specialized reagents or conditions. Potential clinical applications discussed include injectable drug depots, active enzyme gels, and injectable cell scaffolds that protect therapeutic cells from shear damage. This work is pending submission.[59]

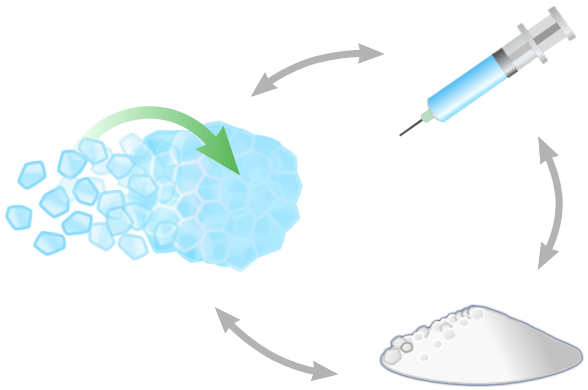

Figure 1.9 – Injectable "ZIP" PCB hydrogels

Chapter 2

POLYMER SIDE CHAIN CHEMISTRY FOR GENE DELIVERY

2.1 Chapter overview

In this chapter, I present how variations in the polymer side chains of polycarboxybetaine methacrylate (PCBMA) can enable its use as a effective and nontoxic polymeric vector for gene delivery applications. One unique aspect of carboxybetaine monomers (all CBMA-based in this chapter) is that nearly every functional part can be modified to integrate additional features, often with little detriment to its core nonfouling function. PCBMA substituting tertiary for quaternary amines is still strongly nonfouling, but also pH-responsive. In addition, hydrolytic or photolabile esters can be added to CBMA, temporarily "hiding" the free carboxylic acid to render the polymer cationic until ester cleavage. Both of these features are explored in this chapter to demonstrate how optimized PCB-based formulations can enable application-specific functionality.

2.2 Introduction

While viral vectors remain the most efficient for systemic gene delivery, nonviral vectors and particularly those based on polymers have gained increasing attention. Several platforms have been show to be capable and broadly-applicable, while mitigating the safety, immunogenicity, manufacturing, and scalability concerns of viruses.[20,60] For over a decade, polyethyleneimine (PEI) has been the benchmark in this class, mediating effective complexation and protection of anionic nucleic acids by virtue of its plentiful amines. Unfortunately, PEI remains cationic under physiological conditions and is not biodegradable, resulting in its well-known cytotoxicity through cell membrane destabilization.[60] An ideal polymeric vector would condense nucleic acids into stable polyplexes that can successfully navigate the extracellular environment and pass through the cell membrane, as well as protect genes from degradation inside and outside the target cells and assist with escape from the endosome or trafficking vesicle. However, many current polymers including PEI fall short when it comes to two final desired functions: controlled DNA release and a lack of inherent toxicity.

Many researchers have modified PEI or other well-studied cationic polymers to reduce their toxicity or boost efficiency.[61–63] Others have focused on engineering new polymers with a rational design or combinatorial chemistry approach, incorporating environmental responsiveness or biodegradability.[64–66] Most of these systems necessarily operate on a principle of compromise-one function of the vector (e.g., toxicity or DNA release) is improved at the expense of another (e.g., transfection rate or polyplex stability) until a balance is found. We have found polycarboxybetaine with degradable esters to offer unique potential in this regard; its charge-switching potential allows optimizing each function without detriment to the others. When the anionic carboxylate groups in zwitterionic PCBMA side chains are esterified, the polymer is rendered cationic and thus able to bind and condense nucleic acids.[47,67] A tertiary amine can be introduced in place of the quaternary ammonium to make the polymer pH-responsive, buffering pH changes during polyplex trafficking and providing a mechanism via the "proton sponge" effect for endosomal escape.[68] Another key function of this platform is the hydrolytic conversion of cationic PCBMA esters to zwitterionic PCBMA. The rate of this charge shifting can be easily modified by the incorporation of different ester leaving groups and different distances between the ester and the tertiary amine groups. This appends a "smart" characteristic to this polymer; DNA is first strongly complexed by cationic PCB-esters, but is efficiently released when ester degradation reveals the anionic carboxylate groups, rendering PCB zwitterionic and nontoxic. Thus, the PCBMA-ester platform is of great potential because its charge-shifting ability remedies the delicate binding-release compromises of other platforms.

Previously, we have demonstrated the in vitro gene transfer potential of the PCBMA-ester platform: an optimized tertiary/quaternary PCBMA-ethyl-ester (PCBMA-EE) copolymer mediated luciferase gene transfection approximately an order of magnitude higher than PEI, but without toxicity.[67] A similar strategy has also been applied to DNA vaccine delivery. This motivated a fundamental study of how altering specific characteristics of the monomers and polymers influenced their functions. Therefore, additional tertiary monomers were developed in this study to arrive at a small library of four unique monomers. Specifically, the side chain length was varied to include either a methyl or ethyl "spacing" length between the amine and the carboxylate/ester groups, denoted as an alkyl spacer length (ASL) of 1 or 2. Additionally, each ASL variation was synthesized with both ethyl ester (EE) and tert-butyl ester (tBu) hydrolytic groups. These molecular modifications produced monomers and resulting polymers with varying proton buffering capacities and

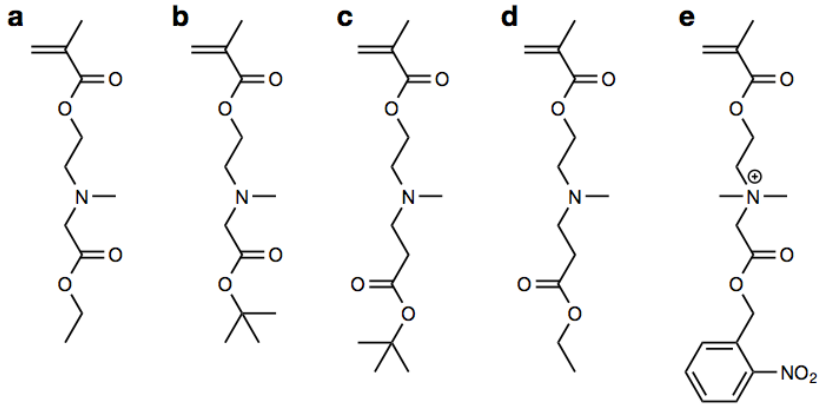

Figure 2.1 – Carboxybetaine methacrylate tertiary amine ester monomers synthesized for this study. By comparing **a-d**, the effects of charge spacing and ester stability were found. **a**, CBMA-1-3°-EE; **b**, CBMA-1-3°-tBu; **c**, CBMA-2-3°-tBu; **d**, CBMA-2-3°-EE. The *o*-nitrobenzyl group added to monomer **e** explores the viability of photolabile charge switching in this system.

hydrolytic profiles. The monomer structures are pictured in Fig. 2.1.

While the post-hydrolysis, zwitterionic form of PCB does not condense DNA, the direct contribution of the ester degradation step to DNA release deserved further study. Therefore, we developed a photolabile *o*-nitrobenzyl derivative of polycarboxybetaine (PCBMA-NBE) to give this platform a UV-sensitive "switch" for active degradation control. The monomer structure of CBMA-NBE is shown in Fig. 2.1e. Similar photoresponsive linkers have been utilized by others to develop photodegradable hydrogels and release DNA from the surface of gold nanoparticles.[53,69,70] We have incorporated it into the multifunctional PCBMA-ester platform to study how the charge neutralization caused by ester degradation directly catalyzes DNA release from a polyplex. The library of PCBMA-3°-esters and the photolabile PCBMA-NBE shows that the rational adjustment of buffering ability and degradation character can tune desired functions of PCBMA-esters and endow them with "smart" abilities.

2.3 Methods

Chemicals used in the synthesis, purification, and characterization of CBMA-ester monomers and polymers, and phosphate-buffered saline (PBS, 138 mM NaCl, 2.7 mM KCl, pH = 7.4) were purchased from Sigma-Aldrich. Dulbecco's Modified Eagle Medium, fetal bovine serum, nonessential amino acids, penicillin-streptomycin, and PicoGreen kit were purchased from Invitrogen/Thermo Fisher. COS-7 cells were purchased from the ATCC. All water

used had been purified to 18.2 MΩ·cm with a Millipore Simplicity water purification system.

2.3.1 *Synthesis and characterization*

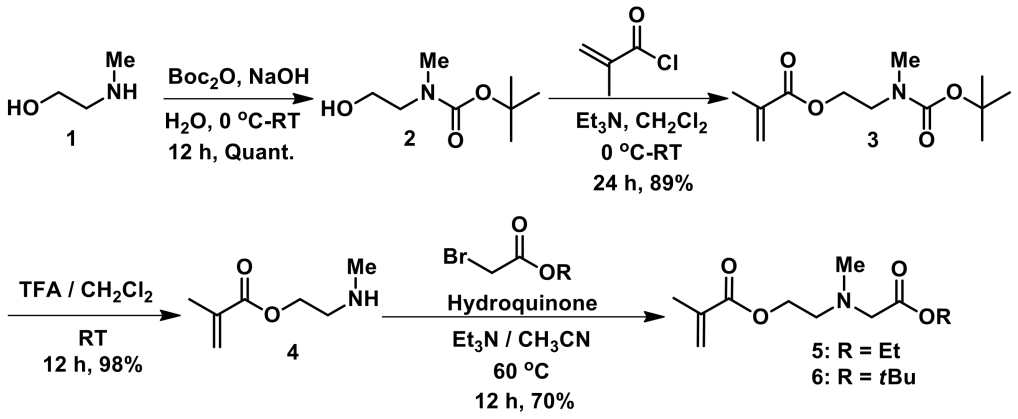

Figure 2.2 – Synthesis of CBMA-1-3°-esters

N-tert-Butoxycarbonyl-N-methyl-ethanolamine (2): N-Methyl-ethanolamine (13.9 g, 185 mmol) was dissolved in 1 N sodium hydroxide (250 mL) and the solution was cooled to 0°C. Di-tert-butyl dicarbonate (45.0 g, 206 mmol) was added to the mixture and the reaction was stirred and allowed to warm to room temperature overnight. The product was then extracted with ethyl acetate (4 x 125 mL) and the combined organic phase was dried over anhydrous sodium sulfate. After removal of the ethyl acetate under reduced pressure, the pure product was obtained as a colorless oil (31.8 g, 181 mmol). Yield: 98%. ^{1}H NMR (300 MHz, $CDCl_3$) δ (ppm): 3.71 (t, 2H, J=6.0 Hz), 3.36 (t, 2H, J=6.0 Hz), 2.90 (s, 3H), 1.44 (s, 9H).

N-tert-Butoxycarbonyl-N-methyl-2-aminoethyl-methacrylate (3): N-tert-Butoxycarbonyl -N-methyl-ethanolamine (14.5 g, 82.7 mmol) and triethylamine (34.7 mL, 249 mmol) were dissolved in anhydrous dichloromethane (150 mL) and the solution was cooled to 0 oC. Methacryloyl chloride (12.3 mL, 125 mmol) was added dropwise and the solution was stirred at room temperature for 24 h. The reaction was quenched at 0°C by slow addition of ice water then diluted with dichloromethane (100 mL). The solvent phases were separated and the organic phase was washed with H_2O (4 x 25 mL) and brine (25 mL). After drying over sodium sulfate, the solvent was removed under reduced pressure and the crude mixture was purified

by silica gel chromatography using a gradient of pure hexane to hexane:ethyl acetate 10:1. The pure product was obtained as a yellow oil (17.8 g, 73.2 mmol). Yield: 89%. ^{1}H NMR (300 MHz, $CDCl_3$) δ (ppm): 6.15 (s, 1H), 5.56 (s, 1H), 4.28 (t, 2H, J=5.9 Hz), 3.27 (s, 3H), 2.90 (t, 2H, J=5.9 Hz), 1.96 (s, 3H), 1.44 (s, 9H).

N-Methyl-2-aminoethyl-methacrylate (4): N-tert-Butoxycarbonyl-N-methyl-2-aminoethyl - methacrylate (15.0 g, 61.7 mmol) was dissolved in anhydrous dichloromethane (100 mL). Trifluoroacetic acid (24.0 mL, 313 mmol) was added and the reaction mixture was stirred at room temperature for 12 h. The solvent was removed under reduced pressure and the crude residue was purified by silica gel chromatography using a gradient of pure dichloromethane to dichloromethane:methanol 2:1. The pure product was obtained as a light yellow oil (8.65 g, 60.4 mmol). Yield: 98%. ^{1}H NMR (300 MHz, $CDCl_3$) δ (ppm): 6.11 (s, 1H), 5.55 (s, 1H), 4.17 (t, 2H, J=5.9 Hz), 3.10 (s, 3H), 2.70 (t, 2H, J=5.9 Hz), 1.94 (s, 3H).

2-((2-Ethoxy-2-oxoethyl)(methyl)amino)ethyl methacrylate (5):
N-methyl-aminoethylmethacrylate (8.18 g, 57.1 mmol) and triethylamine (25.0 mL, 171 mmol) were dissolved in anhydrous acetonitrile (100 mL). Ethylbromoacetate (9.48 mL, 85.6 mmol) was added dropwise and the mixture was stirred at 60°C for 12 h. The reaction was cooled to room temperature and the solvent was removed under reduced pressure. The crude residue was dissolved in ethyl acetate (100 mL) and the organic phase was washed with H_2O (4 x 25 mL). After drying over sodium sulfate and evaporation of the solvent, the crude mixture was purified by silica gel chromatography using a gradient of pure hexane to hexane:ethyl acetate 1:1. The pure product was obtained as a light brown oil (9.56 g, 41.7 mmol). Yield: 73%. ^{1}H NMR (300 MHz, $CDCl_3$) δ (ppm): 6.00 (s, 1H), 5.66 (s, 1H), 4.15 (t, 2H, J= 5.9 Hz), 4.05 (q, 2H, J= 14.3, 7.1 Hz), 2.80 (t, 2H, J= 5.9 Hz), 2.34 (s, 3H), 2.30 (s, 2H), 1.89 (s, 3H), 1.18 (t, 3H, J=7.1 Hz).

2-((2-(tert-Butoxy)-2-oxoethyl)(methyl)amino)ethyl methacrylate (6):
N-methyl-aminoethylmethacrylate (12.1 g, 84.5 mmol) and triethylamine (35.3 mL, 253 mmol) were dissolved in anhydrous acetonitrile (150 mL). t-Butylbromoacetate (19.0 mL, 129 mmol) was added dropwise and the mixture was stirred at 60°C for 12 h. The reaction was cooled to room temperature and the solvent was removed under reduced pressure. The crude residue was dissolved in ethyl acetate (150 mL) and the organic phase was washed with H_2O (4 x 25 mL). After drying over sodium sulfate and evaporation of the solvent, the crude mixture was purified by silica gel chromatography using a gradient of pure hexane to hexane:ethyl acetate 1:1. The pure product was obtained as a light yellow oil (14.5 g, 56.3 mmol). Yield:

67%. ^{1}H NMR (300 MHz, $CDCl_3$) δ (ppm): 6.13 (s, 1H), 5.58 (s, 1H), 4.28 (t, 2H, J= 5.9 Hz), 3.27 (s, 2H), 2.90 (t, 2H, J= 5.9 Hz), 2.48 (s, 3H), 1.96 (s, 3H), 1.47 (s, 9H).

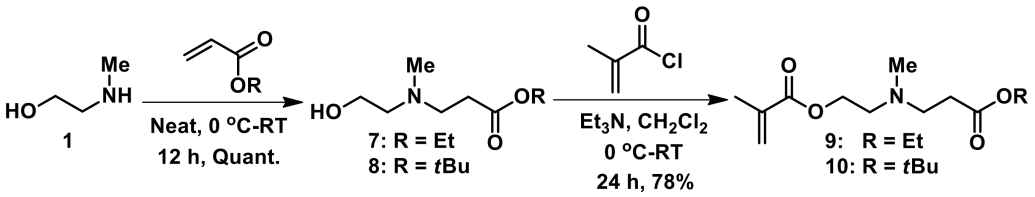

Figure 2.3 – Synthesis of CBMA-2-3°-esters

Ethyl 3-((2-hydroxyethyl)(methyl)amino)propanoate (7): N-Methyl-ethanolamine (10.2 g, 136 mmol) was added to a 250 mL round bottom flask cooled to 0°C. Ethyl acrylate (17.4 mL, 163 mmol) was added and the mixture was stirred at room temperature overnight. The mixture was concentrated on the rotovap to remove unreacted ethyl acrylate and further dried under high vacuum to yield the pure product as a colorless oil (23.8 g, 136 mmol). Yield: 99%. This product was used in the next step without further purification.

tert-Butyl 3-((2-hydroxyethyl)(methyl)amino)propanoate (8):

N-Methyl-ethanolamine (15.6 g, 208 mmol) was added to a 250 mL round bottom flask cooled to 0 oC. tert-Butyl acrylate (45.6 mL, 312 mmol) was added ad the mixture was stirred at room temperature overnight. The mixture was concentrated under vacuum on the rotovap to remove unreacted tert-butyl acrylate and further dried under high vacuum to yield the pure product as a colorless oil (42.1 g, 207 mmol). Yield: 99%. This product was used in the next step without further purification.

2-((3-Ethoxy-3-oxopropyl)(methyl)amino)ethyl methacrylate (9): Compound 7 (23.8 g, 136 mmol) was dissolved in anhydrous CH2Cl2 (200 mL). The solution was cooled to 0°C then triethylamine (47.3 mL, 340 mmol) and methacryloyl chloride (17.0 mL, 170 mmol) were added successively. The mixture was stirred at room temperature for 24 h. The reaction was quenched at 0°C by addition of ice water (50 mL). After separating the phases, the organic solution was extracted with H_2O (3 x 25 mL) and dried over sodium sulfate. After filtration and concentration under vacuum, the crude mixture was purified by silica gel chromatography using a gradient of hexane:ethyl acetate (20:1 to 10:1). The pure product was obtained as a light yellow oil (26.4 g, 109 mmol). Yield: 80%. ^{1}H NMR (300 MHz, $CDCl_3$) δ (ppm): 6.11 (s, 1H), 5.57 (s, 1H), 4.24 (t, 2H, J= 5.9 Hz), 4.14 (q ,2H, J= 14.3, 7.1 Hz),

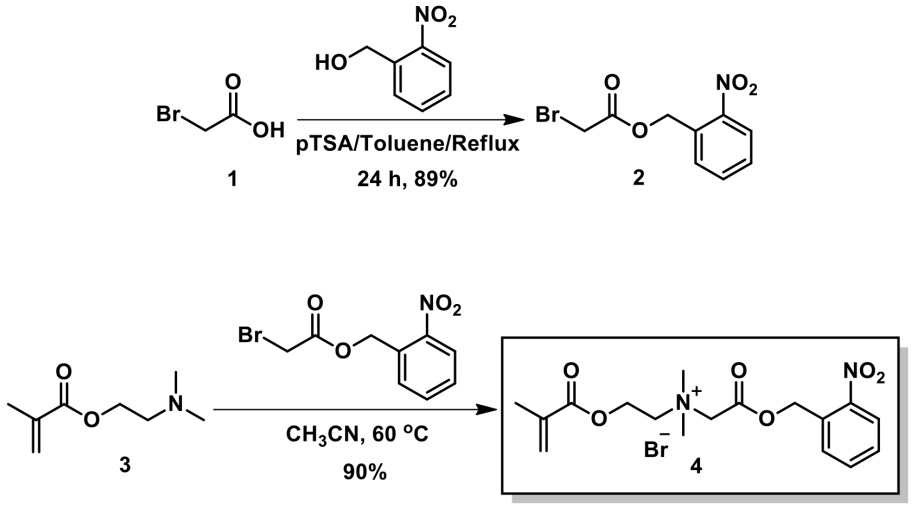

Figure 2.4 – Synthesis scheme of CBMA-*o*-nitrobenzyl ester (CBMA-NBE)

2.79 (t, 2H, J= 7.3 Hz), 2.72 (t, 2H, J= 5.9 Hz), 2.47 (t, 2H, J= 7.3 Hz), 2.32 (s, 3H), 1.95 (s, 3H), 1.26 (t, 3H, J= 7.1 Hz).

2-((3-(tert-Butoxy)-3-oxopropyl)(methyl)amino)ethyl methacrylate (10):

Compound 8 (15.1 g, 74.5 mmol) was dissolved in anhydrous CH_2Cl_2 (150 mL). The solution was cooled to 0°C then triethylamine (31.1 mL, 223 mmol) and methacryloyl chloride (11.0 mL, 112 mmol) were added successively. The mixture was stirred at room temperature for 24 h. The reaction was quenched at 0°C by addition of ice water (50 mL). After separating the phases, the organic solution was extracted with H_2O (3 x 25 mL) and dried over sodium sulfate. After filtration and concentration under vacuum, the crude mixture was purified by silica gel chromatography using a gradient of hexane:ethyl acetate (20:1 to 10:1). The pure product was obtained as a light brown oil.

CBMA-o-nitrobenzyl: The monomer was synthesized in a two-step process as shown in Fig. 2.4. First, 2-Nitrobenzyl-bromoacetate (2) was generated. Bromoacetic acid (11.2 g, 80.6 mmol), p-toluenesulfonic acid (2.78 g, 16.1 mmol) and 2-nitrobenzyl alcohol (14.8 g, 96.6 mmol) were successively dissolved in anhydrous toluene (200 mL). The solution was refluxed at 120 °C for 24 h and toluene was removed via evaporation on a rotovap. The resulting residue was dissolved in ethyl acetate (200 mL) and the organic solution was washed with H_2O (4 x 50 mL). The organic phase was dried over Na_2SO_2, after which the solvent

was removed under reduced pressure and the residue purified by silica gel chromatography using a gradient of pure hexane to hexane:ethyl acetate 3:1. The pure product was obtained as a light yellow oil (19.6 g, 71.5 mmol). Yield: 89%. ^{1}H NMR (300 MHz, $CDCl_3$) δ (ppm): 7.99 (d, 1H, J = 8.0 Hz), 7.59 (m, 1H), 7.43 (m, 2H), 5.49 (s, 2H), 3.89 (s, 2H). 13C NMR (75 MHz, $CDCl_3$) δ (ppm): 166.3, 146.8, 133.7, 130.8, 128.7, 128.5, 124.7, 63.9, 25.3.

Following this, CBMA-Nitrobenzyl-bromoacetate (CBMA-NBE) (4) was synthesized. 2-Nitrobenzyl-bromoacetate (2) (19.5 g, 71.1 mmol) was dissolved in anhydrous acetonitrile (150 mL). Dimethylaminoethylmethacrylate (DMAEMA) (10.8 mL, 63.3 mmol) and hydroquinone (150 mg, 1.36 mmol) were added to the mixture and the solution was stirred at 60°C for 18 h. The solvent was removed under reduced pressure and ether (400 mL) was added to the oily residue. The resulting suspension was stirred for 4 h and the ether phase decanted. The process was repeated three times and the residue was concentrated on the rotovap. The resulting oil was dried further under high vacuum to afford the pure product as a yellow oil (24.6 g, 57.0 mmol). Material was protected from light to avoid unintentional degradation. Yield: 90%. ^{1}H NMR (300 MHz, $CDCl_3$) δ (ppm): 8.05 (d, 1H, J = 8.3 Hz), 7.71 (m, 1H), 7.47 (m, 2H), 6.68 (s, 1H), 6.02 (s, 1H), 5.53 (s, 2H), 5.09 (s, 2H), 4.60 (m, 2H), 4.26 (m, 2H), 3.59 (s, 6H), 3.35 (s, 3H), 1.82 (s, 3H).

Polymerization: Tertiary and quaternary monomers were copolymerized at a molar ratio of 3-to-1 via RAFT polymerization. Various molar ratios of monomer to chain transfer agent ranging from 100 to 400 were used to obtain long, medium, and short length polymer chains. To calculate the molar ratio, total moles of monomer were used (tertiary plus quaternary). Briefly, for each separate tertiary monomer and molar ratio formulation, the appropriate amount of chain transfer agent (4-cyano-4-(phenylcarbonothioylthio) pentanioc acid), initiator (azobisisobutyronitrile), and 4°CBMA-ethyl ester, were weighed sequentially into 5-mL round-bottom flasks. The appropriate volume of tertiary monomer was then added, along with a small stir bar. The reactant flasks were deoxygenated by flowing nitrogen gas for 1 h. Vacuum purges were skipped to avoid loss of the powder reactants. During deoxygenation of the reactants, nitrogen gas was bubbled through anhydrous DMF to deoxygenate the solvent before use. One milliliter of the deoxygenated anhydrous DMF was then added to each reactant flask. Still under nitrogen protection, the flasks were swirled gently to ensure that all reactants dissolved. Once the solutions were uniform, the flasks were sealed and transferred to an oil bath heated to 70°C to initiate polymerization. Polymerization was allowed to continue overnight for up to 24 hours. The polymer solutions were then transferred to

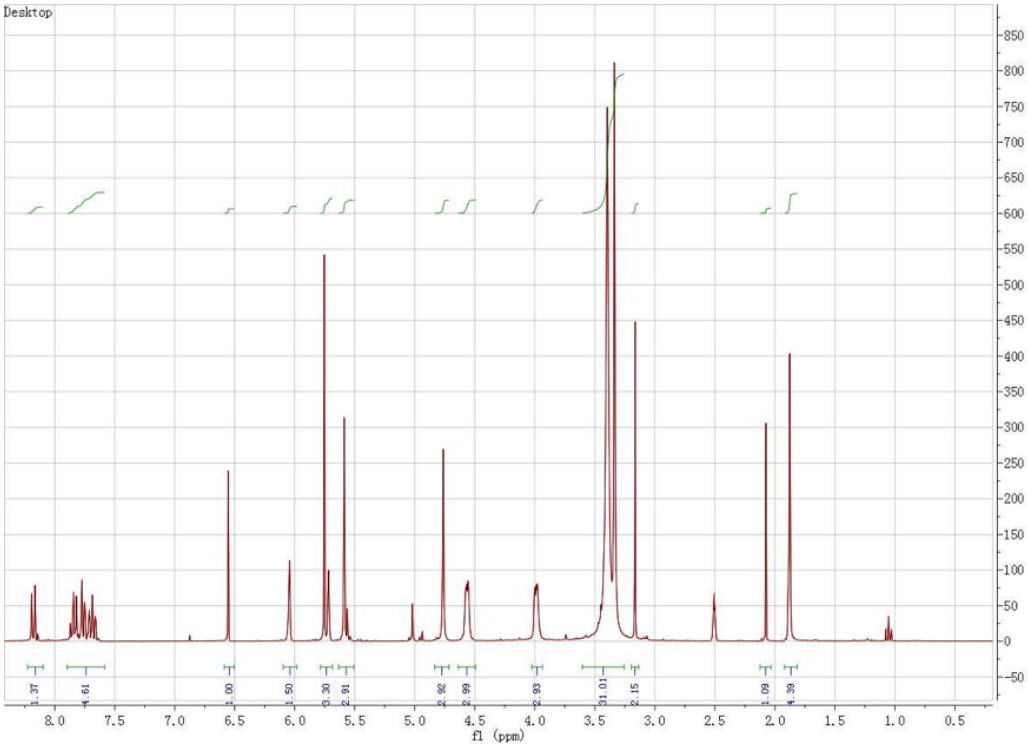

Figure 2.5 – ^{1}H NMR spectrum of CBMA-*o*-nitrobenzyl ester (CBMA-NBE)

hydrated Spectra/Por molecular porous membrane tubing (Spectrum Laboratories) with a molecular weight cutoff of 3.5 kDa and dialyzed overnight in Millipore water. After dialysis, the polymers were lyophilized to powder.

CBMA-NBE monomer was polymerized at a concentration of 10 wt% with an uncontrolled free-radical method in deoxygenated DMF, using 1 wt% azobisisobutyronitrile as an initiator, in a 5-mL round-bottom flask. Once the monomer/initiator solution was checked for uniformity, the flask was deoxygenated for 1 hr, sealed and transferred to an oil bath heated to 70°C to initiate polymerization. Polymerization proceeded for 24 hours. The polymer was then isolated and purified by dropwise precipitation into diethyl ether and dried under high vacuum for 24 h. Polymer purity was confirmed with NMR.

Molecular weights of the polymers were determined using aqueous gel permeation chromatography (GPC), using a Waters 2695 Separations Module fitted with a Waters 2414 refractive index detector and a Waters Ultrahydrogel 1000 column (7.8 mm ×300 mm). The buffer solution (0.05 M sodium acetate, 1.0 M sodium chloride, and 0.02% sodium azide, titrated to pH 5.0) was used as the eluent with a flow rate of 0.5 mL/min at room temper-

ature. The system was calibrated with narrow molecular weight polyethylene oxide standards (Polymer Laboratories, Varian, Inc.) The low pH of the running buffer was chosen to ensure protonation of the tertiary amines and thereby ensure the hydrophilicity of the polymers. Samples of all polymers were completely hydrolyzed before characterization to ensure elution times were more representative of chain length than of any difference in the hydrophobicity or size of the ester side chains. The tBu esters were hydrolyzed in trifluoroacetic acid (TFA) for 2–3 h and then precipitated in ether at 0°C. A small amount of the precipitate was then dissolved in the running buffer. The ethyl esters were hydrolyzed overnight in ammonium hydroxide solution (pH 10) and then mixed at 1:1 volumes with the running buffer.

2.3.2 Characterization of pH-responsiveness

To titrate the monomers and determine their proton buffering capabilities, 5 µL of each pure liquid monomer was dissolved in 0.1 M NaCl to a concentration of 1 mg/mL. The pH of the solution was lowered to 2 with 1 M HCl. Initial titration curves were obtained with sequential 0.1 mL additions of 0.1 M NaOH, with sufficient time between each addition to allow for pH stabilization. After initial curves were obtained and regions of buffering were identified, more thorough titration curves were obtained with additions of 0.02 mL 0.1 M acid or base in the buffering regions. Buffering capacity was calculated with molar equivalency.

2.3.3 Characterization of hydrolytic and photolabile charge switching

Hydrolytic rates of CBMA-1-3°-EE, CBMA-1-3°-tBu, CBMA-2-3°-tBu, and CBMA-2-3°-EE were determined using reverse-phase HPLC, with a C18 column (Econosil, 250×4.6 mm, 5µm, Alltech), and a UV detector (227 nm wavelength). Monomers at a concentration of 1 mg/mL in 100 mM sodium phosphate (pH 7.4) or 100 mM sodium citrate buffer (pH 5.1) were held at 37°C. A chromatography buffer solution of 0.50 vol/vol acetonitrile and aqueous sodium phosphate (100 mM) was used. This buffer caused the monomer to elute based on hydrophilicity; hydrolyzed monomers are significantly more hydrophilic due to their zwitterionic character. Peak areas were normalized and compared to show hydrolytic rate over 48 h. The photodegradation rate of the UV-sensitive CBMA-NBE monomer was determined with a similar method. A handheld UV lamp emitting 365 nm wavelength light was positioned directly above an open-top sample of a 1 mg/mL solution of CBMA-NBE in

pH 7.4 NaAc in a shallow 3 cm^2 glass dish for a radiation rate of 10 mW cm^{-2}. A 10 µL sample was removed each 5 min until a complete shift in peak areas confirmed photodegradation was complete.

2.3.4 Characterization of phototriggered DNA release

PicoGreen quantitative binding assays were adapted from Green et al.[66] PCBMA-NBE and quaternary PCBMA-EE solutions were prepared at 1 mg/mL in 25 mM NaAc buffer, pH 5.2. Then, 50 µL/well of 30 µg/mL gWiz-luciferase DNA plasmid was added to each well of a 96-well plate. The polymer solutions were diluted to correspond to polymer/DNA weight ratios from 1:1 to 20:1 and added to the DNA samples. Initial DNA concentration in each well was set to 1 µg/mL and then condensed with PCBMA-NBE or PCBMA-tBu in NaAc buffer. Solutions were gently mixed with pipetting and allowed to sit for 10 min for polyplex formation. Half of each sample was transferred to another open-top plate and exposed to 365 nm UV light for 1 h via a handheld lamp. Then, 100 µL/well of PicoGreen solution was added. PicoGreen working solution was prepared by diluting 80 µL of the purchased stock into 15.2 mL NaAc buffer. After 5 min, 30 µL/well of polymer-DNA-PicoGreen solution was added to 150 µL/well of NaAC in black 96-well polystyrene plates. The plate fluorescence was then measured on a Perkin-Elmer Victor 3 plate reader using a FITC filter set (excitation 485 nm, emission 535 nm). The relative fluorescence (RF) was calculated using the following relationship:

$$RF = \frac{F_{sample} - F_{blank}}{F_{DNA} - F_{blank}}$$

where F_{sample} is the fluorescence of the polymer-DNA-PicoGreen sample, F_{blank} is the fluorescence of a sample with no polymer or DNA (only PicoGreen), and F_{DNA} is the fluorescence of DNA-PicoGreen (no polymer), but an equivalent amount of DNA. The binding percentage was determined by 1-RF, because DNA bound to polymer or entrapped in a polyplex does not contribute to dye fluorescence. A standard curve of free DNA concentration was used to ensure linear correlation between free DNA content and fluorescence for all measurements and quantify the free DNA concentration of the samples.

2.3.5 Gene transfection studies

DNA-polymer nanoparticles, also referred to as polyplexes, were prepared as follows. Plasmid DNA was diluted from 5 mg/mL stock to 0.1 mg/mL in sterile 25 mM NaAc buffer, pH 5.2. Plasmid solutions were aliquoted in a 96-well plate. Then, the polymer of interest was dissolved in the same NaAc buffer and diluted to a concentration that would lead to the desired polyplex weight or N:P ratio. The polymer solution was added to the DNA and gently mixed with a pipette and allowed to sit for 10 minutes for polyplex formation. Polyplexes were then characterized or used for transfection experiments immediately.

COS-7 cells (African Green Monkey fibroblast cells, ATCC) were grown to 80% confluence in Dulbecco's Modified Eagle Medium (Gibco) supplemented with 10% Fetal Bovine Serum, 1x non-essential amino acids, and penicillin-streptomycin. Cells were incubated at 37°C and 5% CO2. One day prior to transfection, the cells were transferred to 48-well tissue culture plates, at 20,000 cells per well. All cells used in these studies were from passages 5-10.

For each transfection, medium was removed from wells and the cells were washed with sterile filtered PBS. 20 µL of polyplex suspension (prepared as noted in 2.2.9) was added to 180 µL of serum-free medium in a separate 48-well plate. The PBS was removed from cells, and replaced with the polyplex-containing medium. Regardless of the polyplex weight ratio, 1 µg of DNA was added to each well. 25 kDa branched PEI (Aldrich; St. Louis, MO) was used as a positive control for each transfection, at N:P ratios of 5 and 10. DNA-only samples and medium-only samples were used as negative controls. Cells were incubated with the transfection solutions for 3 hours at 37°C, 5% CO2, after which the medium was removed from the cells, they were washed with PBS, and then supplied with 200 µL/well of supplemented medium. Luciferase expression was assayed after 48 hours.

For luciferase expression assays, cells were washed with PBS and lysed with 200 µL 1x Reporter Lysis Buffer (Promega) at room temperature for 10 minutes before a freeze/thaw cycle. 20 µL cell lysate was then transferred to a 96-well polystyrene plate, and 100 µL Bright-Glo Luciferase Assay System (Promega) was added to each well, with minimal delay between substrate addition and luminescence detection. Luminescence of the triplicate samples was measured in a Perkin Elmer Victor 3 microplate reader. For protein content measurement, 20 µL cell lysates were transferred to a 96-well plate and incubated 30 minutes at 37°C with 200 µL BCA protein assay kit working reagent (Pierce). The plate was then allowed to cool to room temperature. Absorbance was measured at 562 nm on a Victor

3 microplate reader and converted to protein concentration using a standard curve made from serially diluted bovine serum albumin (Sigma) solutions in 1x Reporter Lysis Buffer. Luminescence was then normalized to protein concentration.

2.4 Results and discussion

To study the influence of molecular variations on the buffering capacity and degradation behavior of tertiary PCBMA esters, four monomers were synthesized for this study. These monomers are referred to as CBMA-1-3°-EE, CBMA-2-3°-EE, CBMA-1-3°-tBu, and CBMA-2-3°-tBu in the following charts and graphs, in reference to their alkyl spacing length (ASL) between the charged groups (1 or 2) and identity of ester leaving group (2-carbon ethyl ester or 4-carbon tert-butyl). All monomers/polymers in this chapter contain a methacrylate backbone.

Monomers were titrated to identify the pKa of their tertiary amines, with the goal to evaluate how the chemical structure of the monomers affects their potential buffering capacities. For clinical applications, a vector encounters changes in pH as it is trafficked to its target, which can degrade DNA if it is not sufficiently protected. Endocytosed materials are exposed to an increasingly acidic environment; the pH in the endosome is lowered via proton pumps in the endosomal membrane, from physiological pH of 7.4 to approximately 5. Therefore, materials with a pKa and buffering capacity in this endosomally appropriate range can absorb protons as they are pumped into the endosome and help to create an osmotic pressure gradient across the endosomal membrane that may ultimately lead to membrane rupture and endosomal escape, though this "proton sponge" mechanism is still being studied.[68,71] One reason for the high transfection efficiency of PEI may be due to its buffering capacity in this range. Dimethylaminoethyl methacrylate (DMAEMA) has been used as a gene transfer vector, but mediates inferior transfection to PEI.[72,73] The pKa of its tertiary amine is around 8.4, which is not well-suited for endosomal buffering. Both of these polymers remain substantially protonated at physiological pH, leading to post-transfection toxicity.

The monomers in this study have a tertiary amine like DMAEMA, but also have an electron-withdrawing carboxylate ester connected to each amine. The proximity of this ester group decreases the pH required to protonate the amine, shifting the pKa and buffering range down into the pH environment of the endosome, as compared to DMAEMA. Changing the separation distance between the amine and ester changes the extent of this shift.

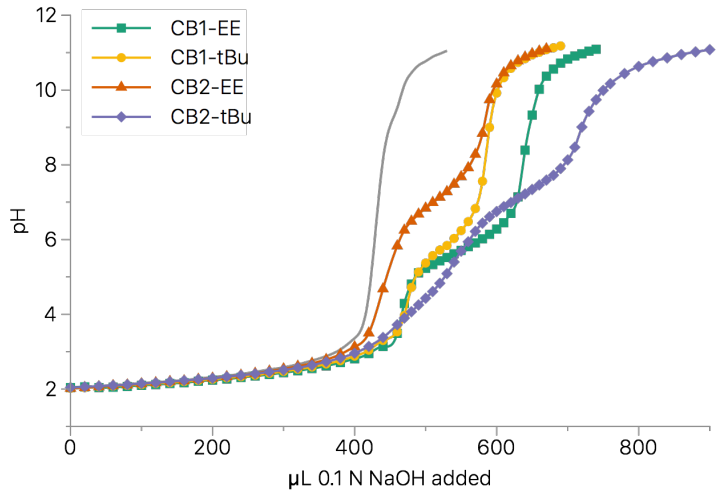

Figure 2.6 – Titration of CBMA-3°-ester monomers, showing their pH buffering ability, tested by titrating with NaOH in 100 mM NaCl. Region of interest is between pH 5.1 and 7.4.

All of these monomers featured either a one- or two-carbon distance (ASL = 1 or 2) between the ester and amine and exhibited pKas that were significantly lower than the pKa of DMAEMA. The four monomers showed pKas in two distinct subsets: ASL 1 monomers had pKas of 5.5-6 and ASL 2 monomers had pKas of approximately 7. Titration curves and the molar buffering capacities of the monomers are shown in Figs. 2.6 and 2.7.

These data show that the pKa is sensitive to the proximity of the electron-withdrawing group down to a one-carbon difference in distance. The pKa values imply that half of the amines on the ASL 2 monomers will be protonated (cationic) at physiological pH, which may aid in DNA packaging. Conversely, few of the amines in the ASL 1 monomers will be protonated at physiological pH, and the fraction available for endosomal buffering will greatly increase. We expect CB esters with this shorter ASL to mediate optimal DNA protection. Their inclusion in copolymers could extend the polymer buffering range to a lower pH without resulting in leftover charge that contributes to toxicity. The pKa of a hydrolyzed ASL 1 monomer (tertiary CB1) is 8.3, very similar to that of DMAEMA. Importantly, this implies that after DNA delivery and transfection, the polymeric residue of the vector will be almost entirely protonated at the amine and unprotonated at the carboxylic acid, rendering it zwitterionic and biocompatible. The size of ester leaving group (ethyl vs tBu) had no significant effect on the pKa, showing that the ester size can be changed without sacrificing the desired buffering range.

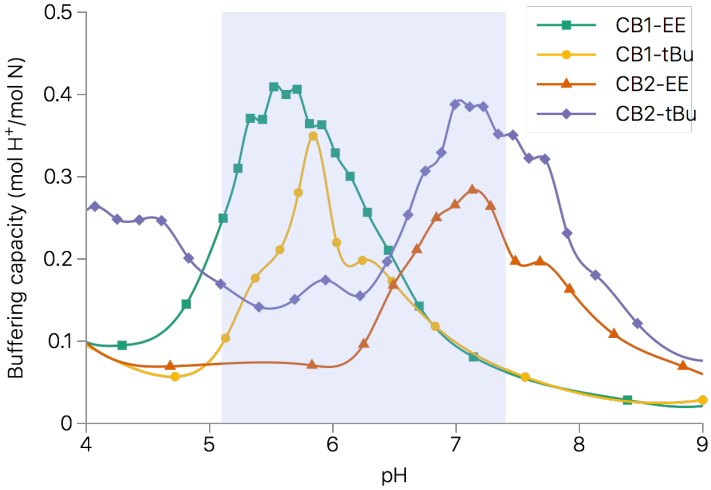

Figure 2.7 – Molar buffering capacity of CBMA-3°-ester monomers, with vertical dashed lines showing the pH range present in the endosome. Curve peaks correspond to the pKa of each monomer.

While others[74,75] have incorporated hydrolytically degradable bonds in polymers, the wide variation in possible hydrolysis profiles necessitate a more discriminating selection of ester leaving group. For example, it could be rationalized that a bond stable at physiological pH (7.4) but labile at the lower endosomal pH (5.1) would ensure that the DNA stays protected for cellular uptake. However, such a strategy may result in DNA release and degradation within the acidic environment of the endosomal pathway. An ester more stable in acidic conditions may remain intact in the endosome, but if it is overly labile at a higher pH, it may experience premature degradation. Therefore, an ester relatively stable at both pH conditions may be desirable, and it is important to study their hydrolytic profiles to help identify unsuitable leaving groups and provide design insight.

The hydrolysis of each ester was monitored over a period of 40 h with reverse-phase HPLC. As seen in Figs. 2.8 and 2.9, CBMA-2-3°-EE and CBMA-1-3°-tBu monomers exhibited pH-dependent hydrolysis behavior. At physiological conditions, the CBMA-2-3°-EE hydrolyzed much more rapidly, reaching more than 80% hydrolysis after 40 h, but only degrading 20% over the same time period at endosomal pH. Conversely, CBMA-1-3°-tBu was more stable at physiological conditions than endosomal ones. The CBMA-1-3°-EE and CBMA-2-3°-tBu esters were relatively stable at both physiological (pH 7.4) and endosomal (pH 5.1) conditions. These data show that the parameters of the CBMA-ester platform can

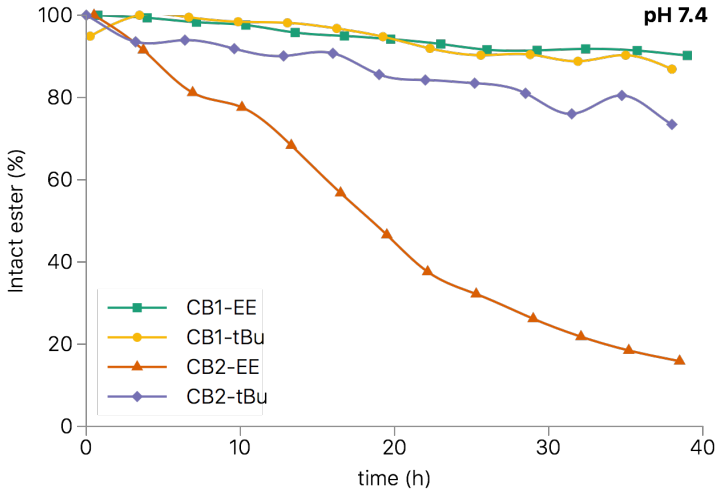

Figure 2.8 – Hydrolysis rates of CBMA-3°-ester monomers at pH 7.4, representative of physiological pH.

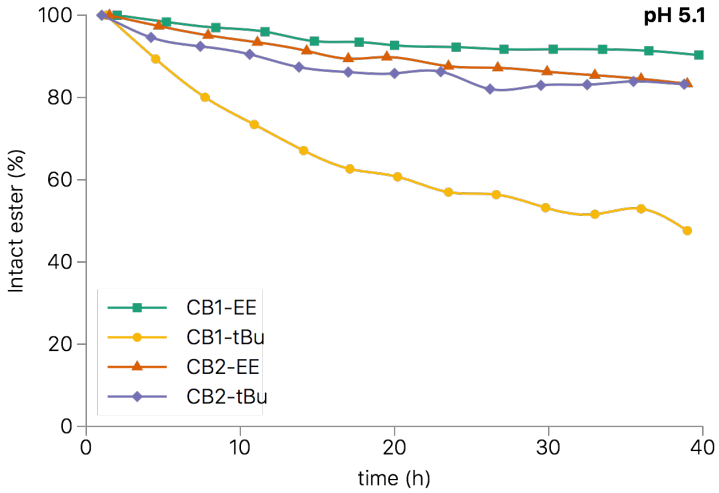

Figure 2.9 – Hydrolysis rates of CBMA-3°-ester monomers at pH 5.1, representative of lowest endosomal pH.

be modified to confer ester stability while maintaining other desirable functions, such as an optimal buffering range. It is apparent that both types of molecular design variations, the ester size and amine–ester ASL, contribute to the stability of these esters. The protonation state of the amines (which is dependent on ASL) may thus play a role. While this could explain the ester stability difference at physiological pH between CBMA-1-3°-EE (de-

protonated amine) and CBMA-2-3°-EE (protonated amine), a larger library of monomers is needed to support this hypothesis. Overly rapid hydrolysis at any relevant pH may sacrifice polyplex stability. Of the two most stable monomers, CBMA-1-3°-EE features a more suitable pKa for endosomal buffering. The hydrolytic product of ethyl esters, ethanol, also is of lowest toxicity.[76] These insights could assist with further platform development.

PCBMA-3°-ester copolymers were used to mediate luciferase expression in COS-7 cells, and the polymer toxicity was evaluated. As our previous work found 3:1 to be the optimal tertiary to quaternary amine ratio in PCB side chains, all polymers were generated with this monomer ratio in the reaction mixture. RAFT polymerization resulted in the generation of well-controlled molecular weights for each polymer, but increased MW beyond 10 kDa (up to 40 kDa) did not result in a statistically significant transfection increase. Therefore, 10 kDa polymers were used to control for this parameter. A nitrogen/phosphorus (N/P) ratio of 20 was found to result in optimal expression for all PCB-based polymers, while N/P ratios of 5 and 10 were used for the 25 kDa bPEI positive control. Copolymers based on the four tertiary CB-esters were all able to mediate transfection without any apparent cytotoxicity. Notably, the two copolymers featuring ethyl esters (PCBMA-1-3°-EE and PCBMA-2-3°-EE) resulted in expression about an order of magnitude higher than both those featuring tBu esters (PCBMA-1-3°-tBu and PCBMA-2-3°-tBu) and bPEI. Transfection and toxicity data are shown in Fig. 2.10. The higher stability of ethyl esters at the lower endosomal pH (PCBMA-2-3°-tBu) or both pH conditions (PCBMA-1-3°-EE) might play a role in their improved transfection, potentially by delaying any DNA release until the polyplexes escape from endosomes.

While more stable esters may complex DNA more efficiently and protect it for a longer time, substantial hydrolysis delay may bottleneck gene release. As the charge-switching behavior of PCB-esters is their key feature, the direct contribution of this charge switch to DNA release from a polyplex deserved further study. PCBMA-NBE, a photolabile *o*-nitrobenzyl ester of PCB, was developed to quantitatively study the charge-switching contribution to DNA release. Photoconversion of CBMA-NBE was verified with reverse-phase HPLC; after 1 h, degradation was complete.

We quantitatively measured DNA binding and release in PCBMA-NBE polyplexes with a PicoGreen assay, in which the fluorescence signal corresponds to the concentration of free (unbound) DNA over a wide range of magnitudes. An initial screening determined the minimum weight ratio of PCBMA-NBE and PCBMA-1-EE required to condense nearly all

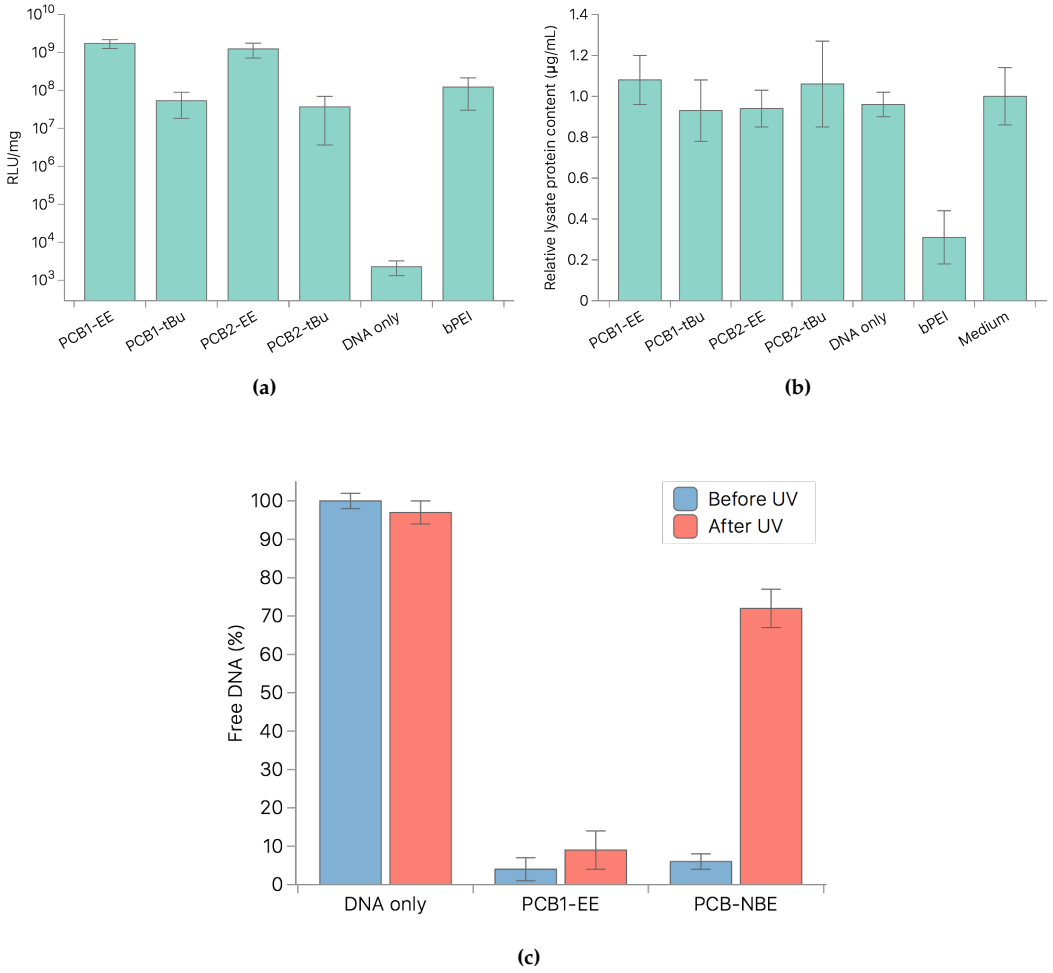

Figure 2.10 – a) Luciferase expression in COS-7 cells mediated by each tertiary copolymer variation. **b)** Relative toxicity, determined by BCA assay of µg protein content per mL cell lysate, normalized to medium only. **c)** DNA release from PCBMA-NBE polyplexes upon photodegradation of *o*-nitrobenzyl groups.

DNA (over 95%) was 5:1. As shown in Fig. 2.10c, both PCBMA-1-EE and PCBMA-NBE at this ratio complexed nearly all the DNA in each sample, quenching fluorescence. A 365 nm wavelength UV lamp was held directly above each polyplex sample for 1 h. This wavelength was chosen because it is least harmful to cells but still catalyzes degradation of the nitrobenzyl ester. The released DNA in these irradiated samples bound to the fluorescent dye, restoring fluorescence. Photoinitiated ester degradation released 72±5% of the DNA from the PCBMA-NBE polyplexes as separation of the ester converted them to zwitterionic PCB. The non-photosensitive PCBMA-1-EE released a statistically insignificant amount under the same conditions, as expected based on its hydrolytic profile. Previously, the post-

degradation form of PCB esters have been simply shown not to condense DNA due to their zwitterionic nature. Here, this photolabile polymer shows that the charge-switching step plays the key role in releasing DNA from an entangled polyplex, which is vital for transfection. This result supports one of the key benefits of the PCB-ester system: since tunable hydrolysis or photoresponsive "smart" ester degradation is the primary driver of DNA release, strong initial binding need not bottleneck eventual polyplex dissociation. Thus, unlike many other platforms, PCB-esters do not need to establish a fragile balance between DNA binding and release, but these parameters can be engineered individually.

2.5 Conclusions

This work demonstrates how rational molecular design can tune the functionality of PCB-esters and add "smart" responsiveness to environmental stimuli. A small library of CB-esters was designed, synthesized, polymerized and characterized to study the role of small modifications on the platform's buffering and hydrolytic characteristics. A methyl spacing (ASL=1) the charged groups was found to shift the pKa of the tertiary amine into the optimal endosomal buffering range. Ester hydrolysis converts this polymer from cationic (DNA binding) to zwitterionic (DNA releasing) form, while enabling nontoxicity. CBMA-1-EE was most stable at both physiological and endosomal pH, while possessing the highest buffering capacity. A copolymer dominated by the CBMA-2-EE monomer mediated transfection an order of magnitude better than bPEI, with no toxicity. To further study how the charge-switching feature affects polymer binding with DNA in polyplexes, a photolabile *o*-nitrobenzyl ester of PCB (PCBMA-NBE) was developed to allow rapid and externally controlled hydrolysis. Quantitative PicoGreen DNA binding assays demonstrated that photo-initiated ester degradation precipitates rapid release of approximately 72% of complexed DNA from PCBMA-NBE polyplexes. Further work will expand the library of ASL-1 non-toxic PCB-esters, and study the role of enzyme-catalyzed hydrolysis.

Chapter 3

POLYMER BACKBONE CHEMISTRY FOR DRUG DELIVERY

3.1 Chapter overview

Polymeric nanoparticles and polymer-protein conjugates represent some of the most promising and actively-developed areas of drug delivery. Almost any desired attribute—biodegradability, size, surface charge, ligand conjugation, stimuli-responsiveness, theranostic capability, or others—can be integrated into polymers through rational design or combinatorial optimization. Polycarboxybetaine is especially interesting as a potentially universal platform for nanocarrier design and protein conjugation. It has proven very successful in recent years as a hydrophilic shell for nanoparticles. PCB-coated nanoparticles exhibit prolonged circulation times, slowed MPS clearance and and do not elicit immunogenicity.[77] It has also demonstrated surprising utility in practical use, simplifying often-overlooked production issues by enhancing diblock self-assembly and preventing aggregation upon freeze-drying.[34] These benefits have been attributed to its "super-hydrophilicity" that few other materials can match. Similarly, proteins conjugated to PCB[40,41] or encapsulated in PCB nanogels[8,42] see their circulation half-lives enhanced, stability heightened and opsonization reduced or eliminated—all without a significant reduction in bioactivity. This positions PCB modification of biologics as a promising alternative to PEGylation.

In this chapter, a new polymerization strategy will combine the hydrophilicity advantages of current PCB polymers with advantages of more flexible and degradable biomaterials. These step-growth polymers change the distribution of zwitterionic CB moieties and move the cationic amine centers to the backbone, while incorporating labile esters, stable amides or thioethers between each zwitterionic group. In this way, drug delivery applications—particularly protein conjugation where degradability and increased hydrodynamic volume is desirable—will be enhanced by this versatile new class of polyzwitterions.

3.2 *Introduction*

Current zwitterionic polymers feature a backbone/side-chain design, which is also common among other engineered biomaterials. This enables researchers to design and synthesize homopolymers and copolymers or various linear and branched architectures tailored for biological and engineering applications. Chain-growth polymerization techniques—including ATRP, RAFT, and photopolymerization—are now routinely used to generate ionic, nonionic and zwitterionic polymers. Structures of selected polymeric biomaterials with acrylic backbones and functional side chains are shown in Fig. 3.1. Those in the top row (a-d) are examples of popular zwitterionic polymers, while the bottom row shows poly(NIPAM) (e) and poly(HEMA) (f), examples of non-ionic acrylic polymers, as well as PLGA (g) and PEG (h), non-ionic linear polymers typically formed through polycondensation reactions.

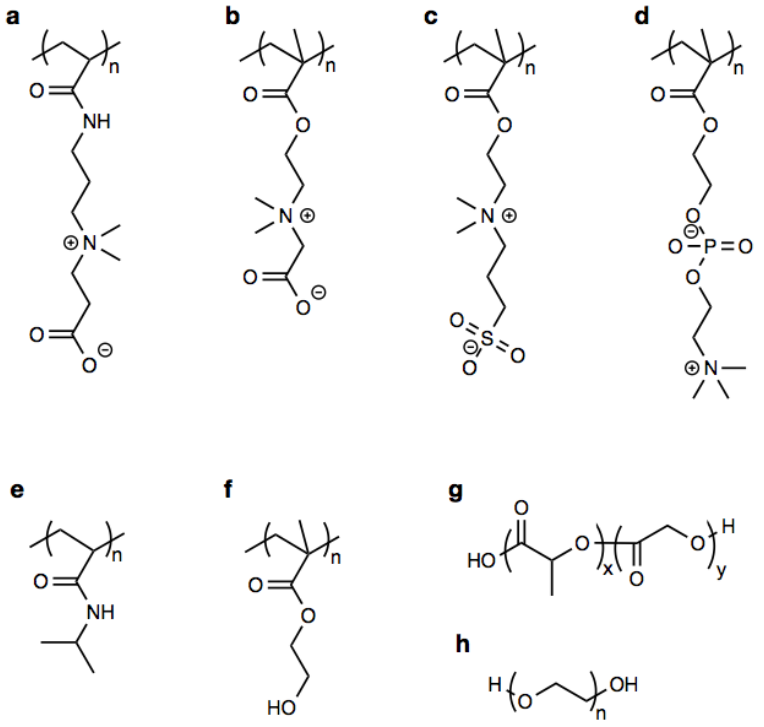

Figure 3.1 – Selected zwitterionic and non-ionic biomaterials. Top: zwitterionic polymers **a)** poly(carboxybetaine acrylamide) (pCBAA) **b)** poly(carboxybetaine methacrylate) (pCBMA) **c)** poly(sulfobetaine methacrylate) (pSBMA) **d)** poly(methacryloyloxyethyl phosphorylcholine) (MPC). **Bottom:** nonionic polymers **e)** poly(n-isopropyl acrylamide) (pNIPAM) and **f)** poly(hydroxyethylmethacrylate) (pHEMA).

As shown in Fig. 3.1, these zwitterionic polyacrylamides (e.g., PCBAA) and polymethacrylates (e.g., PCBMA, PSBMA, and MPC) share backbones with several other polymeric biomaterials, such as PNIPAM and PHEMA. However, polymers such as PEG and PLGA feature a markedly different structure—their structural backbone and defining functionality are one and the same. In the case of PEG, its simple linear polyether structure allows it to occupy a relatively large hydrodynamic volume for a given molecular weight.[78,79] This feature is one of the mechanisms by which PEGylation improves the circulation time of small proteins. Likewise, the hydrolytically degradable polyester backbone of PLGA enables it to be metabolized completely, which has led to many commercially successful PLGA-based drug delivery platforms.[80–82]

Inspired by simple structure-function relationships of flexible PEG and biodegradable PLGA, we propose a new class of "linear" polycarboxybetaines, containing charged groups directly along or adjacent to the backbone. As with PCBAA and PCBMA, the plentiful carboxylates enable robust functionalization. Uniquely, we expect the structure of linear PCBs to give them greater flexibility and hydrodynamic volume than acrylic-backbone PCBs for a given molecular weight. In one variation, labile backbone esters allow complete hydrolytic degradation. Thus, we hypothesize linear PCBs conjugated to therapeutic proteins will extend conjugate circulation times beyond that of comparable PEG-protein and PCBAA-protein conjugates, as they combine the key benefits of both materials for protein modification.

To realize such a polymer, we explored polymerization strategies beyond chain-growth radical polymerization. Two classes of polymers were notable as templates because of their broad tunability and amine-containing backbones: poly(β-amino esters) (PBAEs) and polyamidoamines (PAAs). The synthesis methods and generalized structures of PBAEs and PAAs are very similar.[83,84]

Fig. 3.2 shows examples of typical monomers and synthesis strategies. Both types of polymers contain tertiary amines in their main backbone chain, and are formed in a step-growth mechanism through repeated Michael addition reactions. Their main difference is the presence of hydrolytically labile esters or more stable amides in their main chain. PBAEs (Fig. 3.2a) are typically formed through the polyaddition of equimolar amounts of diacrylate monomers and either primary or bis(secondary) amine monomers; numerous choices for each are commercially available, and large libraries of PBAEs were synthesized combinatorially in the mid-2000s by the Langer and Andersen labs at MIT and optimized for nu-

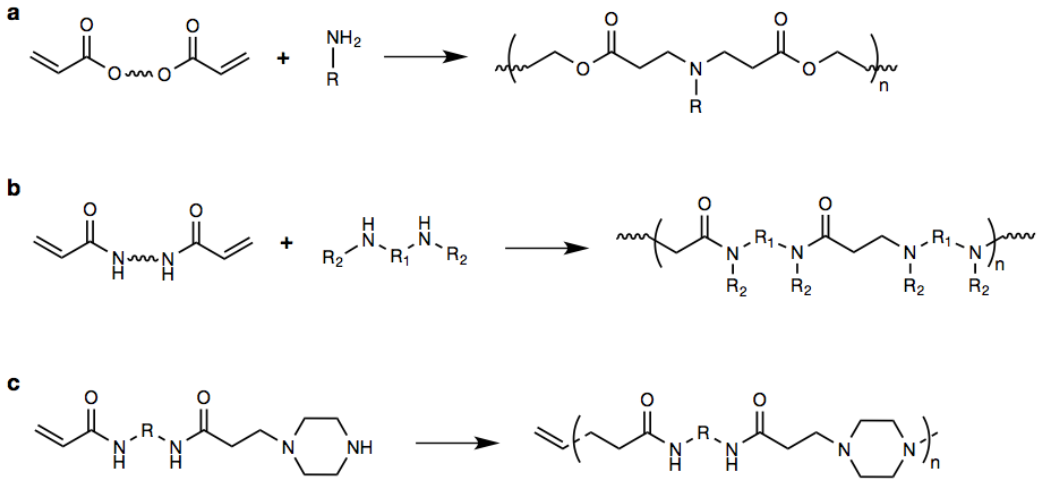

Figure 3.2 – Schematic of representative PBAEs and PAAs, and a heterodifunctional PAA. **a)** poly(β-amino ester) (PBAE) using a primary amine monomer. **b)** poly(amidoamine) (PAA), using a bis(secondary) amine monomer. **c)** Heterodifunctional PAA formed from one monomer.

cleic acid complexation and delivery.[22,75] Similarly, PAAs (Fig. 3.2b) are formed through the polyaddition of bisacrylamides to primary or bis(secondary) amines, and have been developed since the 1970s primarily by Ferruti and coworkers at the University of Milan, Italy[85–87] Notably, poly(amidoamine) dendrimers (typically referred to as PAMAM dendrimers) have a similar structure to linear polyamidoamines, though they are branched. The synthesis of PAMAM dendrimers involves iterative steps to reach higher generations, whereas linear PAAs are synthesized continuously in one step.

As PBAE structures were developed as a gene delivery platform, amino alcohols represent the most commonly used amine monomers; several variations of pH-responsive, weakly cationic PBAEs with alcohol side chains have demonstrated excellent efficacy as nonviral gene vectors. No zwitterionic PBAEs or quasi-zwitterionic PBAEs have been reported. On the other hand, PAAs have seen decades of study from a polymer chemistry perspective, and been tested in widely varying applications as biomaterials and otherwise. Quasi-zwitterionic or amphoteric poly(amidoamino acids) have been sporadically reported by Ferruti et al over the past 30 years, both for their metal-ion-chelating ability and potential biomedical applications.[88,89] Insight from the synthesis of amphoteric poly(amidoamino acids) has proven particularly valuable in our development of zwitterionic polymers formed through similar mechanisms. Specifically, Ferruti et al recently first reported PAAs with het-

Type	Analogous to?	Degradable?
PACB	Poly(amido amine)	No
PECB	Poly(β-amino ester)	Yes
PSCB	Polysulfide	Either

Table 3.1 – Variations of linear polycarboxybetaines

erodifunctional terminating groups,[90] formed from a single 'A-B'-type monomer (Fig. 3.2c). Most polymers produced via Michael polyaddition have utilized two symmetrical monomers, 'A-A' and 'B-B', producing matching or random end groups depending on reaction stoichiometry. This proves problematic for bioconjugation applications, as it results in many polymer chains containing either zero or two terminal groups amenable to a chosen conjugation reaction. This lowers conjugation efficiency, reduces predictability, and results in "looped" polymers conjugated at both ends. Heterodifunctional polymers have reliably asymmetrical terminating groups, enabling more reliable surface grafting, bioconjugation and other post-polymerization reactions.

In this work, we propose a new class of heterodifunctional zwitterionic polymers and three constituent variations, each with the cationic amine moiety contained in the functional polymer backbone. The basic illustration to the right shows the key difference between current polyzwitterions and these new "linear" polyzwitterions, and the key differences between each type is summarized in Table 3.1.

All three types are formed through step-growth, Michael-type polyaddition reactions. The first type is a PAA-based, denoted poly(amidocarboxybetaine) (PACB), containing alternating carboxybetaine and hydrolytically stable amides in the main chain. We expect PACB to maintain a stable molecular weight in physiological conditions and be especially useful for applications necessitating long-term stability, circulation, or implantation. The second type is PBAE-based, though also derived from a single 'A-B'-type monomer. We denote this type poly(estercarboxybetaine) (PECB), and it contains alternating carboxybetaine and hydrolytically labile esters along its main chain. This biodegradable zwitterionic polymer may be optimal in short-term drug and gene delivery formulations—a hydrophilic analogue to hydrophobic polyesters like PLGA and amphiphilic ones like most PBAEs. The third type, poly(sulfidecarboxybetaine) (PSCB), is derived from a zwitterionic monomer that contains

a thiol group in addition to the betaine functionality. This thiol is designed to participate in the polyaddition reaction in place of the cationic ammonium, which may enhance the reaction efficiency and simplify post-polymerization modification steps.[91–93]

3.3 Methods

3.3.1 Synthesis of PACB

A schematic outlining the synthesis of poly(aminocarboxybetaine) is shown in Fig. 3.3. Briefly, aminoethyl methacrylamide is added to tert-butyl 3-bromoproionate in THF to form an acrylamide monomer containing a secondary amine and tBu-protected carboxylate (Fig. 3.3a). Then, the ester is removed under acidic conditions using TFA (Fig. 3.3b) and the monomer is placed in a basic aqueous solution (pH=9, adjusted with triethylamine) to initiate Michael-type polyaddition (Fig. 3.3c). The reaction is allowed to proceed at room temperature for up to one week. Finally, iodomethane is added to quaternize the tertiary backbone amines and produce a zwitterionic PACB (Fig. 3.3d). Polymers are purified by dialysis.

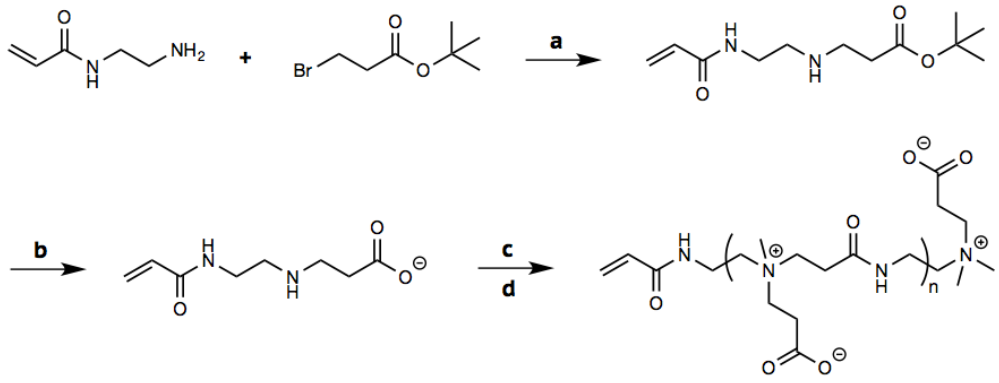

Figure 3.3 – Scheme showing typical synthesis of heterodifunctional zwitterionic PACB. a) 'A-B'-type monomer syntheized in one step reaction. **b)** Monomer deprotection (can also occur following polymerization). **c)** Polymerization through Michael-type polyaddition in mild aqueous basic conditions. Alternate conditions and catalysts are also under investigation. **d)** Methylation of tertiary amines in backbone for truly zwitterionic polymer.

3.3.2 Synthesis of PECB

A schematic outlining the synthesis of poly(estercarboxybetaine) is shown in Fig. 3.4. Briefly, aminoethyl methacrylate is added to tert-butyl 3-bromoproionate in DCM to form an acry-

late monomer containing a secondary amine and tBu-protected carboxylate (Fig. 3.4a). Then, the ester is removed under acidic conditions using TFA (Fig. 3.4b), which were chosen to avoid degrading the acrylate ester. The monomer is placed in triethylamine to initiate Michael-type polyaddition (Fig. 3.4c). Reaction is allowed to proceed at room temperature for up to one week. Finally, iodomethane is added to quaternize the tertiary backbone amines and produce a zwitterionic PECB (Fig. 3.3d). Polymers are purified by dialysis at 4°C. Synthesis procedures are substantially similar to PACB, with extra care taken not to hydrolyze the backbone esters prematurely.

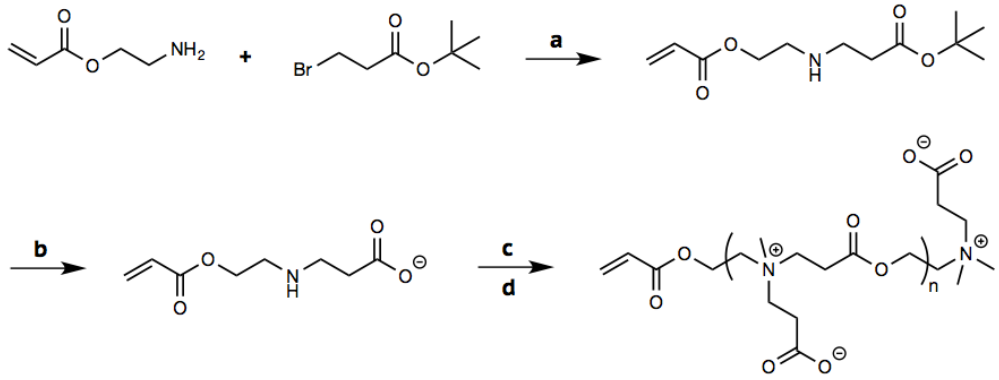

Figure 3.4 – Scheme showing typical synthesis of heterodifunctional zwitterionic PECB. a) 'A-B'-type monomer syntheized in one step reaction. **b)** Monomer deprotection in basic conditions. **c)** Polymerization through Michael-type polyaddition in triethylamine to avoid hydrolysis in aqueous solution. **d)** Methylation of tertiary amines in backbone.

3.3.3 Synthesis of PSCB

A schematic outlining the synthesis of poly(sulfidecarboxybetaine) is shown in Fig. 3.5. This synthesis differs markedly from PACB and PECB, and care is taken throughout not to oxidize thiol groups so as to avoid disulfide formation. In part **I**, a tBu-protected acrylate monomer containing a tertiary amine is formed (Fig. 3.5, **A**). In part II, a trityl-protected, bromoacetamide thiol component is produced (Fig. 3.5, **B**). Finally, these two molecules are reacted in acetonitrile at 70 °C to generate the trityl-protected monomer used to produce PSCB. Next, this monomer is deprotected and polymerized in one pot to minimize the chance of disulfide formation after deprotection. To deprotect the thiol, triethylsilane and TFA are added in a 1:2 volume ratio to the protected monomer dissolved in degassed DCM with a stir bar. The reaction is vented with a needle and stirred rapidly for 15 min until color

change indicates the deprotection is complete. The triethylsilane acts as a scavenger to prevent reprotection of the thiol. The solution is once again degassed and polymerization is initiated by adding TEA (basic catalyst) or hexylamine (nucleophilic catalyst). Polymerization reaction is stirred for 48 h and watched for color or viscosity changes. Finally, product is purified through repeated precipitation and dialysis.

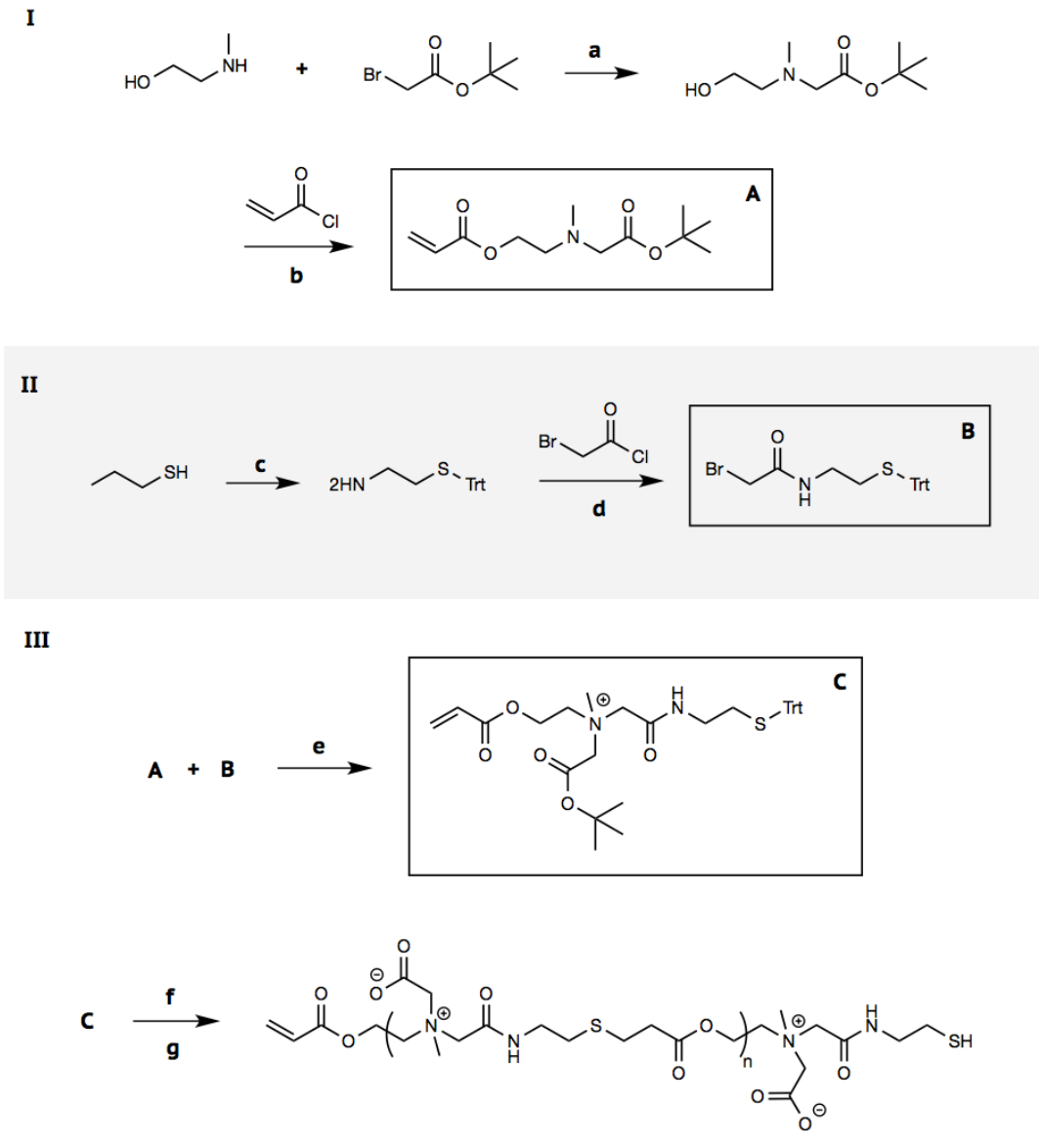

Figure 3.5 – Synthesis of CB-SH monomer and PSCB

3.3.4 Polymer characterization

PACB, PECB, and PSCB molecular weights were first analyzed for their molecular weight using aqueous gel permeation chromatography (GPC) (Agilent 1200 Separations Module) fitted with a Wyatt refractive index detector and a Waters Ultrahydrogel 250 column. The buffer solution (0.05 M Tris buffer + 1.0 M NaCl) was used as the eluent with a flow rate of 0.5 mL/min at 35°C. All samples were filtered through 0.2 micron PTFE filters prior to injection. The system was calibrated with narrow molecular weight polyethylene oxide standards.

Matrix-assisted laser desorption/ionization time-of-flight mass spectrometry (MALDI-TOF MS) spectra of crude and purified samples were obtained in both linear and reflected modes. Each polymer was mixed with DHB or CHCA matrix and spotted on a steel plate, then allowed to dry at room temperature. Using a Bruker Autoflex II, mass spectra were obtained, with the laser power adjusted for each sample and dependent on matrix and polymer concentration. While polymer characterization via MALDI-TOF is less common than GPC, this method is growing in popularity due to improvements in spectrometer sensitivity.[94]

3.4 Results and discussion

While step-growth polymerization can present some challenges in obtaining products of low polydispersity and high molecular weight, it enables fundamentally different structures and functionality than typical chain-growth, radical-mediated strategies. For the majority of polymerizations, both GPC and MALDI-TOF analysis found predominantly oligomers of 3-15 monomers in length.

3.4.1 PACB synthesis and characterization

While this variation initially appeared to be the most straightforward, we have experienced some challenges in its synthesis. First, the secondary amine critical to the polyaddition reaction is the same moiety destined to be the cationic charge in the final polymer. While this results in one of the most structurally simple forms of amidoamine-backbone PCB, it also means that molecular modifications of and near the zwitterions can also affect the polymerization kinetics. This may be the biggest challenge in obtaining high molecular weight polymers of this class. Our previous work has demonstrated the hydration and nonfouling character of polyzwitterions to decrease rapidly with a three-or-more carbon length distance between the charged groups.[32] This suggests that for any polymer architecture, there is an apparent ceiling on the zwitterionic moiety spacing before key hydration properties are lost.

Sample	Solvent	Conditions	Mn (kDa)
PACB-1	water/CaCl2, pH 8.5 (NaOH)	25°C, 6 d	1.6
PACB-2	water, pH 8.5 (TEA)	40 °C, 5 d	8.5
PACB-3	water, pH 9 (NaOH)	25 °C, 11 d	4.1

Table 3.2 – GPC characterization of PACB synthesis

At the same time, work by Ferruti has reported extremely slow reaction rates for symmetrical PAAs using alpha amino acids such as glycine,[88] but reasonable rates for species such as β-alanine. It is with these constraints we chose the ethyl spacer when designing the PACB and PECB monomers.

Based on GPC characterization, we achieved slow but progressive polymerization of PACB in aqueous basic conditions. A summary of the molecular weights achieved as determine by GPC comparison with PEG standards is shown in Table 3.2. In addition, we used MALDI-TOF to characterize PACB polymers. As shown in Fig. 3.7, the signal decreases substantially as the molecular weight increases, though the distance between major peaks indicates short polymers (or long oligomers) were formed. We are conducting further tests to determine if this is an accurate characterization method for this polymer.

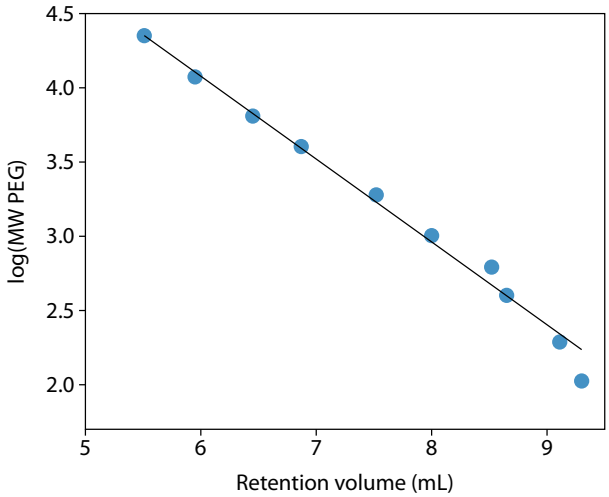

Figure 3.6 – PEG MW standard curve used for GPC characterization of PACB and PECB polymers

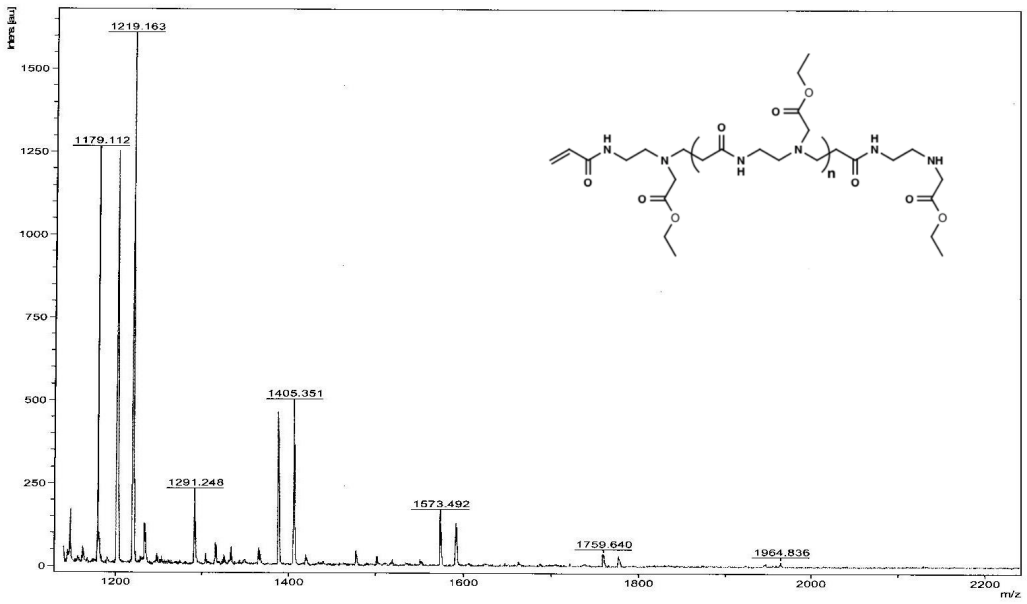

Figure 3.7 – MALDI-TOF mass spectrum of PACB polymer/oligomers

3.4.2 PSCB synthesis and characterization

The PSCB variation of this class is advantageous in that neither the zwitterionic moiety (nor precursors to it) are involved in the polymerization reaction. This makes it easier to adjust the structure of each part to optimize the overall characteristics of the polymer. Also, in addition to Michael-type polyaddition synthesis, the acrylic moiety could be substituted with an alkene to be more reactive under thiol-ene "click" conditions, such as norbornene.[95–98] MALDI mass spectra of the protected CB-SH monomer and resulting PSCB polymer are shown in Figs. 3.8 and 3.9.

3.4.3 Use of nucleophilic catalysts

While mild basic conditions are typically used for polyaddition-based synthesis of PBAEs and PAAs, nucleophilic catalysis has recently been shown to improve reaction efficiency, in some cases considerably. Relevant catalysts in this class include hexylamine and triphenylphosphine.[93] One issue with any type of step-growth polymerization as compared to chain-growth methods is only low-molecular weight products are obtained until very high conversion is reached. This has inspired us to further tune the PSCB strategy to utilize thiol-ene photopolymerization, which can be more rapid than Michael additions. For this, we are in the process of designing a monomer incorporating a norbornene group in addition to the

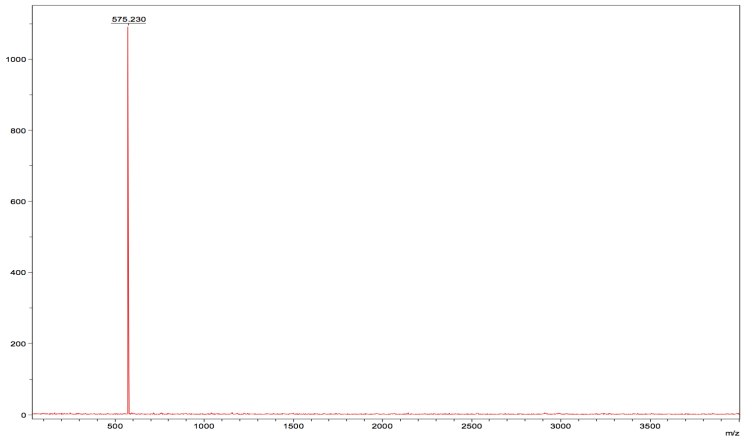

Figure 3.8 – The protected CB-SH monomer was easily detected with MALDI-TOF mass spectroscopy, suggesting this may be the best method to analyze the polymer.

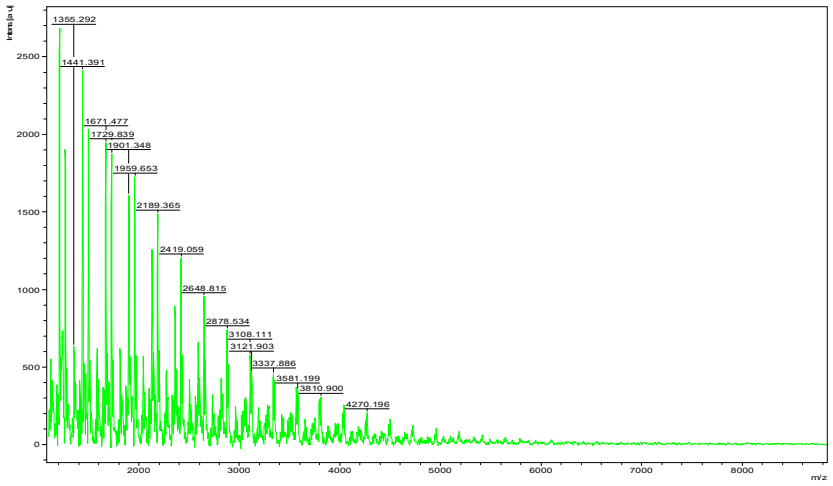

Figure 3.9 – PSCB polymer as characterized by MALDI-TOF MS.

thiol, as this group has been reported the most reactive in these reactions.

3.4.4 Protein conjugation

In future work, we plan to conjugate these polymers to model enzyme β-lactamase. This is a naturally stable and well-characterized protein produced by E. coli, and many surface amines are available as conjugation sites. In one potential conjugation strategy, a crosslinker

will be attached to the enzyme as reported previously.[40] The modified enzyme will be characterized with MALDI-TOF, which was shown to work well in our recent work reporting amino acid conjugation.[18] Enzymatic stability will then be assayed through temperature, salt, and chemical denaturant challenges, and the remaining activity measured with nitrocefin color change.

3.5 Conclusions

We have designed a new polymerization strategy aiming to combine the hydrophilicity of current zwitterionic polymers with advantages of more flexible and degradable biomaterials. These step-growth change the spacing of CB moieties and move the amines to the backbone, while incorporating labile esters, stable amides or thioethers between each zwitterionic group. While promising, the majority of products obtained were of insufficient molecular weight for protein conjugation.

Chapter 4

HYDROGEL CHEMISTRY FOR *IN SITU* CELL ENCAPSULATION

4.1 Chapter overview

In this chapter, I present cytocompatible and degradable thiol-based crosslinking chemistries aimed to enable *in situ*-forming PCBAA hydrogels for stem cell expansion. First, PCBAA star polymers (spCB) were synthesized found to be cytocompatible. These star polymers were end-modified with either thiol (spCB-SH) or disulfide pyridine (spCB-DP) groups to enable cytocompatible *in situ* gelation via a thiol-disulfide exchange reaction. Several cell lines including mesenchymal stem cells were encapsulated in this hydrogel, and demonstrated high expansion rates of 25–30-fold in two weeks. Through analyzing characteristic biomarkers and gene expression, we found spCB-expanded hMSCs to retain their multipotent phenotype and full differentiation potential. As most non-zwitterionic biomaterial platforms provide encapsulated cells with nonspecific interactions that trigger phenotype change and contribute to cellular senescence, this spCB platform is a useful 3D growth platform that avoids damaging encapsulation chemistries and difficult recovery procedures.

4.2 Introduction

As the clinical importance of cell-based therapies continues to grow, the ability to sufficiently and reliably expand cells *ex vivo* is proving to be a key challenge; cells frequently lose bioactivity and change their phenotype when expanded using typical culture platforms, which dramatically reduces their therapeutic value. As a large and homogeneous population of mesenchymal stem cells (hMSCs) is needed for their clinical use, the limited number of cells obtained from a primary culture or patient must typically be expanded through multiple passages. Cells are routinely cultured on 2D hydrophobic surfaces or in stirred bioreactors, but these methods expose cells to many nonspecific material interactions, promote aggregation, and exhibit progressive losses in bioactivity.[99] Increasing evidence highlights the importance of mechanical signals or environmental interactions to the long-term fate of cultured cells; these signals can trigger phenotype change or differentiation independent of biochemical cues.[26] Maintaining stem cell multi- or pluripotency during *in vitro* expan-

sion is particularly important and challenging, deeply affecting the study and application of these sensitive cells.

A promising way to tackle this long-standing problem is culturing cells in a biomimetic 3D niche that more accurately models their *in vivo* extracellular matrix.[26] However, very few biomaterials are suitable for 3D culture platforms due to concerns about their long-term biocompatibility and immunogenic potential. Hydrophilic polymers are desirable to minimize unwanted interactions, and many cell scaffolds have thus been based on the perennially popular poly(ethylene glycol) (PEG).[100] However, PEG is actually amphiphilic instead of purely hydrophilic as generally assumed, and is under increasing scrutiny as reports of its immunogenicity suggest it is not as bio-inert as originally thought. Among next-generation biomaterials that improve upon PEG's weaknesses, zwitterionic polymers, and particularly poly(carboxybetaine) (PCB), are unique for several reasons. A hydrogel matrix constructed exclusively from PCB will provide zero nonspecific signals to encapsulated cells—we recently found this unique characteristic to result in mesenchymal stem cells temporarily 'losing' their ability to differentiate inside pure PCB hydrogels.[44] The carboxyl group in each monomer side chain can be functionalized using straightforward EDC/NHS chemistry to immobilize biomolecules with a high efficiency and capacity, and unreacted groups can be easily restored to their original nonfouling state. In one example, the important cellular recognition and adhesion peptide RGD can be functionalized to PCB in this way while maintaining the polymer's overall zwitterionic character. These combined attributes make PCB particularly amenable to specifically targeting desired biomolecules or promoting integrin mediated cellular adhesion while remaining highly resistant to any other non-specific interactions. In contrast, PEG and its derivatives are relatively difficult to functionalize, and unreacted activated carboxylate or amine groups still carry charge and remain as fouling moieties after this process.

We have typically used free radical polymerization to produce pCB hydrogels in our previous work.[101] This often makes dialysis or prolonged soaking necessary to remove all unreacted monomers and initiators, and if cells are encapsulated during gelation the free radicals generated can cause irreversible cellular damage and compromise their viability and function. This damage is especially concerning for sensitive and clinically valuable cell lines such as stem cells. To avoid free radical exposure, injectable or thermoresponsive hydrogels incorporating zwitterionic components have been reported, that can gel under physiological conditions without radical-mediated chemical crosslinking.[102] However, all

of these "injectable" hydrogels have been based on copolymers with zwitterionic and hydrophobic portions; if used as a stem cell scaffold, the hydrophobic content in these copolymers will trigger differentiation as we have demonstrated. A strategy for forming a purely zwitterionic hydrogel under physiological conditions is highly desirable for this reason.

In the strategy presented here, we synthesized four-arm, star-shaped PCB (spCB), and modified their termini with complementary reactive moieties—either thiols (spCB-SH) or disulfide pyridine groups (spCB-DP). These two functionalized star polymers can be simply mixed to spontaneously form a disulfide-crosslinked, bioreducible and fully zwitterionic hydrogel. As this gelation process generates no cytotoxic species or free radicals, we applied this platform to cell encapsulation and expansion. We hypothesized the purely zwitterionic and degradable spCB network may present an effective matrix for the expansion of therapeutic cell lines, while preserving their bioactivity and phenotype. To test the suitability of spCB hydrogels for this purpose, we encapsulated and expanded several cell lines, including human mesenchymal stem cells (hMSCs). We then used immunofluorescent sorting, histological marker staining and mRNA expression to evaluate their expansion rates, phenotype, multipotency and differentiation potential.

4.3 Methods

4.3.1 Zwitterionic star polymer synthesis

PCBAA star polymers were synthesized using atom-transfer radical polymerization (ATRP) as previously reported and briefly summarized in Figs. 4.1 and 4.2. In brief, appropriate amounts of carboxybetaine acrylamide (CBAA), 2,2'-bipyridine (BPY) catalyst, and tetrafunctional initiator pentaerythritol tetrakis(2-bromoisobutyrate) were placed in a 10 mL reaction tube. The mixture was subjected to three freeze-pump-thaw cycles, and equilibrated at room temperature for 20 min before water and methanol were added at a 1:1 ratio. The polymerization reaction was stirred at room temperature for 8 h, after which the polymer product was treated with alumina, recovered, and purified by precipitation twice into acetone. Desired molecular weights of the polymers were tuned by adjusting the stoichiometric ratio between the monomer and the initiator. Polymers were then partially functionalized with cyclic RGD to mediate cell attachment via an EDC/NHS reaction, using conditions previously reported. Star-shaped pCBAA (spCB) samples with targeted molecular weights of 5, 20, 50, 80 and 120 kDa were synthesized.

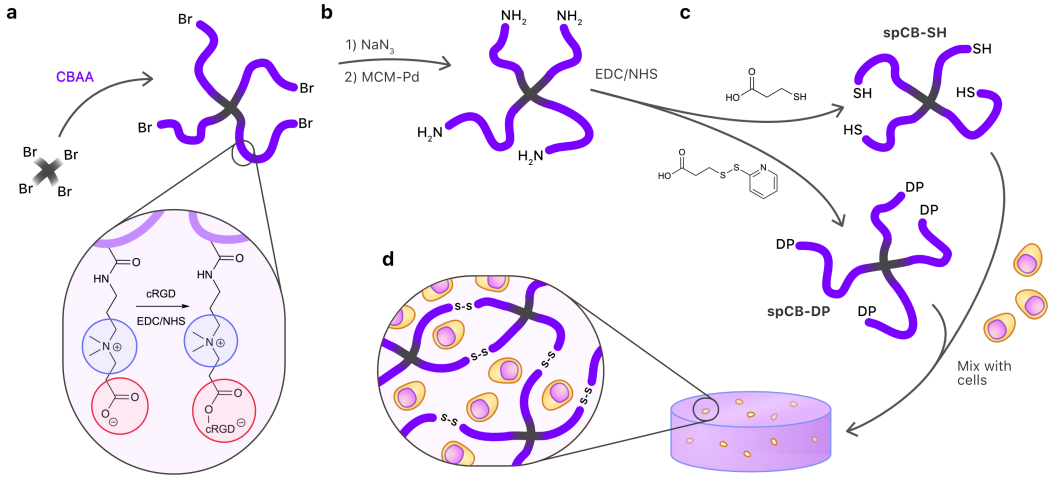

Figure 4.1 – Star-shaped PCB (spCB) strategy for cytocompatible cell encapsulation. **a)** Br-terminated spCB synthesized with ATRP at various molecular weights, and functionalized with cRGD to mediate cell attachment. **b)** End groups modified to primary amine groups to enable EDC/NHS functionalization with complementary thiol and disulfide pyridine groups. **c)** Batches of spCB were functionalized with each terminal group and solutions of each were mixed with cells. **d)** Complementary spCB termini react in situ to form a soft matrix for cell expansion.

4.3.2 Star polymer functionalization

Purified spCB polymers were first end-functionalized with azide (N_3) groups by reacting 2 g of each polymer with 50 mg of sodium azide for 48 h in water at room temperature. N_3-functionalized polymers were purified using dialysis and lyophilized. Azide groups were then reduced to NH_2 using a MCM-Silylamine Pd(II) Complex, which was prepared as previously reported. Here, 1.5 g of azide-terminated spCB and 10 mg of MCM-Silylamine Pd(II) Complex were dissolved in 10 mL of methanol and reacted for 3 h at room temperature, after which the complex was removed by filtration and the polymer dried under vacuum. To functionalize spCB with thiol (SH) or disulfide pyridine (DP) groups, 3-Mercaptopropionic acid or 3-(2-Pyridyldithio) propanoic acid, respectively, were used. In brief, equimolar amounts of N-(3-Dimethylaminopropyl)-N'-ethylcarbodiimide hydrochloride (EDC) (Sigma) and N-Hydroxysuccinimide (NHS) (Sigma) were added an aqueous solution of 3-Mercaptopropionic acid or 3-(2-Pyridyldithio) propanoic acid. After incubation at 25°C for 1 h to activate the carboxylate group, 1 g of NH_2-terminated spCB was added to each activated reagent. The molar concentration of in the reaction solution was set at 100 µM. The reaction proceeded for 24 h at 25°C before purification via LC-MS. The efficiency of the reaction was also calculated by LC-MS (Yield 68%).

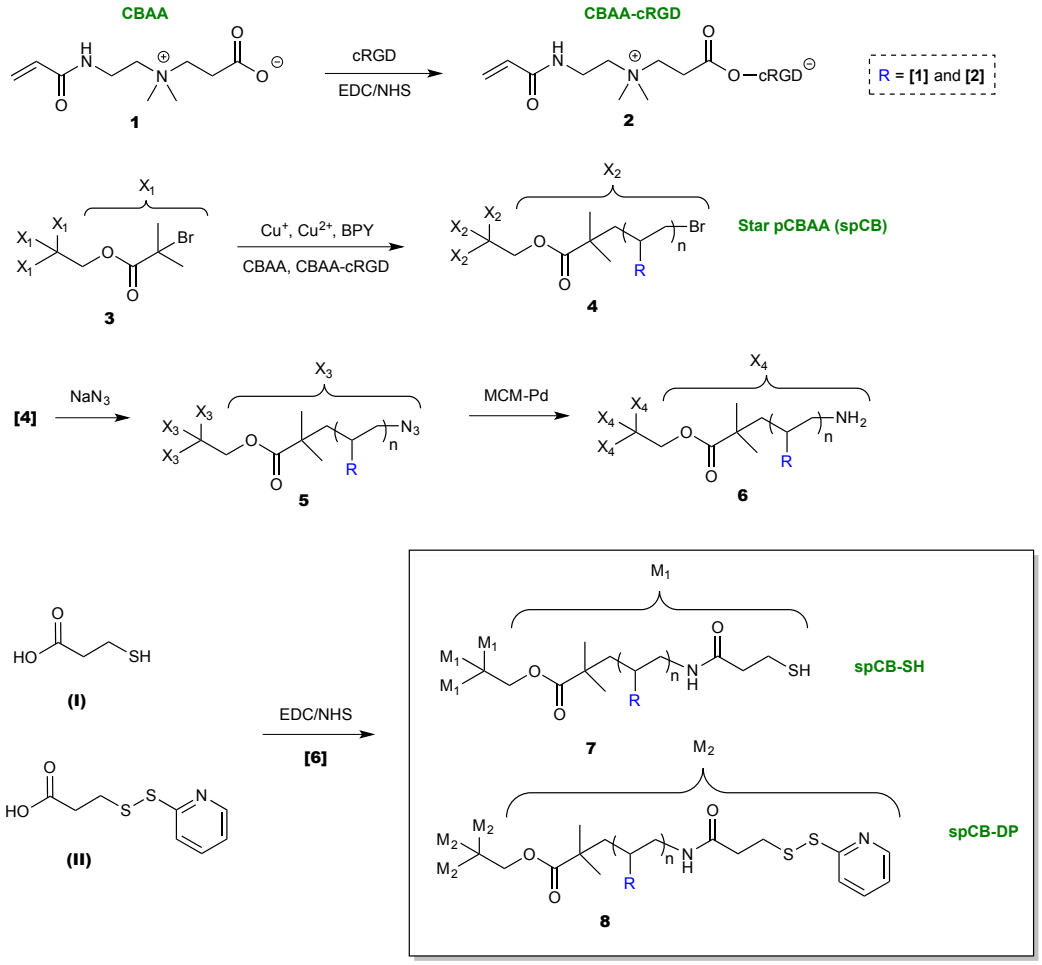

Figure 4.2 – sPCB synthesis and functionalization. CBAA monomer (**1**) was functionalized with cRGD (**2**) to mediate cell attachment. A tetrafunctional initiator (**3**) was used to initiate an ATRP reaction forming the star PCB polymers of various molecular weights (**4**). End groups were modified azides (5), after which azide groups were then reduced to NH_2 using a MCM-Silylamine Pd(II) Complex (**6**) Batches of spCB were functionalized with each terminal group (**I** and **II**) once again using EDC/NHS to produce spCB-SH (**7**) and spCB-DP (**8**).

4.3.3 Characterization and purification of spCB polymers

An Agilent 1200 LC 6520 Q-Tof MS system was employed to purify the functionalized star polymers and quantify the efficiency of the conjugation reactions. In brief, after the reaction, functionalized star polymer sample was injected. The chromatographic separation was performed in hydrophilic interaction chromatography (HILIC) mode on a SeQuant ZIC-cHILIC column (150 x 2.1 mm, 3.0 µm particle size, Merck KGaA). The flow rate was 0.500 mL/min,

auto-sampler temperature was kept at 4°C, the column compartment was set at 40°C, and total separation time for both ionization modes was 40 min. The mobile phase was composed of Solvents A (5 mM ammonium acetate in 90% H_2O/10% acetonitrile + 0.2% acetic acid) and B (5 mM ammonium acetate in 90% acetonitrile/10% H_2O + 0.2% acetic acid).

The Q-Tof mass spectrometer was equipped with an electrospray ionization (ESI) source. The instrument was controlled by an Agilent Mass Hunter Workstation (Agilent Technologies). The ESI voltage was set at 3800 volts. The source gas was N_2 (99.999% purity). The ion source conditions in positive mode were: drying gas = 10 L/min, nebulizer gas = 45 psi, temperature = 325°C. The extracted ion chromatography (EIC, 3-Mercaptopropionic acid m/z=106.14, 3-(2-Pyridyldithio) propanoic acid m/z=312.36) peaks were integrated using Agilent Mass Hunter Qualitative Analysis software (Agilent Technologies). The functionalized star polymers were purified by the LC system and obtained via lyophilization.

The functionalization efficiency (FA) was determined using:

$$FA = \frac{V_c - V_f}{V_c} * 100\%$$

where V_f is the integrated value of the free 3-Mercaptopropionic acid or 3-(2-Pyridyldithio) propanoic acid after the reaction and V_c is the integrated value of the free 3-Mercaptopropionic acid or 3-(2-Pyridyldithio) propanoic acid in the aqueous solutions in which no coupling agents (EDC or NHS) were added.

Molecular weights of the polymers were determined using aqueous gel permeation chromatography (GPC) (Waters 2695 Separations Module) fitted with a Waters 2414 refractive index detector and a Waters Ultrahydrogel 250 column (7.8 mm 300 mm). The buffer solution (0.05 M Tris buffer + 1.0 M NaCl) was used as the eluent with a flow rate of 0.5 mL/min at 35°C. All samples were filtered through 0.2 micron PTFE filters prior to injection. The system was calibrated with narrow molecular weight polyethylene oxide standards.

4.3.4 Cytotoxicity evaluation

The polymers were dissolved directly in the cell culture medium at 10 mg/mL. NIH-3T3, COS-7, HEK293 and hMSC cell lines (ATCC) were plated at 2 x 10^4 cells/mL in a 96-well tissue culture treated plate and incubated at 37°C in 5% CO2 and 100% relative humidity. After culture for 24 h, the culture medium was removed and 100 uL of monomer solution was added in each well. Fresh medium was used as a control. After the cells were exposed to the polymer-containing medium for how long, the medium was removed and the cells

were rinsed with PBS. An MTT assay was then used to evaluate cell viability after exposure to each spCB polymer. 100 uL of MTT solution (5 mg of MTT/mL serum-free DMEM) was added to each well and incubated for 4 h, then replaced with 100uL of DMSO per well. The optical absorbance of formazan production was measured at 570 nm (OD_{570}) and 630 nm (OD_{630}). The relative cell viability (RCV) was calculated using the following equation:

$$RCV = \frac{OD570_{treated} - OD630_{treated}}{OD570_{control} - OD630_{control}} * 100\%$$

4.3.5 Hydrogel preparation and characterization

Degradable spCB hydrogels were prepared via a disulfide exchange reaction between spCB-SH and spCB-DP. SpCB-SH was dissolved in 100 uL PBS to make a 5% (w/v) solution. Three amounts of spCB-DP (0.5, 1, and 2 mg) were added to the spCB-SH solution and mixed briefly to initiate gelation. Gelation was monitored by inverting the tubes until the gel solution stopped flowing.

Dynamic viscoelasticity of the spCB hydrogels was measured with a Kinexus Pro rheometer (Malvern) using parallel plates 40-mm in diameter and a plate-to-plate distance of 900 µm. The frequency-sweep spectra were recorded in a constant-strain (10%) mode over the frequency range of 0.1-100 rad/s at 25°C. The time-sweep spectra were recorded at a constant-strain (10%) mode and constant frequency of 10 rad/s over time at 25°C. The strain-sweep spectra were recorded in a constant frequency of 10 rad/s over the strain range of 0.01-10 at 25°C. The temperature dependence of the storage and loss moduli was determined by oscillatory shear deformation over a temperature range of 20°C to 50°C.

4.3.6 Cell encapsulation, expansion, and recovery

Four cell types (NIH3T3, COS-7, HEK293, and hMSC, all from ATCC) were encapsulated in the spCB hydrogels, all at seeding densities of $2x10^5$ cells/mL. To encapsulate cells, cells were suspended in their appropriate media and mixed with media aliquots containing spCB-SH and spCB-DP, with each star polymer at a final concentration of 5% (w/v) to allow gelation. The resulting hydrogels embedded with cells were incubated at 37°C in 5% CO_2 and 100% relative humidity to promote cell expansion. Immediately after encapsulation, selected cell-hydrogel constructs for each cell type were assayed for viability. For this viability test, constructs were stained with 1 mg/ml fluorescein diacetate (FDA) and 1 mg/ml propidium iodide (PI) for 30 min at 37°C in the dark. The samples were then washed with

a large amount of PBS and observed under a Nikon Eclipse TE2000-U flurorescence microscope. The initial viability was calculated as the number of live cells/the number of total cells*100(%).

After a specified number of days of culture (3, 5, 7, 9, 11, and 15), the cell-laden hydrogels were incubated with hydrogel-dissociation medium (cell medium containing 2 mM L-cysteine) at 37°C for 30 min, and cells were recovered upon hydrogel decomposition and then collected by centrifugation. Cells were stained with Trypan blue, and their viability and proliferation rate was calculated using a hemacytometer. The rate of cell expansion was also determined by staining for DNA and glycosaminoglcan (GAG) content in each hydrogel. After each chosen time point, cell-hydrogel constructs from each group (n=5) were recovered and dehydrated by lyophilization. The dried constructs were then crushed with a tissue grinder and digested in 1 mL of papainase for 15 h at 60°C. The DNA content (nanograms of DNA per milligram dry weight of the hydrogel) was determined by staining with Hoechst 33258 and measuring fluorescence (Ex 352 nm, Em 461 nm). The GAG content was determined by chondroitin sulfate using dimethylmethylene blue dye.

4.3.7 Mesenchymal stem cell differentiation

Multicolor analysis for progenitor and stem cell phenotyping was performed on a LSR II flow cytometer (Becton Dickinson). Cells were stained in staining media (HBSS supplemented with FBS [2%] and EDTA [2 mM]) at 4°C for 1 h with Alexa Fluor®647 anti-STRO-1 (Biolegend), FITC anti-ALCAM (AbD Serotec), then washed with staining media and analyzed. At least 10,000 events were acquired for each analysis.

To test gene expression of hMSCs cultured in spCB hydrogels, constructs were removed from culture media at specified time points and assayed with quantitative real-time PCR (qRT-PCR). The constructs were transferred to TRI Reagent (Sigma) in RNase-free test tubes and homogenized with a tissue homogenizer. Total RNA was extracted according to the manufacturer's instructions. Total RNA for each sample was quantified with a UV spectrophotometer and converted to cDNA using the QuantiTect Reverse Transcription Kit. After amplification using SYBR Green PCR Master mix (Qiagen), thermocycling was carried out in a solution with primers (Integrated DNA Technologies) and cDNA. PCR conditions were as follows: 15 s at 94°C, 30 s at 55°C, and 30 s at 72°C. Here, we used RNase-free DNase (Qiagen) to prevent genomic DNA contamination.

To test for differentiation of expanded hMSCs encapsulated in spCB hydrogels, hydro-

gel constructs were first cultured in basal medium for 3 days. Following this time point, the basal medium was replaced with bipotential differentiation medium to promote adipogenic and osteogenic differentiation of hMSCs. This medium contained: low glucose DMEM supplemented with 20% FBS and 1% penicillin/streptomycin (Invitrogen); an adipogenic supplement: 1 µM dexamethasone, 50 µM indomethacin (Sigma), 0.5 µM 3-isobutyl-1-methylxanthine (IBMX; Sigma) and 10 µg/mL human recombinant insulin (Invitrogen); and an osteogenic supplement: 10 mM β-glycerol phosphate (Sigma) and 50 µg/mL ascorbic acid (Sigma). Media changes were performed every 3 days. As a parallel control, a mixed adipogenic/osteogenic inductive media was made by combining commercially available osteogenic and adipogenic inductive media (R&D Systems) in a 1:1 ratio and supplementing with 1% (v/v) penicillin-streptomycin (Gibco). The mixed media was also used for differentiation experiments and no significant difference was observed compared to the lab-made bipotential differentiation medium.

After incubation for one week, cell-hydrogel constructs were fixed in 4% paraformaldehyde in PBS for 8 hours, transferred to 30 wt% sucrose for 72 h, frozen in Cryo-gel (Instrumedics, Inc.) and cryosectioned (10 µm sections) to prepare for histological staining. Osteogenic marker alkaline phosphatase (ALP) was visualized by staining with Fast Blue BB (Sigma), while lipid accumulation was examined by staining with Oil Red O (Sigma) to assay adipogenic activity. The total cell counts were obtained by staining the nuclei with DAPI. The percentage of hMSCs that differentiated down an osteogenic or adipogenic pathway was calculated by dividing the number of cells stained positive for ALP or lipids by the total cell counts, respectively. Color micrographs were acquired using a Nikon E800 upright microscope.

Examination and quantification of histological sections was done by three independent researchers blinded to sample identity with at least five random images/fields in each section per sample. A two-tailed Student's t-test was used for all statistical analyses, with *$p<0.01$ being considered as statistically significant.

4.4 Results

4.4.1 Star polymer cytotoxicity and hydrogel mechanical properties

We synthesized spCBs targeting a wide range of molecular weights (MWs), ranging from 5 kDa to 120 kDa. Modifying the ratio between monomer and initiator in the initial polymerization reaction tuned the degree of polymerization, and we found the conversion to

Polymer (MW target)	Monomer : Initiator	Mn (kDa)	Conversion (%)
spCB-5K	5 : 1	4.2	73%
spCB-20K	20 : 1	17.8	76%
spCB-50K	50 : 1	42.7	76%
spCB-80K	80 : 1	73	80%
spCB-120K	120 : 1	103	79%

Table 4.1 – Targeted and characterized molecular weights of spCB samples

be high (between 70-80%) upon characterizing the polymers with GPC. The targeted and characterized MWs of all spCBs along with their polymerization conditions are shown in Table 4.1.

Then, we exposed cell lines to each spCB sample to ascertain their cytotoxicity. As shown in Fig. 4.3, the higher MW spCBs were nontoxic to all cell lines, as we expected based on the demonstrated cytocompatibility of linear pCB. The lower MW spCB polymers and oligomers (each 'arm' of 5-kDa spCB is only ∼4-5 monomers in length) resulted in lower cell viability, possibly due to the reduced ratio of nontoxic zwitterionic moieties to the required initiator component. We thus used high-MW spCB for further cell encapsulation and expansion experiments.

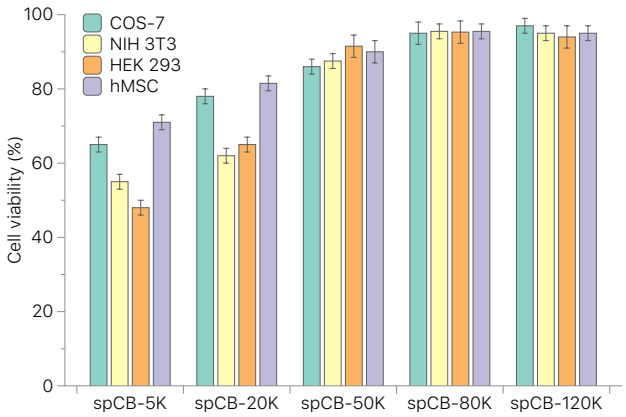

Figure 4.3 – Star-shaped PCB (spCB) of varying molecular weights was tested for cell compatibility. spCB polymers 50-kDa and higher were nontoxic to cells because of the plentiful zwitterionic groups.

We next examined how the molecular weight of spCBs influenced the mechanical and viscoelastic properties of corresponding spCB hydrogels. As all hydrogels formed were designed to be very soft to allow robust cell expansion, the tensile strength and compressive modulus measured with an Instron instrument were imprecise and rotational rheometry proved to be a better characterization approach. To measure the dynamic viscoelasticity of each spCB sample, we conducted a time sweep at constant strain (10%) and frequency (10 rad/s) and assessed the maximum storage (G′) and loss (G") moduli reached upon gelation. When functionalized spCBs of a low MW (spCB-5K and spCB-20K) were mixed to initiate crosslinking and examined rheologically, G" remained greater than G′ through the time sweep, indicating insufficient crosslinking to form a free-standing elastic hydrogel at the concentration used for cell encapsulation. In comparison, spCBs of high MW displayed higher elasticity, forming soft elastic hydrogels with G′ and G" both between 200 and 400 Pa. This data is shown in Fig. 4.4.

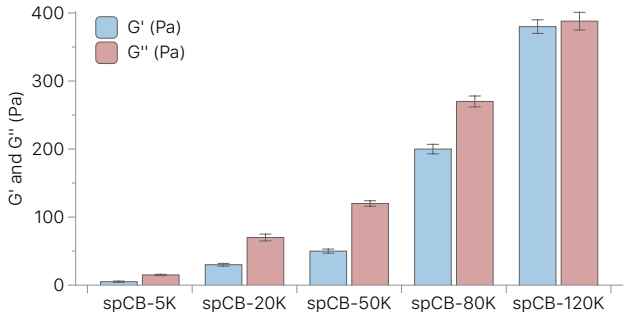

Figure 4.4 – Star-shaped PCB (spCB) of varying molecular weights were tested using time sweeps at constant strain (10%) and frequency (10 rad/s) to find their maximum elastic and viscous moduli after gelation

4.4.2 Cell expansion in and recovery from spCB hydrogels

We encapsulated cells in spCB hydrogels and assessed their viability after 14 days of expansion. As shown in the Live/Dead-stained micrographs in Fig. 4.5a, all cells showed excellent (over 95%) viability after expansion in spCB gels.

To quantify expansion, we immersed cell-hydrogel constructs in dissociation media and counted viable cells after recovery. Fig. 4.5b displays the expansion rate of each cell line, which were all between 25x and 35x. These expansion rates were corroborated by quan-

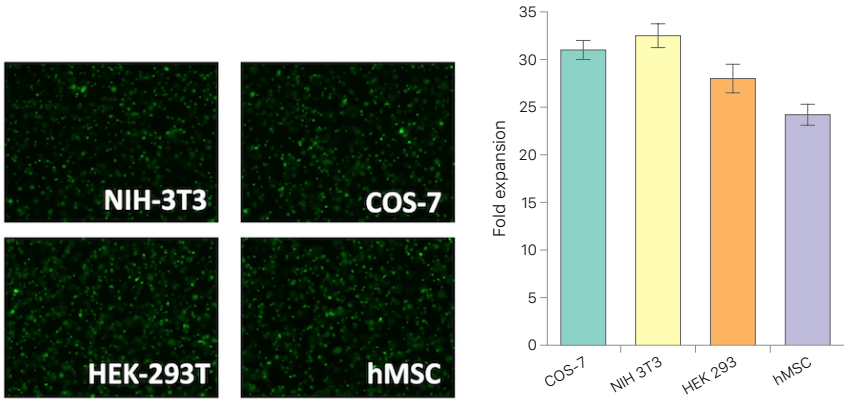

Figure 4.5 – **Left**: Micrographs of LIVE/DEAD stained cells after 14 days of culture in spCB hydrogels. **Right**: Fold expansion of each line after 14 days, from counting.

tifying total DNA and glycosaminoglycan (GAG) content in dried cell-hydrogel constructs using fluorescent markers; DNA content increased between 3000 and 3500% and GAG content increased between 4000 and 6000%. The DNA and GAG content found at each time point are shown in Fig. 4.6.

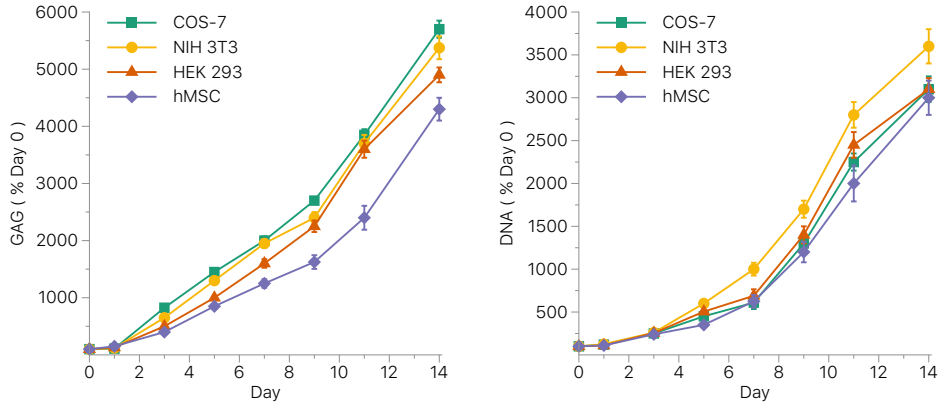

Figure 4.6 – **Left**: Total glycosaminoglycan (GAG) content over time relative to Day 0. **Right**: Total DNA content over time relative the Day 0.

4.4.3 Preservation of mesenchymal stem cell bioactivity

Robust cell expansion is only clinically useful if expanded therapeutic cells maintain their bioactivity or specific functionality. In the case of hMSCs, multipotency after expansion must be maintained so their differentiation pathway can be deliberately chosen for optimal therapeutic benefit. To test the multipotency of hMSCs expanded in spCB gels, we used immunofluorescence staining to visualize the expression of multipotency biomarkers ALCAM and STRO-1. As shown in Fig. 4.7a, we used flow cytometry to count cells expressing these biomarkers after one week of culture in spCB gels or in standard tissue culture flasks and compared them to the multipotent cells initially seeded. The hMSCs expanded in spCB hydrogels displayed positive expression of both biomarkers, equivalent to the population initially seeded. In contrast, hMSCs expanded in a flask were heterogeneous in ALCAM and STRO-1 expression, with around half of the population appearing to lose multipotency.

To further examine hMSC differentiation or multipotency, we used qRT-PCR to quantify the expression of mRNA characteristic to adipogenic (ADIPOQ, FABP4, LPL, PPARG) or osteogenic (COL1A1, OCN, OPN, RUNX2) lineages. After one week, none of these genes showed significantly enhanced expression in hMSCs cultured in spCB hydrogels, suggesting neither adipogenic nor osteogenic fates had been chosen by the cells. The expression measured for all genes relative to the initial population is shown in Fig. 4.7b. Notably, hMSCs that have conclusively chosen an adipogenic or osteogenic lineage typically show between 100x and 10000x higher expression of these characteristic mRNAs.

We finally recovered the hMSCs expanded in spCB gels or in flasks and cultured them in bipotential (adipogenic and osteogenic) differentiation-promoting media. In this way, we could assay their functional bioactivity and therapeutic potential after expansion. After one week of culture, cells were fixed and histologically stained with Fast Blue salts to mark osteogenic expression of alkaline phosphatase (ALP), and with Oil Red O to examine lipid accumulation characteristic of adipogenesis. As shown in Fig. 4.7, there was no difference in the differentiation capacity of the initial hMSC population and cells expanded in spCB gels, indicating their full bioactivity was preserved during expansion. Conversely, hMSCs expanded in flasks displayed a significantly reduced ability to differentiate down adipogenic and osteogenic lineages, signifying a loss in functional bioactivity.

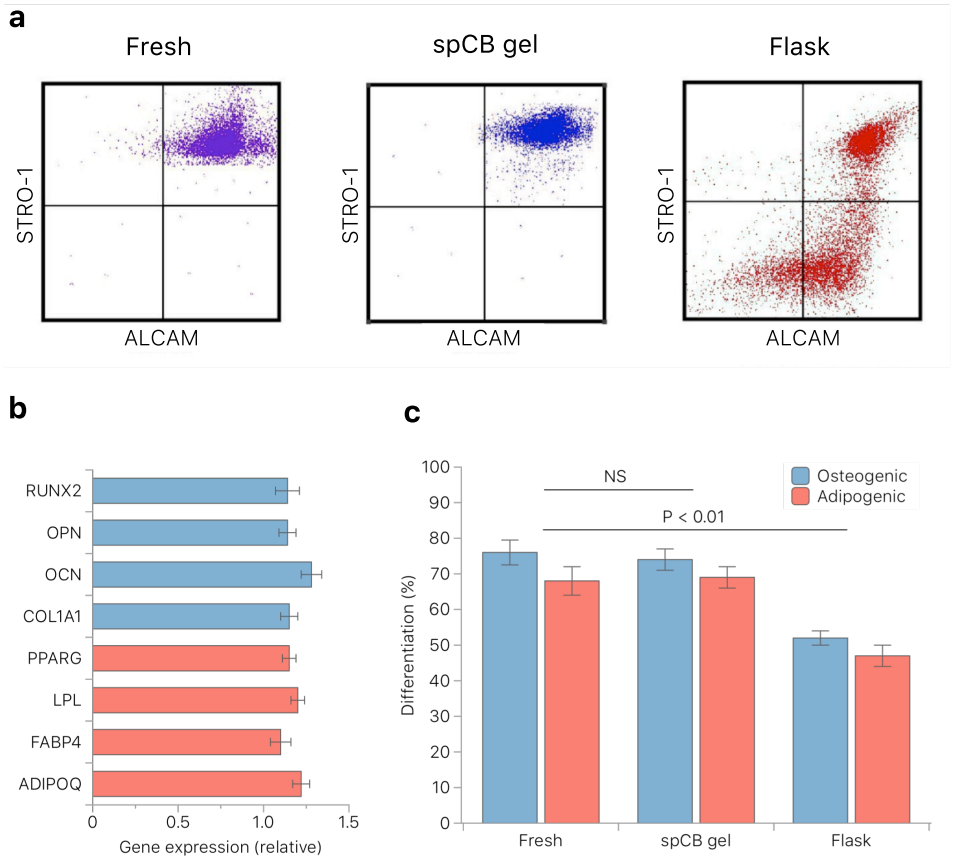

Figure 4.7 – **a)** Flow cytometry analysis of immunofluorescently stained expanded cells from spCB hydrogels compared to a control flask made of TCPS. **b)** Expression of mRNA characteristic to adipogenic (red) and osteogenic (blue) lineages. **c)** Differentiation rate of expanded MSCs, analyzed with histological staining. The spCB-expanded population was functionally equivalent to the original stock, whereas control populations cultured on TCPS lost substantial bioactivity.

4.5 Discussion

The challenge of expanding a patient's lifesaving cells *ex vivo* while maintaining their bioactivity calls for interdisciplinary collaboration. In the case of stem cell expansion, its becoming clear that biochemical signals and physical interactions between a stem cell and its niche are both key to triggering differentiation or maintaining multi- or pluripotency. While several reports have claimed hydrogel scaffold *stiffness* is the key physical trigger of differentiation lineage in these systems, we believe this is an incomplete explanation of the phenomenon. Truly hydrophilic polyzwitterions, especially PCB, have unlocked deeper studies of cell-biomaterial interactions since PCB itself presents no nonspecific cues to cells

but can be easily functionalized to induce specific signaling or binding.[44] Notably, when we cultured mesenchymal stem cells in PCB hydrogels in our previous work, we found the material stiffness *irrevelvant* to whether stem cells remain multipotent or commit to a differentiated lineage; instead, precise tuning of *nonspecific interaction sites* in the hydrogel drives fate choice, and these can be controlled independently of modulus. Pure PCB hydrogels can maintain stem cell multipotency for an unprecedented length of time,[44] and if we add photo-switchable moieties to the network we can reversibly trigger differentiation through specified wavelength exposure.[45]

This advance encouraged us to explore key applications in which premature cell phenotype change or senescence *in vitro* is bottlenecking advances in cell-based regenerative medicine. Many treatments require growing a substantially expanded yet homogeneous cell population in which expanded cells must retain their potency and specific bioactivity. Although cell populations are routinely expanded in flasks and bioreactors, nonspecific interactions from growth surfaces or aggregation reduce the usefulness of the population as they exhaust their limited lifespan and change phenotype unpredictably. Many of these same cell types are sensitive to external inputs such as UV light, so encapsulation through a radical-mediated gelation reaction can also cause damage.

The spCB zwitterionic star polymers we developed in this work present several advantages for cell expansion. First, polymerization and end-group functionalization both occur independently of any cell interactions, so we were able to carefully tune spCB molecular weight through robust living polymerization procedures as detailed in Table 4.1. Any unreacted reagents were removed after functionalization with LC-MS purification so sensitive cells are only exposed to a pure, well-defined material. This high level of control proved useful when optimizing spCB cytocompatibility and efficient gelation, as shown in Fig. 4.3.

Second, the star-shaped architecture ensures each functionalized "point" of the star can quickly react with a complementary point on another, so simple mixing in the presence of cells rapidly establishes a soft yet elastic supportive network that maintains high cell viability, as presented in Fig. 4.5. Many cytocompatible reactions in the growing toolbox of bioorthogonal chemistries could be used to crosslink this platform while maintaining the overall zwitterionic nature of the network.[103] In this work, we used a disulfide exchange reaction to add degradable disulfide linkages between star building blocks, which allowed us to easily break down the hydrogel by adding L-cysteine after expanding cells. These mild conditions enable the robust expansion rate shown in Fig. 4.6 to translate to a large

population of viable recovered cells.

And finally, this flexible new strategy did not hinder the ability of PCB niches to reliably maintain the multipotency and full differentiation capacity of encapsulated hMSCs. As shown in Fig. 4.7, we combined immunofluorescence labeling, quantification of mRNA expression and histological staining to test the bioactivity of expanded cells. Even at a 25-fold rate of expansion, cells in the dramatically enlarged population demonstrated equivalent potency and function to cells in the initial seeded culture. Many cell-based therapies have a success rate directly proportional to the number of functional cells available for infusion, so a simple platform mediating high expansion, simple cell recovery, and high bioactivity of recovered cells could broaden the reach, reduce the cost, and improve the success rate of these lifesaving treatments immediately.

4.6 Conclusions

We have developed a robust platform for expanding cell populations while maintaining their full bioactivity, based on encapsulated culture in zwitterionic hydrogels that form spontaneously by simply mixing two poly(carboxybetaine) star polymers end-functionalized with bioorthogonal reactive groups. This strategy extends the excellent reported capacity of zwitterionic pCB hydrogels to act as cytocompatible scaffolds for tissue culture and regenerative medicine applications. The unique star architecture and spontaneous crosslinking without external input or radical generation is a gentle and facile way to expand and recover valuable cell lines without any loss in functionality. Reliable and broadly-applicable methods to expand rare cell populations could extend the reach of cutting-edge personalized medicine.

Chapter 5

ZIP HYDROGELS AS VERSATILE AND INJECTABLE FORMULATIONS

5.1 Chapter overview

Injectable hydrogels combining high biocompatibility, physiological stability and practical ease-of-use are highly desirable for biomedical applications. Zwitterionic PCB forms superhydrophilic and non-immunogenic hydrogels completely devoid of nonspecific cell and tissue interactions, uniquely enabling PCB to mitigate the foreign body reaction. In this chapter, I present a simple and scalable strategy to create injectable, shear-thinning, and self-healing PCB hydrogels by reconstructing microgel units into new bulk materials. The unique combination of chemical crosslinking and dynamic supramolecular interactions in these zwitterionic injectable pellet (*ZIP*) constructs gives them a supportive modulus and tunable viscoelasticity. Lyophilized *ZIP* powders retain their strength and elasticity upon rehydration, simplifying sterilization and storage. When reconstituted with aqueous suspensions of cells, proteins, or drug-loaded microspheres, *ZIP* powders rapidly self-heal into a homogeneous composite hydrogel formulation without requiring any specialized reagents or conditions, forming an injectable drug depot or cell scaffold.

5.2 Introduction

Hydrogels are hydrated and elastic polymer networks that share many properties with natural tissues. Many of their growing clinical applications—including cosmetic procedures, localized chemotherapy and as regenerative cell scaffolds—demand injectable hydrogels to avoid invasive implantation surgery and enable reshaping to fill unique 3-D spaces.[55–57] Among the numerous natural and synthetic polymers used to construct hydrogels, polyzwitterions have gained particular attention in recent years because of their superhydrophilic, highly biocompatible, and non-immunogenic attributes.[6,41] These polymers contain repeated pairs of cationic and anionic groups along their chain, mimicking the phospholipids comprising cell membranes or the mixed-charge surfaces of many proteins.[30] As biomaterials, polyzwitterionic brushes or crosslinked hydrogels confer ultra-

low levels of nonspecific protein fouling from complex physiological fluids, exceeding the performance of popular hydrophilic and amphiphilic polymers like PEG.[104,105] Zwitterionic hydrogels formed from pure carboxybetaine monomers and crosslinkers have been recently shown to inhibit the foreign-body response and resist collagenous capsule formation when implanted in mice[43] as well as shield proteins from immunogenic responses in the bloodstream.[8,41,42] Key to regenerative medicine applications, stem cells cultured in PCB hydrogel scaffolds maintain their therapeutic pluripotency and avoid nonspecific differentiation.[44,45] These exciting findings motivate accelerated development of PCB hydrogels towards clinical applications, many of which require injectability. However, no straightforward strategy to make pure zwitterionic hydrogels injectable has been reported to date.

Making any hydrogel injectable while maintaining its tissue-like elasticity is challenging, and two general classes of injectable hydrogels have emerged. The first class is more precisely termed *in situ forming*, and a cell expansion platform using this strategy was discussed in Chapter 4. While especially useful for cell encapsulation, *in situ*-forming hydrogels typically undergo an irreversible sol-gel transformation reminiscent of epoxy glues, and can be complex and expensive to develop and use. An alternative class of injectable soft materials are often referred to as viscoelastic hydrogels.[106] Instead of a single in situ reaction triggering irreversible gelation, viscoelastic hydrogels incorporate some form of dynamic or reversible crosslinking, which enables repeated switching between "solid-like" and "liquid-like" forms under different conditions.[107,108] For many real-world applications, this produces more practical and useful materials. Most are designed to flow in response to increased shear (such as when pushed through a needle) and then self-heal into a new elastic shape.[109,110] Polysaccharides such as alginate, dextran, and hyaluronic acid are the basis for many materials in this class; these natural polymers can reversibly crosslink by chelating divalent ions such as Ca^{2+} and Mg^{2+}.[111] Many polysaccharide gels are further modified with covalent crosslinks to increase their strength or resistance to degradation; for example, crosslinked hyaluronic acid is produced for cosmetic applications.[112] Hyaluronic acid has also been extensively modified by Burdick et al to incorporate adamantine, facilitating reversible "guest-host" interactions with cyclodextrins.[113,114] However, these complex modifications fail to eliminate several inherent limitations of polysaccharide gels, which have poor long-term physiological stability, varying biocompatibility, and are difficult to purify from natural sources to medical grade materials.[10]

The biocompatibility and non-immunogenicity achieved by zwitterionic PCB hydrogels

surpasses those based on polysaccharides, PEG, and alternative materials such as NIPAM and PEG-based poloxamers.[40,115,116] We therefore aimed to develop injectable PCB hydrogels while maintaining their unique "stealth" properties. Ideally, their preparation and use would be simple, easy to scale up, and useful in real-world applications without requiring specialized knowledge or laboratory conditions. While exploring dynamic crosslinking strategies, we speculated a set of attributes collectively referred to as "zwitterionic fusion" may provide the key—this concept integrates strong hydration, intermolecular zwitterion pair attraction, and H-bonding between side chains and backbone amides to facilitate time-independent self-healing in some zwitterionic materials.[58,117] Here, we explore how zwitterionic fusion can play a role in hydrogels developed to meet practical clinical needs. We hypothesized that zwitterionic microgels could act as self-healing "building blocks" with which to reconstruct macroscopic materials featuring desirable injectable and viscoelastic characteristics.

5.3 Methods

5.3.1 Bulk hydrogel synthesis

We first made bulk zwitterionic hydrogels with a photopolymerization method. Carboxybetaine acrylamide (CBAA) monomer (2.5 M), CBAA-X crosslinker (0.01-1% mol/mol), and photoinitiator 2-hydroxy-1-[4-(2-hydroxyethoxy)phenyl]-2-methyl-1-propanone (I2959) were dissolved in water, mixed well, and degassed under vacuum. The concentrated solution was then cast into a 1-mm thick glass mold and polymerized in a UV oven (Spectroline). The resulting hydrogels were equilibrated in water for several days to remove any unreacted reagents and allow swelling. We generated a small library of these parent hydrogels, using either CBAA-1 or CBAA-2 monomer and several CBAA-X crosslinker concentrations between 0.025 and 1 mol%, relative to CBAA monomer.

5.3.2 Microgel production

Bulk zwitterionic hydrogels were then converted into zwitterionic microgels of tunable size. The equilibrated bulk hydrogels were roughly cut into pieces and placed into an extrusion apparatus, consisting of a tightly-fit piston and cylinder, capped with a section of micronic steel mesh (TWP, Grainger). The steel piston apparatus was custom-built by Arne Biermans (pictured in Fig. 5.1 below). Mesh of various weaves can be used, but typically we have found Dutch-weave mesh made of 316 stainless steel, with pore sizes of 120 µm, 80 µm, 40

µm, and 25 µm, to be most appropriate. Bulk gels generally must be progressively passed through meshes of decreasing pore size, starting at 120 µm and decreasing to 25 µm. At the final mesh size used, the material is extruded at least three times to improve pellet size homogeneity. The final pellets can be stored in a hydrated state, or lyophilized for long-term storage (Labconco FreeZone).

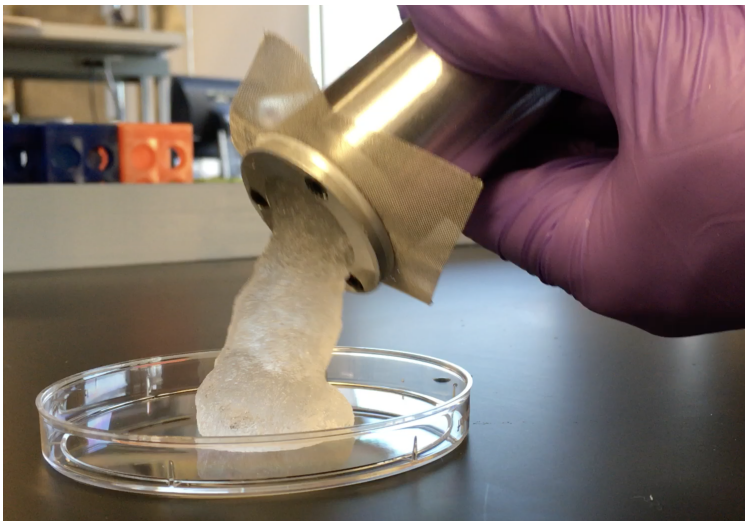

Figure 5.1 – Steel piston assembly used to produce microgels by repeated mesh extrusion.

5.3.3 Rheological evaluations

Dynamic viscoelasticity properties of all *ZIP* constructs were measured with a Physica MCR 301 Rheometer (Anton Paar) using parallel plates of 40-mm diameter and a plate-to-plate distance of 900µm. Dynamic oscillatory frequency sweeps were conducted at a constant 10 %strain over a frequency range of 0.1-100 rad/s at 25°C. Oscillatory strain sweeps were conducted from 0.1% to 100% strain, and G', G" and the complex viscosity were recorded. Step-strain experiments were conducted by toggling the strain between 1% and 300% for three or more cycles.

5.3.4 Production of PLGA microspheres for depot formulation

Several drugs and dyes were encapsulated in PLGA microspheres to evaluate and optimize *ZIP* depot formulations. We first manufactured dye-loaded PLGA microspheres by mixing

(PLGA) copolymers of varying compositions (Evonik) with Methylene blue or Crystal violet dyes in an organic phase (4 mL dichloromethane containing 400 mg PLGA and 100 mg dye). This phase was slowly added to an aqueous phase (100 mL of 0.5% poly(vinyl alcohol) in 5% NaCl) under mixing with a high-shear impeller at 2500 RPM. After 5 min, emulsification was stopped and solution was stirred with a magnetic stir bar at 300 RPM overnight. Microspheres were washed and lyophilized.

To make doxorubicin (DOX) and peptide-loaded MS, either DOX (DOX HCl, Sigma) or peptide (experimental cationic peptide SS31, donated by Stealth Biopharma) were encapsulated in PLGA using a W/O/W double emulsion method adapted from several similar protocols.[118,119] The inner aqueous phase (400 µL DI water containing 40 mg DOX or SS31) was emulsified with the organic phase (4 mL dichloromethane containing 400 mg PLGA, acid terminated) on ice, for 30 s. This emulsion was slowly added to the outer aqueous phase (100 mL of 0.5% poly(vinyl alcohol) in 5% NaCl) while being stirred with a high-shear impeller at 2500 RPM. After 5 min, impeller was removed and solution was stirred with a magnetic stir bar at 300 RPM overnight. Hardened microspheres were washed through repeated centrifugation in sterile water, and lyophilized. DOX and peptide loading were found by dissolving a known mass of particles in DMSO and measuring the absorbance at 480 nm (for DOX) or 280 nm (for SS-31 peptide) with a microplate reader (BioTek Cytation 5). Surface characterization of microspheres was done via SEM.

5.3.5 In vitro drug release

DOX-PLGA and SS-31-PLGA microspheres were mixed with *ZIP* powder and reconstituted formulation to 40 mg DOX-PLGA or SS-31-PLGA (containing 2 mg total DOX or 3.5 mg total SS-31) per mL of *ZIP* gel. We evaluated the drug release rates at 37°C *in vitro* by dispensing the *ZIP*-drug-PLGA depot (or drug-PLGA microspheres without gel) into porous Transwell inserts suspended in PBS. The buffer was sampled and replaced at selected time intervals and the cumulative amount of released DOX or SS-31 assayed spectroscopically, at 480 nm or 280 nm, respectively.

5.3.6 Enzyme assays

TEM-1 β-Lactamase was diluted to 5 nM in 20 mM sodium phosphate, pH 7.0, with 10 µg/mL bovine serum albumin (BSA, Sigma-Aldrich) added as a blocking agent. Nitrocefin (Life Technologies) solution in the same buffer was added to enzyme samples or *ZIP*-

enzyme formulations in UV-transparent 96-well microplates (Corning) at saturating concentration and enzyme activity (V) was measured using a microplate reader (BioTek Cytation 5) as the initial linear rate of increase in substrate absorbance at 490 nm.

5.3.7 Cell growth, expansion and injection

Media containing cells (1 mL, 10^6 cells /mL) was used to rehydrate 50 mg of lyophilized *ZIP* powder of a particular formulation. The cells were gently mixed well with the gel. This construct was transferred to a Corning Transwell tissue culture insert with a porous bottom (8-micron pore size) which was then placed in a 12-well plate with cell media even with the level of the microgels-cells construct. After two days of culture, cells were Live/Dead stained with calcein-AM and ethidium bromide homodimer and imaged with a fluorescent microscope (Nikon T2000U).

To evaluate cell expansion, a purified CD4+ human T lymphocyte population (Lonza) was cultured in the *ZIP* scaffold and its proliferation was tracked. For the first part of this experiment, cells were stained with 10 uM CellTrace carboxyfluorescein succinimidyl ester (CFSE) and resuspended in RMPI media containing 10% FBS, 1% penicillin and streptomycin. Stained cells were stimulated to proliferate with Dynabeads Human T-Activator CD3/CD28, at a ratio of 1:1 bead:cell (seeded at 1x10^6 cells/mL), and 30 U/mL Interleukin-2 (IL-2), and incubated at 37°C and 5% CO_2 for 7 days. Cells were analyzed via fluorescence flow cytometry on an LSR II instrument equipped with a 488 nm excitation source and a 530/30 nm band pass filter; the excitation and emission peaks of the CellTrace product after hydrolysis are 492nm and 517nm, respectively. Proliferation analyses were performed using FlowJo software for a control and both high and low cell seeding density samples within the *ZIP* construct. Cells generations stained with CellTrace CFSE reagent were visualized by separated fluorescence intensity peaks, in which the initial peak on the far right was assumed to be the parent peak and subsequent peaks to the left represented subsequent generations.

To evaluate cell protection during needle flow, healthy HEK 293T cells were resuspended in PBS at 10^6 cells/mL and used to rehydrate an appropriate amount of *ZIP* powder (CB-1, CB-X = 0.05%) to a gel while gently mixing. Then, the soft *ZIP*-cell construct was carefully transferred to a 1 mL syringe and injected into a well plate through a 28G needle. A control suspension was left in PBS and also injected. LIVE/DEAD reagents (calcein AM and EtBr homodimer) were added to each sample to assay the resulting viability.

5.4 Results and discussion

5.4.1 Design and production of ZIP hydrogels

To create zwitterionic microgels in bulk, we first produced macroscopic PCB hydrogels using a photopolymerization casting method previously reported.[44] All hydrogels in this work were constructed solely from zwitterionic carboxybetaine acrylamide monomers (CB-1 or CB-2) with various crosslinker (CB-X) concentrations. Bulk hydrogel sheets were equilibrated in water for several days until they reached their equilibrium water content (EWC), between 97% and 99.5% w/w. After equilibration, we generated microgel "pellets" by repeatedly extruding these large sheets through micronic steel mesh using a custom-fabricated piston assembly. Changing the mesh weave and pore size allowed us to easily tune the average diameter of equilibrium-swollen microgels. Similar hydrogel "sizing" methods have been reported in the manufacture of some cosmetic dermal fillers.[120,121] In this work, pellets were designed to be similar in scale to mammalian cells (10-100 μm), and we initially observed these microgels to heal into moldable constructs with consistent properties between batches. We refer to this class of reconstructed materials as "zwitterionic injectable pellet" (of *ZIP*) hydrogels or constructs. As illustrated in Fig. 5.2, the overall production process is straightforward and amenable to small or large scales.

We have previously shown that zwitterionic PCB hydrogel scaffolds act as a truly "blank slate" to restrain stem cell differentiation,[44,45] but only when all components are zwitterionic: adding even trace amounts of hydrophobic compounds compromises this feature. Similarly, pure zwitterionic gels are the only synthetic materials demonstrated to evade the foreign body reaction upon subcutaneous implantation.[43] Therefore, one of our key goals when designing injectable gels was to preserve zwitterionic purity and retain these unique attributes. Extensive "guest-host"-type material modifications would add synthetic complexity, batch variability and—our biggest concern—hydrophobicity.

5.4.2 Rheological behavior of ZIP hydrogels

In single-charged or non-ionic self-healing materials, hydrophobic surface reconstruction or a pH-dependent charge barrier limits their healing.[58,122] The zwitterionic fusion healing mechanism we previously reported[58] is unique because it is time- and pH-independent. Even so, only polymer chains near the exposed interface of crosslinked PCB hydrogels have sufficient mobility to rearrange and form new supramolecular interactions. In *ZIP* con-

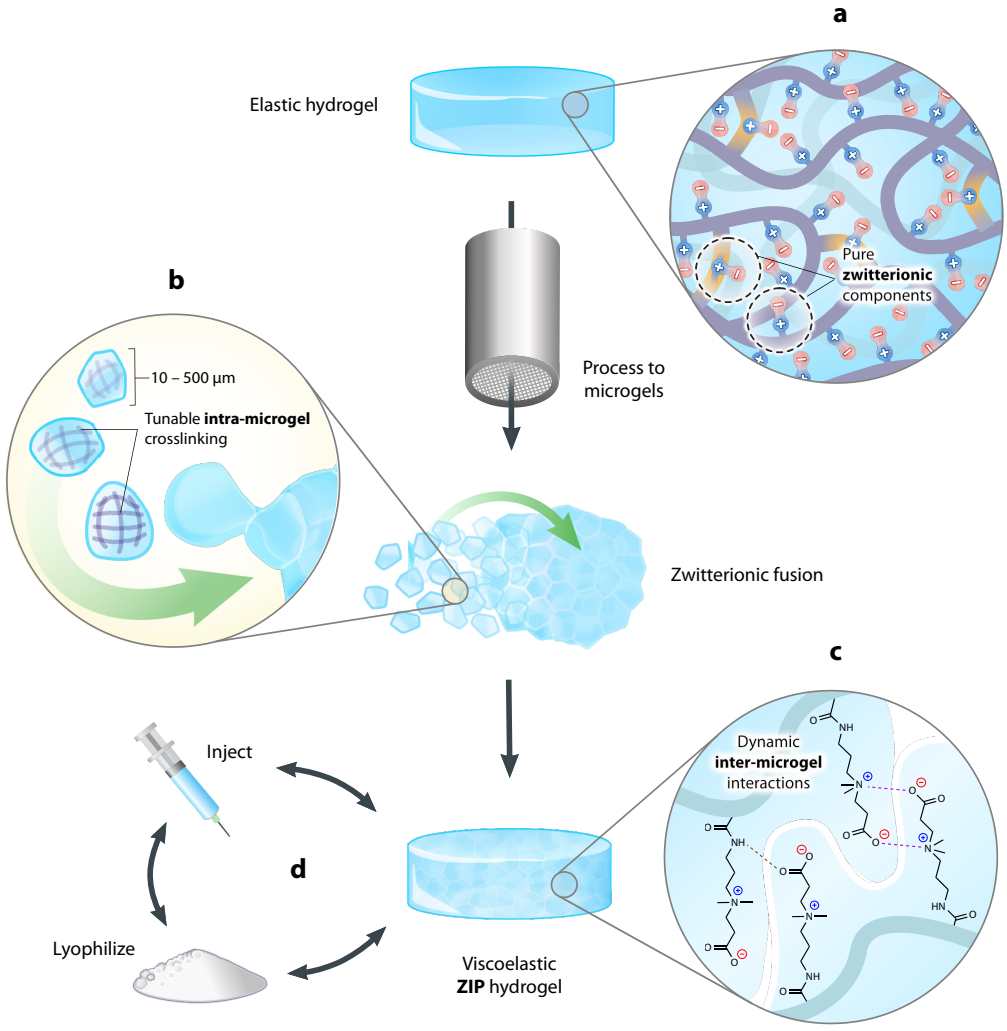

Figure 5.2 – Combination of tunable covalent and dynamic *zwitterionic fusion* crosslinking enables unique *ZIP* hydrogels. Overview schematic showing the production and key features of viscoelastic "zwitterionic injectable pellet" *ZIP* gels. After mechanical processing of a bulk polycarboxybetaine hydrogel to microgels, zwitterionic fusion enables their reconstruction into a viscoelastic gel that can be injected through needles and lyophilized for simplified storage and formulation. **a**, Schematic showing the makeup of starting elastic hydrogels, formed by crosslinking carboxybetaine acrylamide monomers (CBAA-1 or CBAA-2) with carboxybetaine diacrylamide crosslinker (CBAA-X) via photoinitiated free radical polymerization in glass molds. **b**, Bulk hydrogels are mechanically processed to microgels, with each microgel possessing similar elastic characteristics to its parent hydrogel. **c**, When microgels are brought into contact, dynamic inter-microgel supramolecular interactions (zwitterionic fusion) enable rapid self-healing and tunable shear-thinning characteristics. **d**, The resulting *ZIP* constructs can be injected and lyophilized for storage and formulation.

structs, each internally crosslinked microgel participates in dynamic healing interactions with multiple neighboring pellets in 3D—at this scale, each individual gel is large enough to retain strength and elasticity, yet small enough to involve a high percentage of its polymer chains in dynamic interactions. While the molecular identity of each microgel is the same as the bulk hydrogel, inter-microgel zwitterionic fusion interactions are key to the tunable rheological behavior of the aggregate material. This balance is illustrated in Fig. 5.2b-c.

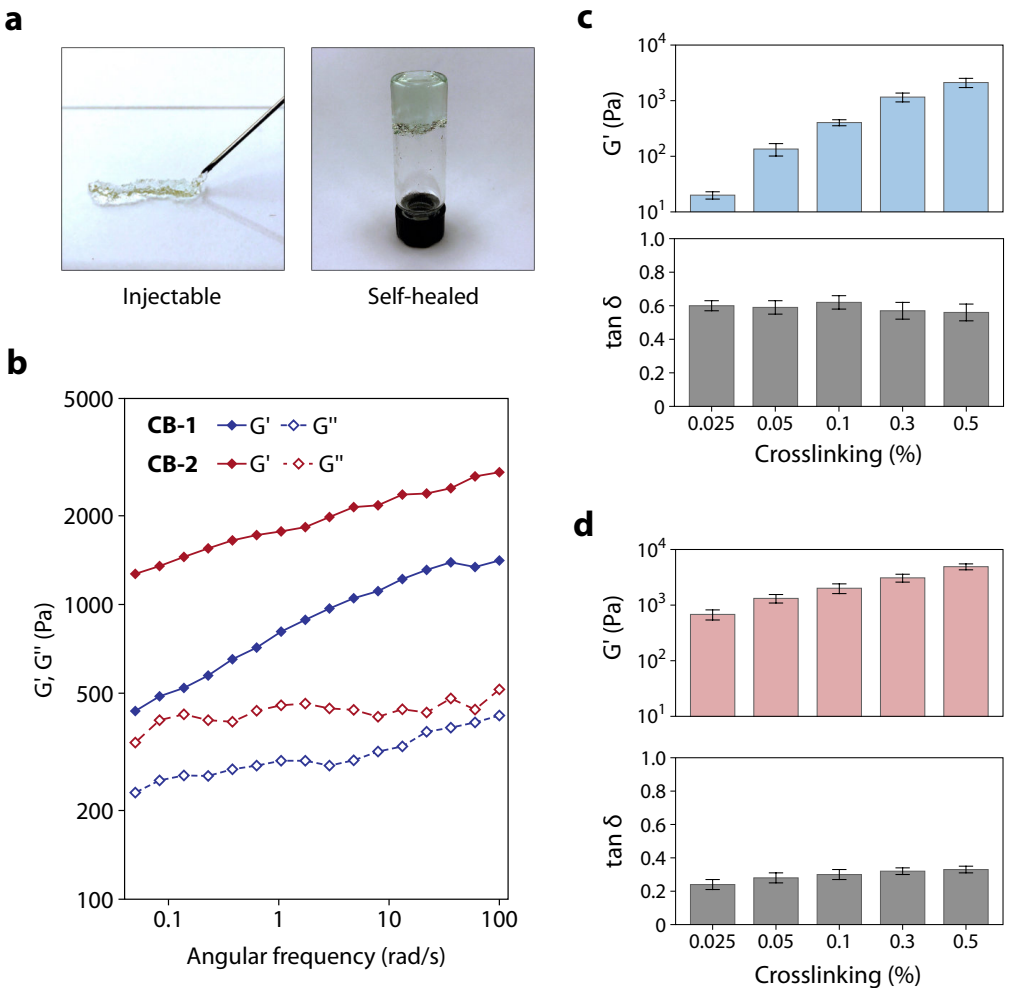

Figure 5.3 – Rheological characterization of viscoelastic *ZIP* hydrogels. a, Photos highlighting the injectability (left) and self- healing ability (right) of ZIP gels. Gels tinted for visual inspection. **b,** Dynamic oscillatory frequency sweeps of CB-1 and CB-2- based *ZIP* hydrogels formed with 0.1% (mol/mol) CB-X. **c,d** Storage modulus (G′) and loss tan δ (G"/G′) found for CB-1 (**c**) and CB-2 (**d**) based *ZIP* hydrogels formed at different CB-X concentrations.

To evaluate the injectability and self-healing capabilities of *ZIP* constructs, we observed their behavior and used rheology to study their viscoelasticity. All *ZIP* hydrogels in this work were injectable through a 25G needle and rapidly reverted to a solid-like state in an inverted vial (Fig. 5.3a). When transferred to a flat surface, *ZIP* constructs maintained self-supporting shapes that varied in rigidity. We conducted dynamic oscillatory frequency sweeps on *ZIP* gels based on CB-1 and CB-2 monomers, each incorporating 0.1 mol% of CB-X crosslinker. This data showed the storage modulus (G′) to be dominant over the loss modulus (G") over the full frequency range examined (0.1 - 100 rad/s), suggesting that both reconstructed *ZIP* materials behaved like a hydrogel (Fig. 5.3b). Summaries of G′ (used as a measure of strength) and tan δ (G"/G′, used as a measure of elasticity) values are shown in Fig. 5.3c and Fig. 5.3d for CB-1 and CB-2 *ZIP* gels, respectively. These data were recorded at 1% strain and 10 rad/s. Notably, CB-2 *ZIP* gels displayed higher G′ values at each crosslinking level compared with CB-1, especially at very low crosslinker content (0.025 mol% CB-X). In addition, CB-2 constructs all exhibited lower tan δ values (around 0.25) compared with CB-1 (around 0.6). As tan δ is inversely associated with elasticity, this indicated CB-2 produced more elastic constructs—these results were consistent across all crosslinking concentrations and between differently-crosslinked CB-1 and CB-2 samples with similar G′, suggesting zwitterionic fusion interactions endow CB-2 constructs with additional bulk strength and elasticity.

We further characterized *ZIP* gels with oscillatory strain sweep and step-strain experiments. Fig. 5.4a shows these relationships for the lowest-crosslinked CB-1 construct, which had a maximum G′ around 20 Pa. Similarly, Fig. 5.4b shows comparable plots for the highest-crosslinked CB-2 sample (G′ = 5kPa). We found G′ to dominate over G" in these and all intermediate formulations at low strains (0.1 - 1%). The complex viscosity and G′ began to decrease as we pushed the strain towards 100%, with most samples exhibiting a crossover point (tan δ = 1) between 10% and 30% strain. Above this strain, G" becomes dominant and the gels begin to adopt liquid-like behavior as inter-microgel associations break. When the strain was toggled between 1% and 300%, both formulations showed inversion of G′ and G" at high strain followed by a rapid recovery of elastic properties when low strain returned. This is indicative of efficient self-healing across all samples. While the data shown in Fig. 5.4a and b are several orders of magnitude apart, axes are scaled appropriately for direct visual comparison of their relative behavior.

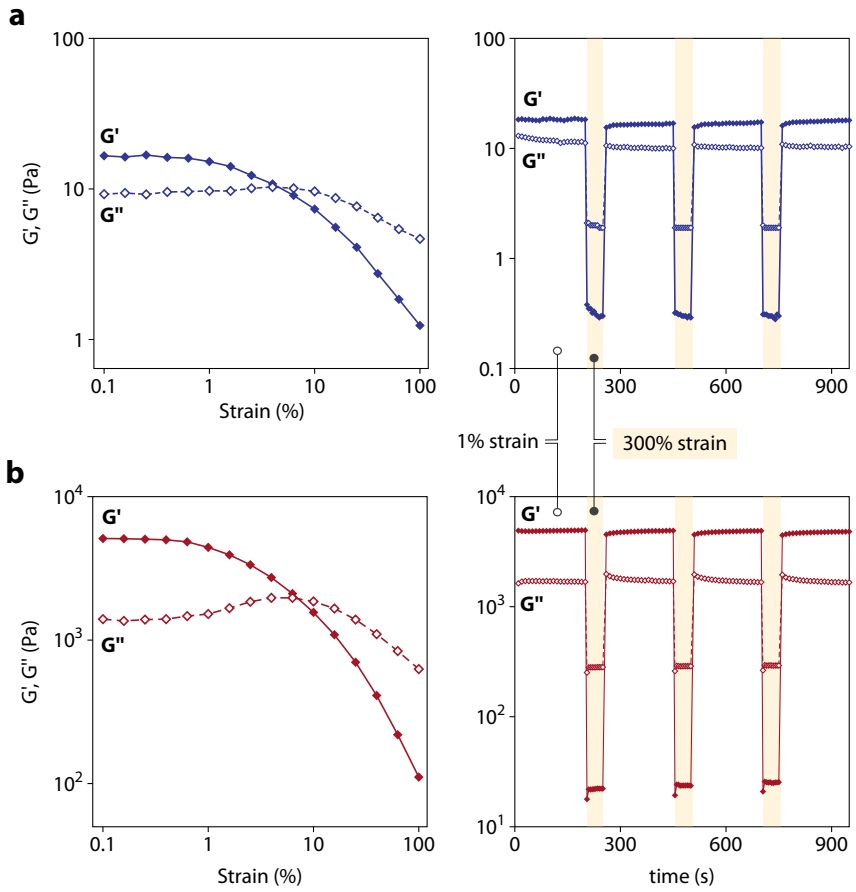

Figure 5.4 – Strain sweep and step-strain experiments. Oscillatory strain sweeps (**left**) and step-strain tests (**right**) of the lowest-crosslinked CB-1 sample (0.025%) (**a**) and the highest-crosslinked CB-2 sample (**b**). Storage (G', solid markers) and loss (G", open markers) moduli plotted as strain increases from 0.1% to 100% (**left**) or toggles between 1% and 300% (**right**). While the data shown in (**a**) and (**b**) are several orders of magnitude apart, axes are scaled for direct visual comparison between relative behavior.

5.4.3 Lyophilization and reconstitution

Freeze-drying *ZIP* gels to store them as sterile lyophilized powders is practical and enables simplified formulation of many drug- or cell-encapsulating constructs. But while several types of macroscopic hydrogels have been lyophilized to create porous scaffolds for drug delivery or cell attachment, the freeze-drying process is known to irreversibly change some aspects of their structure and behavior.[123] Lyophilized gels commonly require immersion in water for hours to days to fully rehydrate; even then, they fail to reach their original water

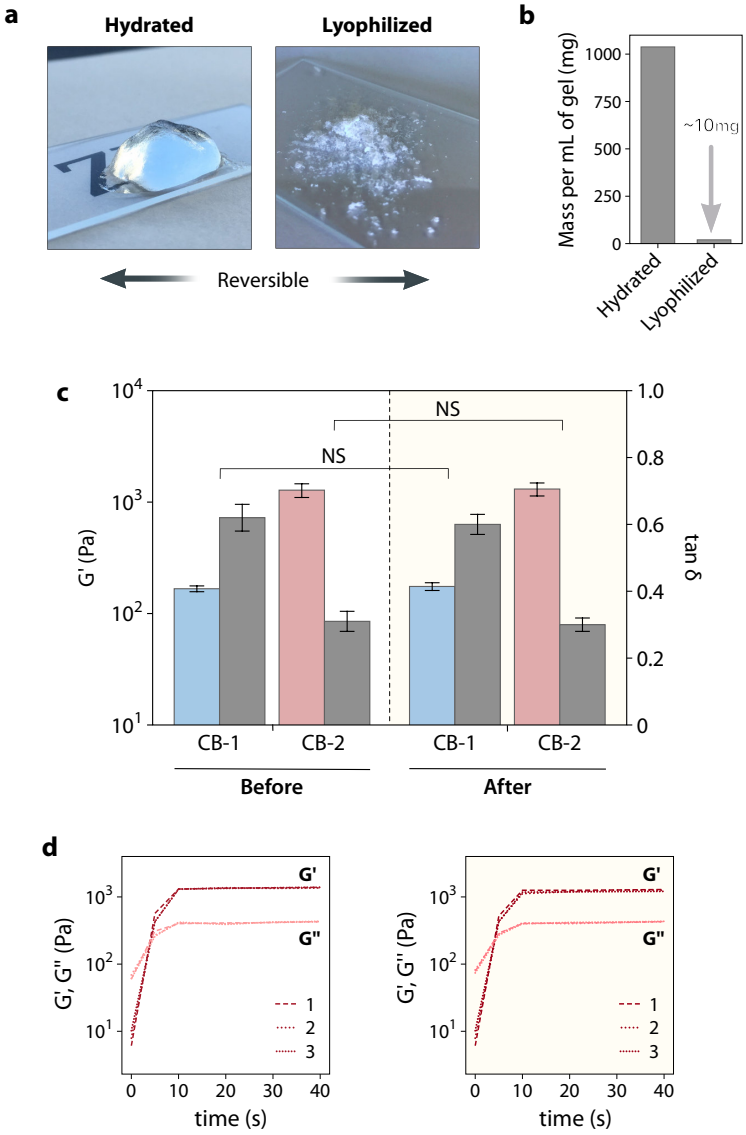

Figure 5.5 – Lyophilization simplifies storage and formulation without detriment to strength, elasticity and healing time. **a**, Soft *ZIP* hydrogel dollop on a glass slide (**left**) and lyophilized to powder (**right**). **b**, Lyophilization dramatically reduces storage demands of sterile microgel material. **c**, Strength (G′, left axis) and elasticity (tangent δ, right axis) of CB-1 (blue/grey) and CB-2 (red/grey) *ZIP* gels before and after lyophilization; both gels contain 0.05% CB-X. Post-lyophilization gels were rehydrated to their EWC. **d**, Recovery of G′ and G" by CB-2 (CB-X = 0.05%) *ZIP* gels upon reverting from high (300%) to low (1%) strain after step-strain cycles 1-3. Left: prior to lyophilization; right: post lyophilization and rehydration to original EWC.

content and display uneven shapes, surface roughness, and modified material properties.[124]

Due to the particularly strong hydration of zwitterionic materials[101] and the high surface-area-to-volume ratio of microgels compared to their macroscopic counterparts, we speculated lyophilization may not have a detrimental impact on *ZIP* hydrogels. We tested this by freeze-drying a volume of each *ZIP* formulation to desiccated powder; as the EWC of lightly-crosslinked PCB hydrogels is near 99%, each mL of gel only contained around 10 mg of dry material, which could be combined from multiple batches for simplified storage (Fig. 5.5a-b). Notably, when we mixed dry *ZIP* powder with the volume of water necessary to return them to their original EWC, hydration completed within seconds. The rapidly rehydrated gel constructs retained their transparency, homogeneity, and practical attributes (e.g., injectability and self-healing), so we conducted further rheological testing to compare samples before and after lyophilization and rehydration. As highlighted in Fig. 5.5c, freeze-drying CB-1 and CB-2 *ZIP* constructs had no effect on their bulk strength (G') or elasticity (G") post-rehydration. In addition, their high self-healing efficiency was unchanged, with no difference in step-strain recovery time after multiple cycles (Fig. 5.5d). We believe both the superhydrophilicity and scale/geometry of the microgel units enables this helpful attribute. To sterilize the ZIP gels for tissue culture applications, we first added EtOH in excess of 70%[125] and then washed out this solution with sterile water before freeze-drying.

5.4.4 Formulation and characterization of drug and protein depots

Injectable drug depot formulations that release therapies at a predictable rate over a designated period of time represent one example of a clinical need motivating the development of biocompatible injectable hydrogels.[56,126,127] Reconstitution of drug-loaded PLGA or PCL microspheres in an injectable crosslinked gel facilitates accurate volumetric dosing and keeps the formulation localized at the injection site. Based on the ability of zwitterionic hydrogel to mitigate the foreign body reaction,[43] we envision they may also be helpful in shielding otherwise-immunogenic materials from immune recognition and attack in a composite formulation.[42]

To explore these possibilities, we first manufactured dye-loaded PLGA microspheres (MS) using low-speed emulsification and simply mixed these dried MS with lyophilized *ZIP* powder in a vial. The lyophilized mix reconstituted to a homogeneous formulation in seconds, with only brief vortexing required during hydration to disperse particles evenly. PLGA MS were held in place by the gel in an inverted vial; no obvious changes, settling,

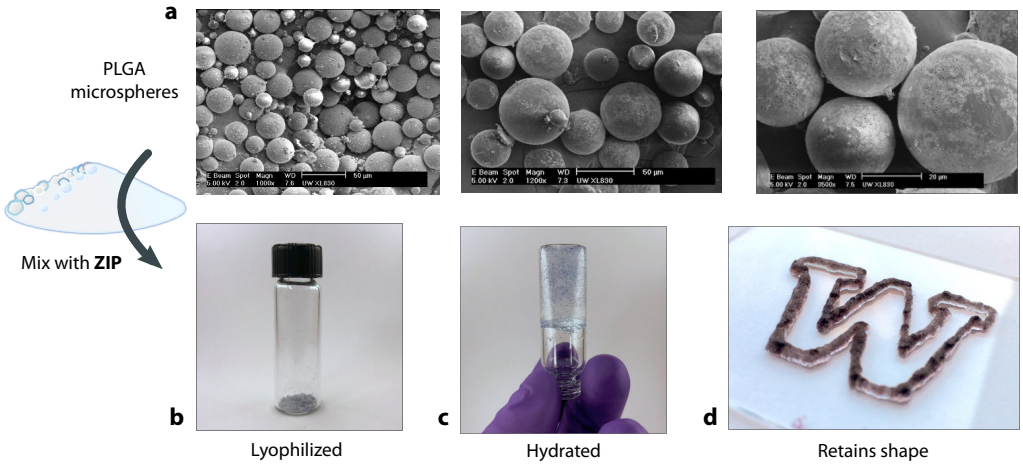

Figure 5.6 – *ZIP* hydrogels enable injectable and versatile extended release drug depot formulations. a, Poly(lactic-co-glycolic) microspheres (PLGA MS) loading various drugs and dyes were produced and characterized with SEM. **b**, PLGA MS were mixed with lyophilized *ZIP* powder and **c**, evenly suspended in injectable gel upon water addition. MS in (**c**) loaded with Methylene Blue for visualization. **d**, injection through a 25G needle was used to trace a *ZIP* formulation containing Crystal violet-dyed MS into a 3-D "UW" logo on a glass slide, representing precise depot placement or topical application.

or separation were observed in undisturbed vials for at least six weeks. To demonstrate the injectability and self-healing capacity of these drug formulations, we used a syringe to accurately dispense reconstituted *ZIP* gel containing Crystal violet-loaded PLGA MS onto a slide in the shape of a "UW" logo. These features are summarized in Fig. 5.6.

Then, we encapsulated chemotherapeutic drug doxorubicin (DOX) inside PLGA MS using a double (W/O/W) emulsion method, tuning the process parameters to achieve smooth particles 30 µm in diameter and targeting a 2-3 week controlled release period. After confirming DOX was loaded successfully, we mixed DOX-PLGA MS with *ZIP* powder and reconstituted this formulation to 40 mg DOX-PLGA MS (containing 2 mg total DOX) per mL of *ZIP* gel. We evaluated the DOX release rate at 37°C *in vitro* by dispensing the *ZIP*-DOX-PLGA depot (or DOX-PLGA without gel) into porous Transwell inserts suspended in PBS (Fig. 5.7a). This was designed to simulate the in vivo environment of a subcutaneously injected cancer treatment, as might be administered to prevent tumor recurrence after surgery. The buffer was sampled and replaced at selected time intervals and the cumulative amount of released DOX assayed spectroscopically; the resulting release data are shown in Fig. 5.7b.

Both *ZIP*-formulated and control MS samples released 90% of their total DOX cargo within two weeks, with an insignificant difference in overall release. This indicates the injectable gel did not significantly inhibit or accelerate PLGA hydrolysis and erosion overall, and that DOX could diffuse out through the zwitterionic matrix. However, it's worth noting that the ZIP-DOX-PLGA formulation seemed to show a lower level of "burst" release in the first 24 h, which would be another advantage of ZIP depot formulations if found to extend to *in vivo* studies. The schematic in Fig. 5.7c illustrates some potential in vivo advantages of injectable ZIP depots—the evenly dispersed drug carriers are free to degrade and release their cargo, while the zwitterionic gel holds the construct in place and prevents immunogenicity and the foreign body reaction.

In recent years, biologic protein drugs such as therapeutic enzymes and monoclonal

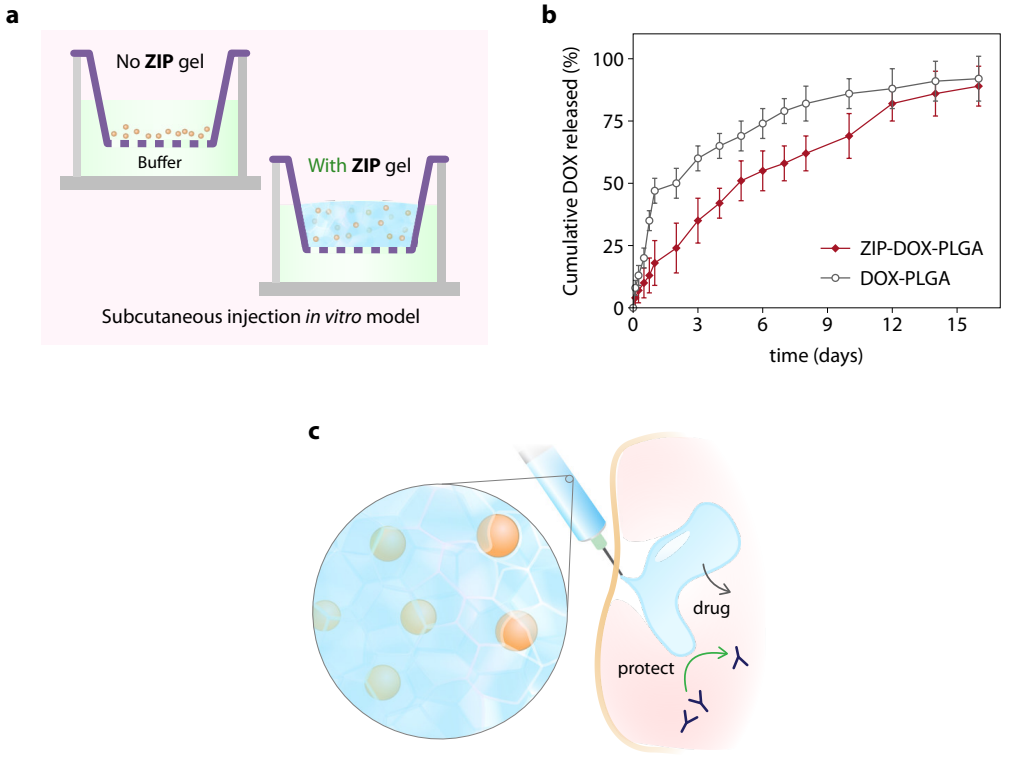

Figure 5.7 – Release of doxorubicin from *ZIP*-PLGA formulation. **a**, PLGA MS alone or suspended in *ZIP* gel inside porous Transwell insert as an *in vitro* model of subcutaneous injection. **b**, DOX release over two weeks in vitro from PLGA MS (grey open markers) and PLGA MS suspended in *ZIP* gel (red solid markers). **c**, Schematic of *ZIP* drug depot in vivo; injectable zwitterionic hydrogel prevents immune reaction while facilitating localized drug release.

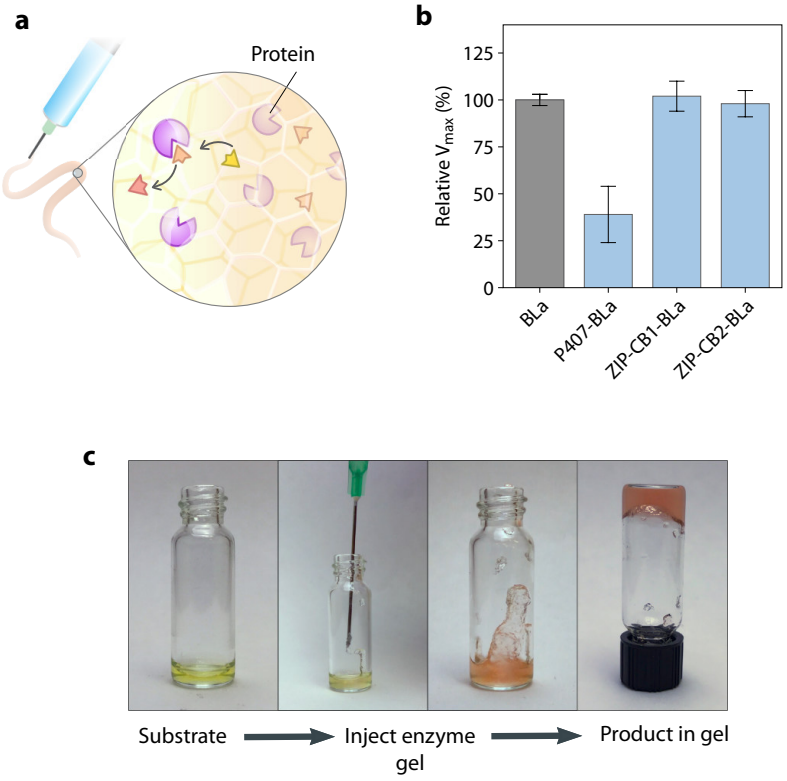

Figure 5.8 – *ZIP*-based injectable active enzyme gel. **a**, Schematic showing concept of injectable enzyme gel. **b** Kinetic evaluations of active enzyme gels formulated with CB-1 or CB-2 and β-Lactamase (BLa) show V_{max} equivalent to BLa in buffer; Pluronic/poloxamer-based injectable enzyme gel (P407; PEG-PPG-PEG triblock) significantly reduced activity. **c**, β-Lactamase (BLa)-loaded *ZIP* gel injected over nitrocefin substrate (yellow) rapidly catalyzed substrate conversion inside gel.

antibodies have grown to dominate the pharmaceutical landscape.[12,41] These drugs can precisely target many debilitating diseases, but remain expensive and are plagued by short circulation half-lives and immunogenic issues.[17,18,128] We recently demonstrated that conjugating zwitterionic PCB to proteins[40,41] or encapsulating them in individual PCB nanogels[8,42] can improve their stability, maintain their bioactivity, and mitigate immunogenic reactions in vivo. The zwitterionic moiety in PCB, glycine betaine, is widely known to stabilize protein structures and prevent denaturation and aggregation.[28,29] We speculated that simply reconstituting ZIP powder with an enzyme solution may produce an "active enzyme gel" for localized injectable or topical biologic therapies. This concept is illustrated in Fig. 5.8a.

As pictured in Fig. 5.8c, when we mixed the model enzyme β-Lactamase (BLa)[18,129] with *ZIP* gel and injected it into a small amount of colorimetric substrate nitrocefin, the enzyme catalyzed substrate conversion as intended inside the healed gel construct. We followed this by quantitatively comparing the maximum activity of BLa (V_{max}) inside a *ZIP* gel and in buffer. No difference was observed in the substrate conversion rates, showing this simple formulation strategy may be useful for topical biologic delivery without harming activity (Fig. 5.8b). For comparison, an injectable hydrogel based on temperature-responsive Pluronic PEG-PPG-PEG triblocks was formulated with BLa. This alternative formula reduced the enzyme activity by over half, consistent with the well-known and deleterious effects of high PEG content on protein bioactivity.[130]

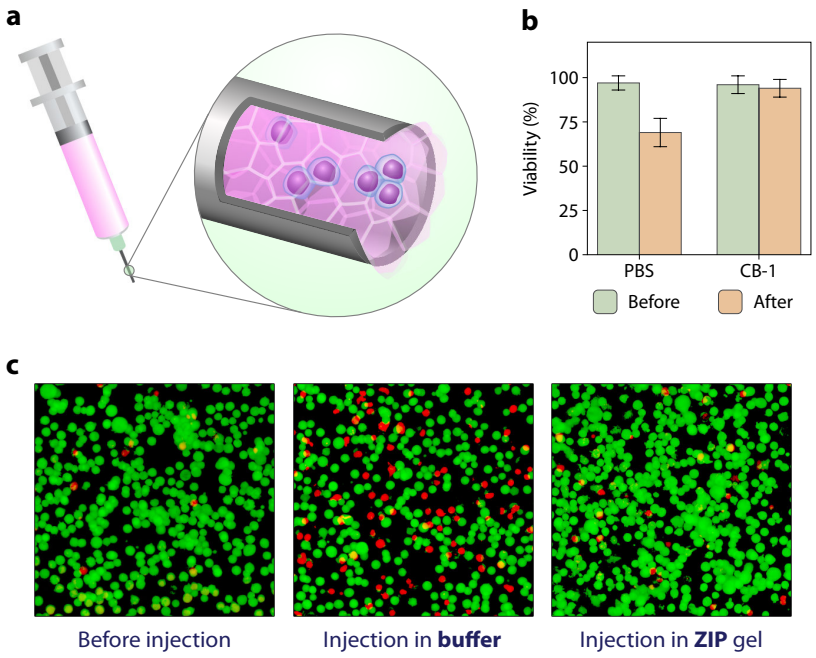

Figure 5.9 – *ZIP* hydrogel protects cells from shear damage during injection. **a**, Schematic showing mammalian cells mixed with ZIP hydrogel to evaluate protection from shear damage during injection. **b**, LIVE/DEAD viability of HEK 293T cells suspended in either PBS or CB-1 gel, before and after injection through 28-g needle. **c**, LIVE/DEAD fluorescent images of viability before and after injection.

5.4.5 Cell protection in injectable ZIP scaffolds

Several reports by Heilshorn et al[108,131,132] have highlighted the protective role some injectable hydrogels can play in shielding therapeutic cells from shear damage as they pass through a needle. In general, soft shear-thinning hydrogels (G′ ∼ 100 Pa) have been reported to have the best protecting effect; we were curious if injectable *ZIP* constructs of similar rheological properties have a similar benefit. Many varieties of zwitterionic gels have shown exceptional promise as cytocompatible synthetic scaffolds for tissue culture and cell expansion, so an injectable version offering additional mechanical protection could prove useful for formulating regenerative therapies. As summarized in Fig. 5.9, healthy HEK 293T cells were resuspended in PBS at 10^6 cells/mL and used to rehydrate an appropriate amount of *ZIP* powder (CB-1, CB-X = 0.05%) to a gel while gently mixing. This *ZIP* formulation was selected to match the rheological attributes of other cell-protective hydrogels. Then, the soft *ZIP*-cell construct was carefully transferred to a 1 mL syringe and injected into a well plate through a 28G needle. A control suspension was left in PBS and also injected. LIVE/DEAD reagents were added to each sample to assay the resulting viability. Promisingly, no significant decrease in viability was seen in the *ZIP*-protected formulation, while a 25-30% decrease was observed in the control buffer sample. Viability results and LIVE/DEAD fluorescent micrographs are shown in Fig. 5.9b-c. These results suggest *ZIP* constructs may also be promising injectable and cell-protective synthetic scaffolds.

5.5 Conclusions

In summary, we have developed a simple and versatile strategy to create shear-thinning and self-healing "zwitterionic injectable pellet" *ZIP* hydrogels based on reconstructed microgel assemblies and zwitterionic fusion. Importantly, these gels consist purely of carboxybetaine polymers and crosslinker, without any of the additional functional groups, chemical modifications, or special reagents typically required to develop hydrogels demonstrating dynamic viscoelasticity. This makes them straightforward to make at any scale, and they can be simply sterilized and lyophilized for long-term storage and facile reconstitution, forming composite injectable formulations with drug-loaded microspheres, biologics or therapeutic cells. *ZIP* hydrogels present a promising platform for a wide variety of biomedical applications requiring biocompatible and injectable materials.

Chapter 6

CONCLUSIONS

In this dissertation, we have described four distinct approaches to add new functionality to PCB-based zwitterionic materials. While the targeted applications varied, we endeavored to find simple ways to enable new features in these materials, using inherent properties of polyzwitterions whenever possible.

We began in *Chapter 1* by identifying the unique attributes characterizing zwitterionic materials, and PCB in particular, compared with other "biocompatible" materials such as PEG. As nanomedicine and regenerative medicine are at the forefront of both medicine and engineering, we set out to leverage the strengths of PCB to find solutions to long-standing problems in these areas.

In *Chapter 2*, we demonstrated how rational molecular design can help develop new cytocompatible biomaterials by systematically tuning the structure of PCB-ester side chains and adding "smart" responsiveness to environmental stimuli. Ester hydrolysis converts these polymers from cationic to zwitterionic forms, while conferring nontoxicity. To further study how the charge-switching feature affects polymer binding with DNA in polyplexes, we developed a photolabile ester of PCB to allow rapid and externally controlled hydrolysis.

Moving on to *Chapter 3*, we designed an approach to combine the hydrophilicity of current PCB with advantages of more flexible and degradable biomaterials. These step-growth polymerizations move the amines to the backbone, while incorporating labile esters, stable amides or thioethers between each zwitterionic group. Future optimization to obtain higher molecular weight products promises to enable protein conjugation and stabilization.

Then in *Chapter 4*, we demonstrated a robust platform for expanding stem cells while maintaining their full bioactivity, based on encapsulated culture inside *in situ* forming "star" PCB hydrogels. This strategy extended the excellent cytocompatibility of PCB to a reliable and broadly-applicable method to expand these valuable cell populations, aiming to relieve a bottleneck in regenerative medicine.

And finally in *Chapter 5*, we developed an "all-in-one" approach to create "zwitterionic injectable pellet" *ZIP* hydrogels. These reconstructed gels consist purely of carboxybetaine,

which has inherent self-healing properties that do not require any of the additional functional groups, chemical modifications, or special reagents typically necessary to enable dynamic viscoelasticity. This makes them straightforward to make, sterilize, and lyophilize, and we discussed several applications in drug depot formulation and cell protection. *ZIP* hydrogels present a promising platform for a wide variety of biomedical applications requiring biocompatible and injectable materials.

BIBLIOGRAPHY

[1] B. D. Ratner, "Biomaterials: Optimism and Pessimism," in *Biomaterials: Optimism and Pessimism*, 2nd International Conference for Bioinspired and Zwitterionic Materials, Seattle, WA, 2015.

[2] B. D. Ratner, "Healing with medical implants: The body battles back.," *Science Translational Medicine*, vol. 7, pp. 272fs4–272fs4, Jan. 2015.

[3] J. D. Faix, "Biomarkers of sepsis*," *Critical Reviews in Clinical Laboratory Sciences*, vol. 50, pp. 23–36, Jan. 2013.

[4] T. Ishida and H. Kiwada, "Accelerated blood clearance (ABC) phenomenon upon repeated injection of PEGylated liposomes.," *International Journal of Pharmaceutics*, vol. 354, pp. 56–62, Apr. 2008.

[5] S. Chen and S. Jiang, "An New Avenue to Nonfouling Materials," *Advanced Materials*, vol. 20, pp. 335–338, Jan. 2008.

[6] S. Jiang and Z. Cao, "Ultralow-fouling, functionalizable, and hydrolyzable zwitterionic materials and their derivatives for biological applications.," *Advanced Materials*, vol. 22, pp. 920–932, Mar. 2010.

[7] J. K. Armstrong, G. Hempel, S. Koling, L. S. Chan, T. Fisher, H. J. Meiselman, and G. Garratty, "Antibody against poly(ethylene glycol) adversely affects PEG-asparaginase therapy in acute lymphoblastic leukemia patients.," *Cancer*, vol. 110, pp. 103–111, July 2007.

[8] P. Zhang, F. Sun, C. Tsao, S. Liu, P. Jain, A. Sinclair, H.-C. Hung, T. Bai, K. Wu, and S. Jiang, "Zwitterionic gel encapsulation promotes protein stability, enhances pharmacokinetics, and reduces immunogenicity.," *Proceedings of the National Academy of Sciences*, vol. 112, pp. 12046–12051, Sept. 2015.

[9] R. P. Garay, R. El-Gewely, J. K. Armstrong, G. Garratty, and P. Richette, "Antibodies against polyethylene glycol in healthy subjects and in patients treated with PEG-conjugated agents.," *Expert Opinion on Drug Delivery*, vol. 9, pp. 1319–1323, Nov. 2012.

[10] K. R. Kamath and K. Park, "Biodegradable hydrogels in drug delivery," *Advanced Drug Delivery Reviews*, vol. 11, no. 1-2, pp. 59–84, 1993.

[11] E. Nance, G. F. Woodworth, K. A. Sailor, T.-Y. Shih, Q. Xu, G. Swaminathan, D. Xiang, C. Eberhart, and J. Hanes, "A dense poly(ethylene glycol) coating improves penetration of large polymeric nanoparticles within brain tissue.," *Science Translational Medicine*, vol. 4, pp. 149ra119–149ra119, Aug. 2012.

[12] M. J. Espiritu, A. C. Collier, and J.-P. Bingham, "A 21st-century approach to age-old problems: the ascension of biologics in clinical therapeutics.," *Drug Discovery Today*, vol. 19, pp. 1109–1113, Aug. 2014.

[13] P. Bailon, A. Palleroni, C. A. Schaffer, C. L. Spence, W.-J. Fung, J. E. Porter, G. K. Ehrlich, W. Pan, Z.-X. Xu, M. W. Modi, A. Farid, W. Berthold, and M. Graves, "Rational Design of a Potent, Long-Lasting Form of Interferon: A 40 kDa Branched Polyethylene Glycol-Conjugated Interferon α-2a for the Treatment of Hepatitis C," *Bioconjugate Chemistry*, vol. 12, pp. 195–202, Mar. 2001.

[14] D. P. Baker, E. Y. Lin, K. Lin, M. Pellegrini, R. C. Petter, L. L. Chen, R. M. Arduini, M. Brickelmaier, D. Wen, D. M. Hess, L. Chen, D. Grant, A. Whitty, A. Gill, D. J. Lindner, and R. B. Pepinsky, "N-terminally PEGylated human interferon-beta-1a with improved pharmacokinetic properties and in vivo efficacy in a melanoma angiogenesis model.," *Bioconjugate Chemistry*, vol. 17, pp. 179–188, Jan. 2006.

[15] J. S. Bomalaski, F. W. Holtsberg, C. M. Ensor, and M. A. Clark, "Uricase formulated with polyethylene glycol (uricase-PEG 20): biochemical rationale and preclinical studies.," *The Journal of rheumatology*, vol. 29, pp. 1942–1949, Sept. 2002.

[16] V. Schellenberger, C.-W. Wang, N. C. Geething, B. J. Spink, A. Campbell, W. To, M. D. Scholle, Y. Yin, Y. Yao, O. Bogin, J. L. Cleland, J. Silverman, and W. P. C. Stemmer, "A recombinant polypeptide extends the in vivo half-life of peptides and proteins in a tunable manner.," *Nature Biotechnology*, vol. 27, pp. 1186–1190, Dec. 2009.

[17] M. Schlapschy, U. Binder, C. Borger, I. Theobald, K. Wachinger, S. Kisling, D. Haller, and A. Skerra, "PASylation: a biological alternative to PEGylation for extending the plasma half-life of pharmaceutically active proteins," *Protein engineering, design & selection : PEDS*, vol. 26, pp. 489–501, July 2013.

[18] E. J. Liu, A. Sinclair, A. Keefe, B. L. Nannenga, B. L. Coyle, F. Baneyx, and S. Jiang, "EKylation: Addition of an Alternating-Charge Peptide Stabilizes Proteins.," *Biomacromolecules*, vol. 16, pp. 3357–3361, Oct. 2015.

[19] C. Sheridan, "Gene therapy finds its niche," *Nature Biotechnology*, vol. 29, pp. 121–128, Feb. 2011.

[20] X. Guo and L. Huang, "Recent Advances in Nonviral Vectors for Gene Delivery," *Accounts of Chemical Research*, vol. 45, pp. 971–979, July 2012.

[21] M. A. Mintzer and E. E. Simanek, "Nonviral Vectors for Gene Delivery," *Chemical Reviews*, vol. 109, pp. 259–302, Feb. 2009.

[22] J. J. Green, R. S. Langer, and D. G. Anderson, "A Combinatorial Polymer Library Approach Yields Insight into Nonviral Gene Delivery," *Accounts of Chemical Research*, vol. 41, pp. 749–759, June 2008.

[23] P. A. Burke, S. H. Pun, and T. M. Reineke, "Advancing Polymeric Delivery Systems Amidst a Nucleic Acid Therapy Renaissance," *ACS Macro Letters*, vol. 2, pp. 928–934, Oct. 2013.

[24] J. Behr, "The proton sponge: a trick to enter cells the viruses did not exploit," *CHIMIA*, vol. 1, no. 2, pp. 34–36, 1997.

[25] C. Yang, M. W. Tibbitt, L. Basta, and K. S. Anseth, "Mechanical memory and dosing influence stem cell fate," *Nature Materials*, vol. 13, pp. 645–652, Mar. 2014.

[26] C. A. DeForest and K. S. Anseth, "Advances in Bioactive Hydrogels to Probe and Direct Cell Fate," *Annual Review of Chemical and Biomolecular Engineering*, vol. 3, pp. 421–444, July 2012.

[27] A. J. Engler, S. Sen, H. L. Sweeney, and D. E. Discher, "Matrix Elasticity Directs Stem Cell Lineage Specification," *Cell*, vol. 126, pp. 677–689, Aug. 2006.

[28] Y. He, S. Jiang, Q. Shao, and A. D. White, "Different effects of zwitterion and ethylene glycol on proteins," *The Journal of Chemical Physics*, vol. 136, no. 22, p. 225101, 2012.

[29] D. R. Canchi and A. E. García, "Cosolvent Effects on Protein Stability," *Annual Review of Physical Chemistry*, vol. 64, pp. 273–293, Apr. 2013.

[30] A. D. White, A. K. Nowinski, W. Huang, A. J. Keefe, and F. Sun, "Decoding nonspecific interactions from nature," *Chemical Science*, 2012.

[31] A. Keefe, S. Jiang, K. B. Caldwell, A. K. Nowinski, A. D. White, and A. Thakkar, "Screening nonspecific interactions of peptides without background interference," *Biomaterials*, vol. 34, pp. 1871–1877, Mar. 2013.

[32] Q. Shao, L. Mi, X. Han, T. Bai, S. Liu, and S. Li, Yutingand Jiang, "Differences in cationic and anionic charge densities dictate zwitterionic associations and stimuli responses.," *The Journal of Physical Chemistry B*, vol. 118, pp. 6956–6962, June 2014.

[33] K. Ishihara, *Novel Bioinspired Phospholipid Polymer Biomaterials for Nanobioengineering*. Weinheim, Germany: Wiley-VCH Verlag GmbH & Co. KGaA, 2014.

[34] Z. Cao, Q. Yu, H. Xue, H. Xue, G. Cheng, and S. Jiang, "Nanoparticles for drug delivery prepared from amphiphilic PLGA zwitterionic block copolymers with sharp contrast in polarity between two blocks.," *Angewandte Chemie International Edition*, vol. 49, pp. 3771–3776, May 2010.

[35] W. Yang, S. Liu, T. Bai, A. Keefe, L. Zhang, J.-R. Ella-Menye, Y. Li, and S. Jiang, "Poly(carboxybetaine) nanomaterials enable long circulation and prevent polymer-specific antibody production," *Nano Today*, vol. 9, pp. 10–16, Feb. 2014.

[36] Y. Zhu, H. S. Sundaram, S. Liu, L. Zhang, X. Xu, Q. Yu, J. Xu, and S. Jiang, "A robust graft-to strategy to form multifunctional and stealth zwitterionic polymer-coated mesoporous silica nanoparticles.," *Biomacromolecules*, vol. 15, pp. 1845–1851, May 2014.

[37] J. M. Cordero, N. Insin, H. Wei, W. Liu, J. Lee, H.-S. Han, and M. G. Bawendi, "Compact zwitterion-coated iron oxide nanoparticles for biological applications.," *Nano Letters*, vol. 12, pp. 22–25, Jan. 2012.

[38] L. Zhang, S. Jiang, H. Xue, C. Gao, L. Carr, J. Wang, and B. Chu, "Imaging and cell targeting characteristics of magnetic nanoparticles modified by a functionalizable zwitterionic polymer with adhesive 3,4-dihydroxyphenyl-l-alanine linkages," *Biomaterials*, vol. 31, pp. 6582–6588, Sept. 2010.

[39] W. Yang, J.-R. Ella-Menye, S. Liu, T. Bai, D. Wang, Q. Yu, Y. Y. Li, and S. Jiang, "Crosslinked Carboxybetaine SAMs Enable Nanoparticles with Remarkable Stability in Complex Media.," *Langmuir*, vol. 30, pp. 2522–2529, Feb. 2014.

[40] A. Keefe and S. Jiang, "Poly(zwitterionic)protein conjugates offer increased stability without sacrificing binding affinity or bioactivity.," *Nature Chemistry*, vol. 4, pp. 59–63, Jan. 2012.

[41] S. Liu and S. Jiang, "Chemical conjugation of zwitterionic polymers protects immunogenic enzyme and preserves bioactivity without polymer-specific antibody response," *Nano Today*, vol. 11, pp. 285–291, June 2016.

[42] P. Zhang, P. Jain, C. Tsao, A. Sinclair, F. Sun, H.-C. Hung, T. Bai, K. Wu, and S. Jiang, "Butyrylcholinesterase nanocapsule as a long circulating bioscavenger with reduced immune response.," *Journal of Controlled Release*, vol. 230, pp. 73–78, Apr. 2016.

[43] L. Zhang, Z. Cao, T. Bai, L. Carr, J.-R. Ella-Menye, C. Irvin, B. D. Ratner, and S. Jiang, "Zwitterionic hydrogels implanted in mice resist the foreign-body reaction.," *Nature Biotechnology*, vol. 31, pp. 553–556, June 2013.

[44] T. Bai, F. Sun, L. Zhang, A. Sinclair, S. Liu, J.-R. Ella-Menye, Y. Zheng, and S. Jiang, "Restraint of the differentiation of mesenchymal stem cells by a nonfouling zwitterionic hydrogel.," *Angewandte Chemie International Edition*, vol. 53, pp. 12729–12734, Nov. 2014.

[45] T. Bai, A. Sinclair, F. Sun, P. Jain, H.-C. Hung, P. Zhang, J.-R. Ella-Menye, W. Liu, and S. Jiang, "Harnessing isomerization-mediated manipulation of nonspecific cell/matrix interactions to reversibly trigger and suspend stem cell differentiation," *Chemical Science*, vol. 7, no. 1, pp. 333–338, 2015.

[46] L. Carr, J. E. Krause, J.-R. Ella-Menye, and S. Jiang, "Functionalizable and nonfouling zwitterionic carboxybetaine hydrogels with a carboxybetaine dimethacrylate crosslinker," *Biomaterials*, vol. 32, no. 33, pp. 8456–8461, 2011.

[47] Z. Zhang, S. Jiang, L. Cheng, Gangand Carr, H. Vaisocherová, and S. Chen, "The hydrolysis of cationic polycarboxybetaine esters to zwitterionic polycarboxybetaines with controlled properties," *Biomaterials*, vol. 29, no. 36, pp. 4719–4725, 2008.

[48] M. Ilčíková, J. Tkáč, and P. Kasák, "Switchable Materials Containing Polyzwitterion Moieties," *Polymers*, vol. 7, pp. 2344–2370, Nov. 2015.

[49] A. Sinclair, T. Bai, L. Carr, J.-R. Ella-Menye, L. Zhang, and S. Jiang, "Engineering buffering and hydrolytic or photolabile charge shifting in a polycarboxybetaine ester gene delivery platform.," *Biomacromolecules*, vol. 14, pp. 1587–1593, May 2013.

[50] C. A. DeForest and D. A. Tirrell, "A photoreversible protein-patterning approach for guiding stem cell fate in three-dimensional gels," *Nature Materials*, vol. 14, pp. 523–531, Feb. 2015.

[51] P. M. Kharkar, K. L. Kiick, and A. M. Kloxin, "Design of thiol- and light-sensitive degradable hydrogels using Michael-type addition reactions," *Polym. Chem.*, vol. 6, no. 31, pp. 5565–5574, 2015.

[52] J. C. Grim, I. A. Marozas, and K. S. Anseth, "Thiol-ene and photo-cleavage chemistry for controlled presentation of biomolecules in hydrogels.," *Journal of Controlled Release*, vol. 219, pp. 95–106, Dec. 2015.

[53] B. J. Adzima, Y. Tao, C. J. Kloxin, C. A. DeForest, K. S. Anseth, and C. N. Bowman, "Spatial and temporal control of the alkyne–azide cycloaddition by photoinitiated Cu(II) reduction," *Nature Chemistry*, vol. 3, pp. 258–261, Jan. 2011.

[54] T. Bai, J. Li, S. Imren, A. Sinclair, F. Merriam, F. Sun, C. Nourigat, P. Jain, J. Delrow, R. Bason, H.-C. Hung, P. Zhang, S. Heimfeld, C. Delaney, and S. Jiang, "Culture in zwitterionic hydrogels promotes expansion of human hematopoietic stem cells," *submitted*, 2017.

[55] L. S. Nair, "Injectable Hydrogels for Regenerative Engineering," 2016.

[56] A. Hatefi and B. Amsden, "Biodegradable injectable in situ forming drug delivery systems.," *Journal of Controlled Release*, vol. 80, pp. 9–28, Apr. 2002.

[57] D. Seliktar, "Designing cell-compatible hydrogels for biomedical applications.," *Science*, vol. 336, pp. 1124–1128, June 2012.

[58] T. Bai, S. Liu, F. Sun, A. Sinclair, L. Zhang, Q. Shao, and S. Jiang, "Zwitterionic fusion in hydrogels and spontaneous and time-independent self-healing under physiological conditions.," *Biomaterials*, vol. 35, pp. 3926–3933, Apr. 2014.

[59] A. Sinclair, M. O'Kelly, T. Bai, P. Jain, and S. Jiang, "Injectable hydrogels based on dynamic crosslinking of zwitterionic microgels present a versatile and self-healing platform for drug and cell delivery formulations," *to be submitted*, 2017.

[60] Y. Teramura and H. H. Iwata, "Cell surface modification with polymers for biomedical studies," *Soft Matter*, vol. 6, no. 6, p. 1081, 2010.

[61] A. Kichler, "Gene transfer with modified polyethylenimines," *The journal of gene medicine*, vol. 6, no. S1, pp. S3–S10, 2004.

[62] S. W. Kim, Z. Zhong, J. Feijen, M. C. Lok, W. E. Hennink, L. V. Christensen, J. W. Yockman, and Y.-H. Kim, "Low Molecular Weight Linear Polyethylenimine- b-poly(ethylene glycol)- b-polyethylenimine Triblock Copolymers: Synthesis, Characterization, and in Vitro Gene Transfer Properties," *Biomacromolecules*, vol. 6, pp. 3440–3448, Nov. 2005.

[63] R. Arote, T.-H. Kim, Y.-K. Kim, S.-K. Hwang, H.-L. Jiang, H.-H. Song, J.-W. Nah, M.-H. Cho, and C.-S. Cho, "A biodegradable poly(ester amine) based on polycaprolactone and polyethylenimine as a gene carrier," *Biomaterials*, vol. 28, pp. 735–744, Feb. 2007.

[64] J. Zhou, J. J. Liu, C. J. C. Cheng, T. R. T. Patel, C. E. C. Weller, J. M. J. Piepmeier, Z. Jiang, and W. M. W. Saltzman, "Biodegradable poly(amine-co-ester) terpolymers for targeted gene delivery.," *Nature Materials*, vol. 11, pp. 82–90, Jan. 2011.

[65] K. Miyata, N. Nishiyama, and K. Kataoka, "Rational design of smart supramolecular assemblies for gene delivery: chemical challenges in the creation of artificial viruses," *Chemical Society Reviews*, vol. 41, no. 7, p. 2562, 2012.

[66] J. J. Green, G. T. Zugates, N. C. Tedford, Y.-H. Huang, L. G. Griffith, D. A. Lauffenburger, J. A. Sawicki, R. S. Langer, and D. G. Anderson, "Combinatorial modification of degradable polymers enables transfection of human cells comparable to adenovirus," *Advanced Materials*, vol. 19, no. 19, pp. 2836–+, 2007.

[67] L. R. Carr and S. Jiang, "Mediating high levels of gene transfer without cytotoxicity via hydrolytic cationic ester polymers.," *Biomaterials*, vol. 31, pp. 4186–4193, May 2010.

[68] T. L. Andresen, R. V. Benjaminsen, M. A. Mattebjerg, J. R. Henriksen, and S. M. Moghimi, "The Possible "Proton Sponge " Effect of Polyethylenimine (PEI) Does Not Include Change in Lysosomal pH," *Molecular Therapy*, vol. 21, pp. 149–157, Oct. 2012.

[69] K. S. Anseth, A. M. Kloxin, A. M. Kasko, and C. N. Salinas, "Photodegradable Hydrogels for Dynamic Tuning of Physical and Chemical Properties," *Science*, vol. 324, pp. 59–63, Apr. 2009.

[70] G. Han, C.-C. You, B.-j. Kim, R. S. Turingan, N. S. Forbes, C. T. Martin, and V. M. Rotello, "Light-Regulated Release of DNA and Its Delivery to Nuclei by Means of Photolabile Gold Nanoparticles," *Angewandte Chemie International Edition*, vol. 118, pp. 3237–3241, May 2006.

[71] S. Y. Wong, J. M. Pelet, and D. Putnam, "Polymer systems for gene delivery—Past, present, and future," *Progress in Polymer Science*, vol. 32, pp. 799–837, Aug. 2007.

[72] D. S. H. Chu, J. G. Schellinger, P. S. P. Stayton, J. Shi, A. J. J. A. Convertine, and S. H. Pun, "Application of living free radical polymerization for nucleic Acid delivery.," *Accounts of Chemical Research*, vol. 45, pp. 1089–1099, July 2012.

[73] S. R. Van Tomme, M. J. van Steenbergen, S. C. De Smedt, C. F. van Nostrum, and W. E. Hennink, "Self-gelling hydrogels based on oppositely charged dextran microspheres," *Biomaterials*, vol. 26, pp. 2129–2135, May 2005.

[74] B. Sun and D. Lynn, "Release of DNA from polyelectrolyte multilayers fabricated using 'charge-shifting' cationic polymers: Tunable temporal control and sequential, multi-agent release," *Journal of Controlled Release*, vol. 148, pp. 91–100, Nov. 2010.

[75] D. Lynn, D. G. Anderson, D. Putnam, and R. S. Langer, "Accelerated Discovery of Synthetic Transfection Vectors: Parallel Synthesis and Screening of a Degradable Polymer Library," *Journal of the American Chemical Society*, vol. 123, pp. 8155–8156, Aug. 2001.

[76] J. L. Fortman, S. Chhabra, A. Mukhopadhyay, H. Chou, T. S. Lee, E. Steen, and J. D. Keasling, "Biofuel alternatives to ethanol: pumping the microbial well," *Trends in Biotechnology*, vol. 26, pp. 375–381, July 2008.

[77] S. Jiang, W. Yang, H. Xue, W. Li, and J. Zhang, "Pursuing "Zero" Protein Adsorption of Poly(carboxybetaine) from Undiluted Blood Serum and Plasma," *Langmuir*, vol. 25, pp. 11911–11916, Oct. 2009.

[78] D. S. Pisal, M. P. Kosloski, and S. V. Balu-Iyer, "Delivery of therapeutic proteins.," *Journal of Pharmaceutical Sciences*, vol. 99, pp. 2557–2575, June 2010.

[79] A. Constantinou, C. Chen, and M. P. Deonarain, "Modulating the pharmacokinetics of therapeutic antibodies.," *Biotechnology letters*, vol. 32, pp. 609–622, May 2010.

[80] S.-Q. Gao, T. Maeda, K. Okano, and K. Palczewski, "A microparticle/hydrogel combination drug-delivery system for sustained release of retinoids.," *Investigative Ophthalmology & Visual Science*, vol. 53, pp. 6314–6323, Sept. 2012.

[81] K. Whitehead, D. Kohane, B. Timko, W. Gao, O. C. Farokhzad, D. G. Anderson, and R. S. Langer, "Advances in Drug Delivery," *Annual Review of Materials Research*, vol. 41, no. 1, pp. 1–20, 2011.

[82] J.-W. Yoo, D. J. Irvine, D. E. Discher, and S. Mitragotri, "Bio-inspired, bioengineered and biomimetic drug delivery carriers," *Nature Reviews Drug Discovery*, vol. 10, pp. 1–15, July 2011.

[83] D. Lynn and R. S. Langer, "Degradable Poly(β-amino esters): Synthesis, Characterization, and Self-Assembly with Plasmid DNA," *Journal of the American Chemical Society*, vol. 122, pp. 10761–10768, Nov. 2000.

[84] C. Lin and J. F. J. Engbersen, "Effect of chemical functionalities in poly(amido amine)s for non-viral gene transfection.," *Journal of Controlled Release*, vol. 132, pp. 267–272, Dec. 2008.

[85] P. Ferruti and F. Danusso, "Synthesis of tertiary amine polymers," *Polymer*, vol. 11, pp. 88–113, Feb. 1970.

[86] P. Ferruti, M. C. Tanzi, L. Rusconi, C. Barozzi, and L. Angiolini, "Synthesis and characterization of piperazine-derived poly(amido-amine)s with different distributions of amido- and amino-groups along the macromolecular chain," *Polymer*, 1984.

[87] P. Ferruti, M. A. Marchisio, and R. R. Duncan, "Poly(amido-amine)s: Biomedical Applications," *Macromolecular Rapid Communications*, vol. 23, no. 5-6, pp. 332–355, 2002.

[88] E. Ranucci, P. Ferruti, E. Lattanzio, A. Manfredi, M. Rossi, P. Mussini, F. Chiellini, and C. Bartoli, "Acid-base properties of poly (amidoamine)s," *Journal of Polymer Science Part A: Polymer Chemistry*, vol. 47, no. 24, pp. 6977–6991, 2009.

[89] R. Cavalli, A. Bisazza, R. Sessa, L. Primo, F. Fenili, A. Manfredi, E. Ranucci, and P. Ferruti, "Amphoteric agmatine containing polyamidoamines as carriers for plasmid DNA in vitro and in vivo delivery.," *Biomacromolecules*, vol. 11, pp. 2667–2674, Oct. 2010.

[90] P. Ferruti, N. Mauro, A. Manfredi, and E. Ranucci, "Hetero-difunctional dimers as building blocks for the synthesis of poly(amidoamine)s with hetero-difunctional chain terminals and their derivatives," *Journal of Polymer Science Part A: Polymer Chemistry*, vol. 50, pp. 4947–4957, Dec. 2012.

[91] W. Xi, T. F. Scott, C. J. Kloxin, and C. N. Bowman, "Click Chemistry in Materials Science," *Advanced Functional Materials*, vol. 24, pp. 2572–2590, Jan. 2014.

[92] J. W. Chan, C. E. Hoyle, A. B. Lowe, and M. Bowman, "Nucleophile-Initiated Thiol-Michael Reactions: Effect of Organocatalyst, Thiol, and Ene," *Macromolecules*, vol. 43, pp. 6381–6388, July 2010.

[93] G.-Z. Li, R. K. Randev, A. H. Soeriyadi, G. Rees, C. Boyer, Z. Tong, T. P. Davis, C. R. Becer, and D. M. Haddleton, "Investigation into thiol-(meth)acrylate Michael addition reactions using amine and phosphine catalysts," *Polym. Chem.*, vol. 1, no. 8, pp. 1196–9, 2010.

[94] "Characterization of synthetic polymers by MALDI-MS," *Progress in Polymer Science*, vol. 31, pp. 277–357, Jan. 2006.

[95] W. H. Binder and R. Sachsenhofer, "'Click' Chemistry in Polymer and Materials Science," *Macromolecular Rapid Communications*, vol. 28, pp. 15–54, Jan. 2007.

[96] A. B. Lowe, "Thiol–ene "click" reactions and recent applications in polymer and materials synthesis: a first update," *Polym. Chem.*, vol. 5, pp. 4820–4870, July 2014.

[97] J. D. McCall and K. S. Anseth, "Thiol-ene photopolymerizations provide a facile method to encapsulate proteins and maintain their bioactivity.," *Biomacromolecules*, vol. 13, pp. 2410–2417, Aug. 2012.

[98] C.-C. Lin, C. S. Ki, and H. Shih, "Thiol-norbornene photoclick hydrogels for tissue engineering applications," vol. 132, pp. n/a–n/a, Oct. 2014.

[99] N. Tandon, D. Marolt, E. Cimetta, and G. Vunjak-Novakovic, "Bioreactor engineering of stem cell environments," *Biotechnology Advances*, vol. 31, pp. 1020–1031, Nov. 2013.

[100] E. A. Phelps, N. O. Enemchukwu, V. F. Fiore, J. C. Sy, N. Murthy, T. A. Sulchek, T. H. Barker, and A. J. García, "Maleimide Cross-Linked Bioactive PEG Hydrogel Exhibits Improved Reaction Kinetics and Cross-Linking for Cell Encapsulation and In Situ Delivery," *Advanced Materials*, vol. 24, pp. 64–70, Dec. 2011.

[101] Q. Shao and S. Jiang, "Molecular Understanding and Design of Zwitterionic Materials," *Advanced Materials*, vol. 27, pp. 15–26, Jan. 2015.

[102] L. Mi, H. Xue, Y. Y. Li, and S. Jiang, "A Thermoresponsive Antimicrobial Wound Dressing Hydrogel Based on a Cationic Betaine Ester," *Advanced Functional Materials*, vol. 21, pp. 4028–4034, Sept. 2011.

[103] C. E. Hoyle, A. B. Lowe, and C. N. Bowman, "Thiol -click chemistry: a multifaceted toolbox for small molecule and polymer synthesis," *Chemical Society Reviews*, vol. 39, no. 4, pp. 1355–1387, 2010.

[104] Y.-N. Chou, F. Sun, H.-C. Hung, P. Jain, A. Sinclair, P. Zhang, T. Bai, Y. Chang, T.-C. Wen, Q. Yu, and S. Jiang, "Ultra-low fouling and high antibody loading zwitterionic hydrogel coatings for sensing and detection in complex media.," *Acta Biomaterialia*, Apr. 2016.

[105] N. D. Brault, A. D. White, A. D. Taylor, Q. Yu, and S. Jiang, "A Directly Functionalizable Surface Platform for Protein Arrays in Undiluted Human Blood Plasma.," *Analytical Chemistry*, pp. –, Jan. 2013.

[106] M. Guvendiren, H. D. Lu, and J. A. Burdick, "Shear-thinning hydrogels for biomedical applications," *Soft Matter*, vol. 8, no. 2, pp. 260–272, 2012.

[107] T. L. Sun, T. Kurokawa, S. Kuroda, A. Bin Ihsan, T. Akasaki, K. Sato, M. A. Haque, T. Nakajima, and J. P. Gong, "Physical hydrogels composed of polyampholytes demonstrate high toughness and viscoelasticity," *Nature Materials*, vol. 12, pp. 932–937, July 2013.

[108] H. Wang and S. C. Heilshorn, "Adaptable hydrogel networks with reversible linkages for tissue engineering.," *Advanced Materials*, vol. 27, pp. 3717–3736, July 2015.

[109] T. L. Sun, F. Luo, T. Kurokawa, S. N. Karobi, T. Nakajima, and J. P. Gong, "Molecular structure of self-healing polyampholyte hydrogels analyzed from tensile behaviors.," *Soft Matter*, vol. 11, pp. 9355–9366, Dec. 2015.

[110] C. B. Highley, G. D. Prestwich, and J. A. Burdick, "Recent advances in hyaluronic acid hydrogels for biomedical applications," *Current Opinion in Biotechnology*, vol. 40, pp. 35–40, Aug. 2016.

[111] E. A. Appel, J. del Barrio, X. J. Loh, and O. A. Scherman, "Supramolecular polymeric hydrogels," *Chemical Society Reviews*, vol. 41, no. 18, pp. 6195–20, 2012.

[112] I. Sall and G. Férard, "Comparison of the sensitivity of 11 crosslinked hyaluronic acid gels to bovine testis hyaluronidase," *Polymer Degradation and Stability*, vol. 92, pp. 915–919, May 2007.

[113] C. B. Rodell, A. L. Kaminski, and J. A. Burdick, "Rational Design of Network Properties in Guest–Host Assembled and Shear-Thinning Hyaluronic Acid Hydrogels," *Biomacromolecules*, vol. 14, pp. 4125–4134, Nov. 2013.

[114] S. Strandman and X. X. Zhu, "Self-Healing Supramolecular Hydrogels Based on Reversible Physical Interactions," *Gels*, vol. 2, pp. 16–31, June 2016.

[115] Y. Zhao, T. Bai, Q. Q. Shao, S. Jiang, and A. Q. Shen, "Thermoresponsive self-assembled NiPAm-zwitterion copolymers," *Polym. Chem.*, vol. 6, no. 7, pp. 1066–1077, 2015.

[116] J. J. Escobar-Chavez, "Applications of thermo-reversible Pluronic F127 gels in pharmaceutical formulations ," *Journal of Pharmacy Pharmaceutical Sciences*, vol. 9, pp. 339–358, Nov. 2006.

[117] D. L. Taylor and M. in het Panhuis, "Self-Healing Hydrogels.," *Advanced Materials*, vol. 28, pp. 9060–9093, Nov. 2016.

[118] L. Hu, H. Zhang, and W. Song, "An overview of preparation and evaluation sustained-release injectable microspheres," *Journal of Microencapsulation*, vol. 30, pp. 369–382, June 2013.

[119] T. Niwa, T. Hino, and M. Nohara, "Biodegradable submicron carriers for peptide drugs: preparation of DL-lactide/glycolide copolymer (PLGA) nanospheres with nafarelin acetate by a novel emulsion-phase separation method in an oil system," *International Journal of Pharmaceutics*, vol. 121, no. 1, pp. 45–54, 1995.

[120] Y. Zhu, C. Crewe, and P. E. Scherer, "Hyaluronan in adipose tissue: Beyond dermal filler and therapeutic carrier.," *Science Translational Medicine*, vol. 8, pp. 323ps4–323ps4, Jan. 2016.

[121] K. M. C. Chan, R. H. Li, J. W. Chapman, E. M. Trac, J. B. Kobler, S. M. Zeitels, R. S. Langer, and S. S. Karajanagi, "Functionalizable hydrogel microparticles of tunable size and stiffness for soft-tissue filler applications.," *Acta Biomaterialia*, vol. 10, pp. 2563–2573, June 2014.

[122] Q. Wang, J. L. Mynar, M. Yoshida, E. Lee, M. Lee, K. Okuro, K. Kinbara, and T. Aida, "High-water-content mouldable hydrogels by mixing clay and a dendritic molecular binder," *Nature*, vol. 463, pp. 339–343, Jan. 2010.

[123] S. Butylina, S. Geng, and K. Oksman, "Properties of as-prepared and freeze-dried hydrogels made from poly(vinyl alcohol) and cellulose nanocrystals using freeze-thaw technique," *European Polymer Journal*, vol. 81, pp. 386–396, Aug. 2016.

[124] N. Guziewicz, A. Best, B. Perez-Ramirez, and D. L. Kaplan, "Lyophilized silk fibroin hydrogels for the sustained local delivery of therapeutic monoclonal antibodies," *Biomaterials*, vol. 32, pp. 2642–2650, Apr. 2011.

[125] W. L. Stoppel, J. C. White, S. D. Horava, A. C. Henry, S. C. Roberts, and S. R. Bhatia, "Terminal sterilization of alginate hydrogels: Efficacy and impact on mechanical properties," *Journal of Biomedical Materials Research Part A*, vol. 102, pp. 877–884, Nov. 2013.

[126] K. Schoenhammer, J. Boisclair, H. Schuetz, H. Petersen, and A. Goepferich, "Biocompatibility of an injectable in situ forming depot for peptide delivery," *Journal of Pharmaceutical Sciences*, vol. 99, pp. 4390–4399, Aug. 2010.

[127] P. Z. Elias, G. W. Liu, H. Wei, M. C. Jensen, P. J. Horner, and S. H. Pun, "A functionalized, injectable hydrogel for localized drug delivery with tunable thermosensitivity: Synthesis and characterization of physical and toxicological properties," *Journal of Controlled Release*, vol. 208, pp. 76–84, June 2015.

[128] A. P. Chapman, P. Antoniw, M. Spitali, S. West, S. Stephens, and D. J. King, "Therapeutic antibody fragments with prolonged in vivo half-lives.," *Nature Biotechnology*, vol. 17, pp. 780–783, Aug. 1999.

[129] G. Georgiou and F. Baneyx, "Expression, purification, and enzymatic characterization of a protein A-β-lactamase hybrid protein," *Enzyme and microbial technology*, vol. 11, no. 9, pp. 559–567, 1989.

[130] F. M. Veronese and A. Mero, "The impact of PEGylation on biological therapies.," *BioDrugs : clinical immunotherapeutics, biopharmaceuticals and gene therapy*, vol. 22, no. 5, pp. 315–329, 2008.

[131] B. A. Aguado, W. Mulyasasmita, J. Su, K. J. Lampe, and S. C. Heilshorn, "Improving Viability of Stem Cells During Syringe Needle Flow Through the Design of Hydrogel Cell Carriers," *Tissue Engineering Part A*, vol. 18, pp. 806–815, Apr. 2012.

[132] K. Dubbin, Y. Hori, K. K. Lewis, and S. C. Heilshorn, "Dual-Stage Crosslinking of a Gel-Phase Bioink Improves Cell Viability and Homogeneity for 3D Bioprinting.," *Advanced healthcare materials*, vol. 5, pp. 2488–2492, Oct. 2016.

[133] A. Sinclair, T. Bai, and S. Jiang, "Degradable zwitterionic star polymer hydrogel for mesenchymal cell expansion without a loss in bioactivity," *to be submitted*, 2017.

[134] B. Xu, T. Bai, A. Sinclair, W. Wang, Q. Wu, F. Gao, H. Jia, S. Jiang, and W. Liu, "Directed neural stem cell differentiation on polyaniline-coated high strength hydrogels," *Materials Today Chemistry*, vol. 1-2, pp. 15–22, Oct. 2016.

[135] F. Sun, H.-C. Hung, A. Sinclair, P. Zhang, T. Bai, D. D. Galvan, P. Jain, B. Li, S. Jiang, and Q. Yu, "Hierarchical zwitterionic modification of a SERS substrate enables real-time drug monitoring in blood plasma," *Nature Communications*, vol. 7, pp. 1–9, Nov. 2016.

[136] J. An, Q. Guo, P. Zhang, A. Sinclair, Y. Zhao, X. Zhang, K. Wu, F. Sun, H.-C. Hung, C. Li, and S. Jiang, "Hierarchical design of a polymeric nanovehicle for efficient tumor regression and imaging," *Nanoscale*, vol. 8, pp. 9318–9327, Apr. 2016.

[137] L. Zhang, A. Sinclair, Z. Cao, J.-R. Ella-Menye, X. Xu, L. Carr, S. H. Pun, and S. Jiang, "Hydrolytic cationic ester microparticles for highly efficient DNA vaccine delivery.," *Small*, vol. 9, pp. 3439–3444, Oct. 2013.

Appendix A

VITA

Andy Sinclair grew up in Grants Pass, Oregon and graduated as valedictorian from Grants Pass High School in 2006. He then attended the Oregon State University Honors College and received his Honors Bachelor of Science in Bioengineering in 2011 with minors in Chemistry and Business & Entrepreneurship. In his spare time, he enjoys playing tennis, drinking craft IPAs with his wife and cats, and graphic design.

Publications

[1] A. Sinclair, M. O'Kelly, T. Bai, P. Jain, and S. Jiang, "Injectable hydrogels based on dynamic crosslinking of zwitterionic microgels present a versatile and self-healing platform for drug and cell delivery formulations," *to be submitted*, 2017

[2] A. Sinclair, T. Bai, and S. Jiang, "Degradable zwitterionic star polymer hydrogel for mesenchymal cell expansion without a loss in bioactivity," *to be submitted*, 2017

[3] T. Bai, J. Li, S. Imren, A. Sinclair, F. Merriam, F. Sun, C. Nourigat, P. Jain, J. Delrow, R. Bason, H.-C. Hung, P. Zhang, S. Heimfeld, C. Delaney, and S. Jiang, "Culture in zwitterionic hydrogels promotes expansion of human hematopoietic stem cells," *submitted*, 2017

[4] B. Xu, T. Bai, A. Sinclair, W. Wang, Q. Wu, F. Gao, H. Jia, S. Jiang, and W. Liu, "Directed neural stem cell differentiation on polyaniline-coated high strength hydrogels," *Materials Today Chemistry*, vol. 1-2, pp. 15–22, Oct. 2016

[5] F. Sun, H.-C. Hung, A. Sinclair, P. Zhang, T. Bai, D. D. Galvan, P. Jain, B. Li, S. Jiang, and Q. Yu, "Hierarchical zwitterionic modification of a SERS substrate enables real-time drug monitoring in blood plasma," *Nature Communications*, vol. 7, pp. 1–9, Nov. 2016

[6] P. Zhang, P. Jain, C. Tsao, A. Sinclair, F. Sun, H.-C. Hung, T. Bai, K. Wu, and S. Jiang, "Butyrylcholinesterase nanocapsule as a long circulating bioscavenger with reduced immune response.," *Journal of Controlled Release*, vol. 230, pp. 73–78, Apr. 2016

[7] Y.-N. Chou, F. Sun, H.-C. Hung, P. Jain, A. Sinclair, P. Zhang, T. Bai, Y. Chang, T.-C. Wen, Q. Yu, and S. Jiang, "Ultra-low fouling and high antibody loading zwitterionic hydrogel coatings for sensing and detection in complex media.," *Acta Biomaterialia*, Apr. 2016

[8] J. An, Q. Guo, P. Zhang, A. Sinclair, Y. Zhao, X. Zhang, K. Wu, F. Sun, H.-C. Hung, C. Li, and S. Jiang, "Hierarchical design of a polymeric nanovehicle for efficient tumor regression and imaging," *Nanoscale*, vol. 8, pp. 9318–9327, Apr. 2016

[9] T. Bai, A. Sinclair, F. Sun, P. Jain, H.-C. Hung, P. Zhang, J.-R. Ella-Menye, W. Liu, and S. Jiang, "Harnessing isomerization-mediated manipulation of nonspecific cell/matrix interactions to reversibly trigger and suspend stem cell differentiation," *Chemical Science*, vol. 7, no. 1, pp. 333–338, 2015

[10] E. J. Liu, A. Sinclair, A. Keefe, B. L. Nannenga, B. L. Coyle, F. Baneyx, and S. Jiang, "EKylation: Addition of an Alternating-Charge Peptide Stabilizes Proteins.," *Biomacromolecules*, vol. 16, pp. 3357–3361, Oct. 2015

[11] P. Zhang, F. Sun, C. Tsao, S. Liu, P. Jain, A. Sinclair, H.-C. Hung, T. Bai, K. Wu, and S. Jiang, "Zwitterionic gel encapsulation promotes protein stability, enhances pharmacokinetics, and reduces immunogenicity.," *Proceedings of the National Academy of Sciences*, vol. 112, pp. 12046–12051, Sept. 2015

[12] T. Bai, F. Sun, L. Zhang, A. Sinclair, S. Liu, J.-R. Ella-Menye, Y. Zheng, and S. Jiang, "Restraint of the differentiation of mesenchymal stem cells by a nonfouling zwitterionic hydrogel.," *Angewandte Chemie International Edition*, vol. 53, pp. 12729–12734, Nov. 2014

[13] T. Bai, S. Liu, F. Sun, A. Sinclair, L. Zhang, Q. Shao, and S. Jiang, "Zwitterionic fusion in hydrogels and spontaneous and time-independent self-healing under physiological conditions.," *Biomaterials*, vol. 35, pp. 3926–3933, Apr. 2014

[14] L. Zhang, A. Sinclair, Z. Cao, J.-R. Ella-Menye, X. Xu, L. Carr, S. H. Pun, and S. Jiang, "Hydrolytic cationic ester microparticles for highly efficient DNA vaccine delivery.," *Small*, vol. 9, pp. 3439–3444, Oct. 2013

[15] A. Sinclair, T. Bai, L. Carr, J.-R. Ella-Menye, L. Zhang, and S. Jiang, "Engineering buffering and hydrolytic or photolabile charge shifting in a polycarboxybetaine ester gene delivery platform.," *Biomacromolecules*, vol. 14, pp. 1587–1593, May 2013